UNIVERSIDADE FEDERAL DO RIO GRANDE DO SUL
PROGRAMA DE PÓS-GRADUAÇÃO EM ENGENHARIA DE MINAS, METALÚRGICA E DE MATERIAIS

ELLEN DAVID CHEPP

MODELAGEM DA OPERAÇÃO DE INSTALAÇÕES FOTOVOLTAICAS COM SOMBREAMENTO PARCIAL E SUA VALIDAÇÃO EXPERIMENTAL

Porto Alegre
2023

ELLEN DAVID CHEPP

MODELAGEM DA OPERAÇÃO DE INSTALAÇÕES FOTOVOLTAICAS COM SOMBREAMENTO PARCIAL E SUA VALIDAÇÃO EXPERIMENTAL

Tese submetida ao Programa de Pós-Graduação em Engenharia de Minas, Metalúrgica e de Materiais da Universidade Federal do Rio Grande do Sul, como requisito parcial à obtenção do título de Doutor (a) em Engenharia.

Orientador: Prof. Dr. Arno Krenzinger
Coorientador: Prof. Dr. Fabiano Perin Gasparin

Porto Alegre
2023

CIP - Catalogação na Publicação

Chepp, Ellen David
MODELAGEM DA OPERAÇÃO DE INSTALAÇÕES FOTOVOLTAICAS COM SOMBREAMENTO PARCIAL E SUA VALIDAÇÃO EXPERIMENTAL / Ellen David Chepp. -- 2023.
59 f.
Orientador: Arno Krenzinger.

Coorientador: Fabiano Perin Gasparin.

Tese (Doutorado) -- Universidade Federal do Rio Grande do Sul, Escola de Engenharia, Programa de Pós-Graduação em Engenharia de Minas, Metalúrgica e de Materiais, Porto Alegre, BR-RS, 2023.

1. Fotovoltaico. 2. Sombreamento. 3. Modelagem. I. Krenzinger, Arno, orient. II. Gasparin, Fabiano Perin, coorient. III. Título.

Elaborada pelo Sistema de Geração Automática de Ficha Catalográfica da UFRGS com osdados fornecidos pelo(a) autor(a).

ELLEN DAVID CHEPP

MODELAGEM DA OPERAÇÃO DE INSTALAÇÕES FOTOVOLTAICAS COM SOMBREAMENTO PARCIAL E SUA VALIDAÇÃO EXPERIMENTAL

Esta tese foi analisada e julgada adequada para a obtenção do título de Doutor (a) em Engenharia e aprovada em sua forma final pelos Orientadores e pela Banca Examinadora designada pelo PPGE3M da UFRGS.

Orientador: Prof. Dr. Arno Krenzinger

Coorientador: Prof. Dr. Fabiano Perin Gasparin

BANCA EXAMINADORA:

Prof. Dr. Adriano Moehlecke

Pontifícia Universidade Católica do Rio Grande do Sul (PUCRS)

Prof. Dr. Giuliano Arns Rampinelli

Universidade Federal de Santa Catarina (UFSC)

Prof. Dr. Marcelo Pinho Almeida

Universidade de São Paulo (USP)

Prof. Dr. Rodrigo de Lemos Peroni

Coordenador do PPGE3M

AGRADECIMENTOS

Agradeço a Deus, meu Senhor, por sua graça e bondade em minha vida.

À minha mãe, Alvina Isabel, por todos os sacrifícios feitos em meu favor e por sempre me apoiar ao longo da minha trajetória acadêmica. Ao meu marido, Douglas, pela paciência e pelos conselhos nos momentos de dúvidas e preocupações.

Às minhas tias, Marilinda e Maria Izabel, pelo amor e cuidado demonstrados a mim e a minha mãe. A toda minha família pelo suporte que recebi nesse período.

Aos professores Arno e Fabiano pela orientação dada a mim durante esses anos de pesquisa, que possibilitou a realização desta tese.

Agradeço à UFRGS, ao PPGE3M e à CAPES pela bolsa de doutorado concedida.

RESUMO

A energia solar fotovoltaica (FV) é a principal fonte utilizada em geração distribuída no Brasil. Esses sistemas FV, principalmente em região urbana, são mais suscetíveis a sombreamentos causados por elementos do entorno. Nesse contexto, o conhecimento dos efeitos do sombreamento parcial e uma modelagem precisa dos módulos FV nessa condição são imprescindíveis. Esta tese teve o objetivo de propor aperfeiçoamentos na modelagem da operação de instalações FV com sombreamento parcial, sendo composta por três artigos científicos publicados em revistas internacionais. No primeiro artigo, foi proposta uma metodologia intuitiva e acessível para análise de sistemas FV parcialmente sombreados, que foi aplicada em um estudo sobre o efeito de diferentes padrões de sombreamento em um módulo FV e em uma análise das sombras de uma usina FV. Foram obtidos dados experimentais de um sistema FV que é sombreado parcialmente ao longo do dia, juntamente com dados de radiação solar e de temperatura no local. Esses dados foram utilizados para analisar, no segundo artigo publicado, a exatidão dos resultados obtidos utilizando diferentes modelos de sombreamento disponíveis nos programas PVSyst e SAM. A partir da análise dos dados medidos, também foi proposta, no terceiro artigo, uma melhoria a um método simplificado de cálculo da energia elétrica produzida por sistemas FV parcialmente sombreados usando um fator de sombreamento difuso. No mesmo artigo, foram analisados os efeitos de diferentes configurações de sombreamento em curvas I-V medidas em um simulador solar. Então, foi proposto um método simplificado de modelagem de curvas I-V de módulos FV nessas condições. No PVSyst e no SAM, as diferenças entre a energia elétrica medida e a simulada variaram de acordo com o modelo de sombreamento escolhido e chegaram a cerca de 20% usando alguns modelos de cálculo. Em relação à modelagem de curvas I-V, a metodologia proposta apresentou vantagens em comparação às outras analisadas, em questão de facilidade de aplicação e precisão dos resultados, principalmente quando os submódulos não são sombreados uniformemente. O uso de um fator de sombreamento difuso para estimativa da eletricidade produzida levou a resultados significativamente mais precisos, sendo a diferença entre a energia elétrica medida e simulada de até 5% quando usada uma base de dados mensal. Concluiu-se que os métodos propostos para a modelagem de curvas I-V e de cálculo simplificado da energia produzida apresentaram vantagem em questão de precisão e simplicidade.

Palavras chave: Fotovoltaico. Sombreamento. Modelagem.

ABSTRACT

Photovoltaic solar energy (PV) is the main source used in distributed generation in Brazil. These PV systems, especially in urban regions, are more susceptible to shading caused by surrounding elements. In this context, the knowledge of the effects of partial shading and accurate modeling of PV modules in this condition are essential. This thesis aimed to propose improvements in modeling the operation of PV installations with partial shading, consisting of three scientific articles published in international journals. In the first article, an intuitive and accessible methodology for analyzing partially shaded PV systems was proposed, which was applied in a study on the effect of different shading patterns on a PV module and in an analysis of shadows on a PV plant. Experimental data were obtained from a PV system that is partially shaded throughout the day, in addition to solar radiation and temperature data measured on site. These data were used to analyze, in the second published article, the accuracy of the results obtained using different shading models available in the PVSyst and SAM programs. Based on the analysis of the measured data, an improvement to a simplified method for calculating the electrical energy produced by partially shaded PV systems using a diffuse shading factor was also proposed in the third article. In the same article, the effects of different shading configurations on I-V curves measured in a solar simulator were analyzed. Therefore, a simplified method for modeling I-V curves of PV modules under these conditions was proposed. In PVSyst and SAM, the differences between measured and simulated electrical energy varied according to the chosen shading model and reached around 20% using some calculation models. Regarding the modeling of I-V curves, the proposed methodology presented advantages compared to the others analyzed, in terms of ease of application and accuracy of results, especially when the submodules are not shaded uniformly. The use of a diffuse shading factor to estimate the electricity produced led to significantly more accurate results, with the difference between measured and simulated electrical energy being up to 5% when using a monthly database. It was concluded that the proposed methods for modeling I-V curves and simplified calculation of the energy produced presented advantages in terms of precision and simplicity.

Keywords: Photovoltaic. Shading. Modeling.

LISTA DE FIGURAS

LISTA DE TABELAS

SUMÁRIO

1 INTRODUÇÃO

A energia solar fotovoltaica (FV) tem ganhado cada vez mais destaque no mundo, conforme pode ser verificado na Figura 1, que apresenta a evolução da capacidade global instalada de energia solar FV de 2013 a 2022. A expansão de fontes renováveis em 2022 foi liderada pela energia solar FV, correspondendo a 65% da potência instalada no ano. A potência de usinas FV alcançou 1,046 TW em 2022, tendo um crescimento de 22% em relação ao ano de 2021 (IRENA, 2023). Em comparação às demais fontes renováveis, a energia solar apresenta 31% da capacidade mundial de produção e é a segunda fonte com maior participação atualmente, como pode ser visto na Figura 2. Ressalta-se que 99% da capacidade de produção da fonte solar é fotovoltaica.

As fontes renováveis de energia correspondem a cerca de 85% da potência de geração centralizada e distribuída no Brasil, conforme pode ser visto na Figura 3 (ANEEL, 2023a, 2023b). Assim como no mundo, a fonte hídrica é a fonte renovável com maior participação no Brasil, correspondendo a cerca de 50% da capacidade de produção brasileira. A fonte solar apresenta a segunda maior parcela de participação, com cerca de 15% da potência instalada no Brasil atualmente.

Figura 1 – Potência instalada de energia solar FV no mundo.

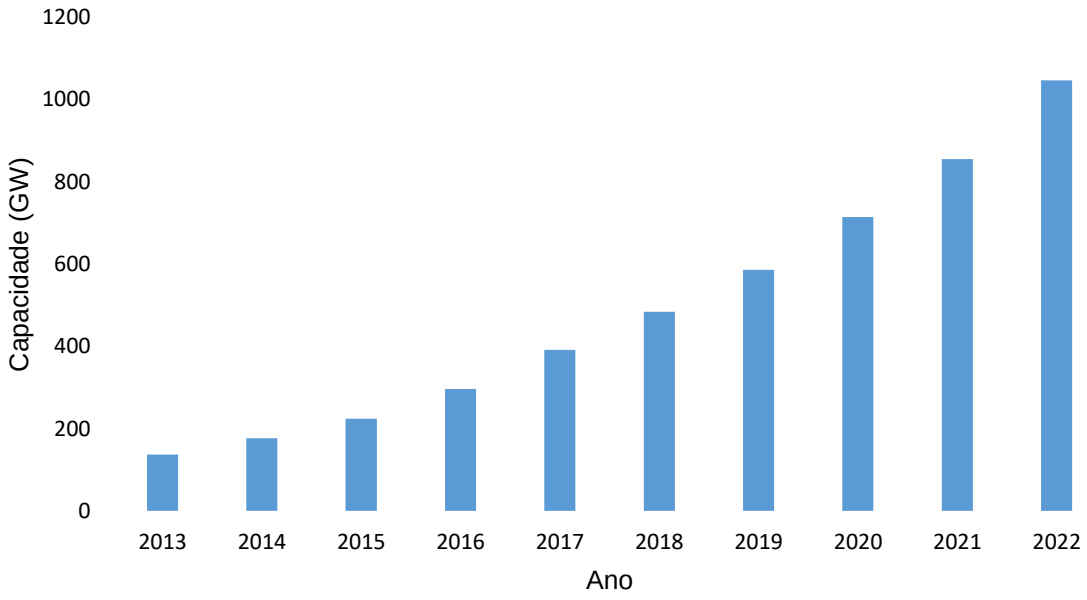

Fonte: IRENA (2023).

Figura 2 – Capacidade mundial de produção renovável por fonte no ano de 2022.

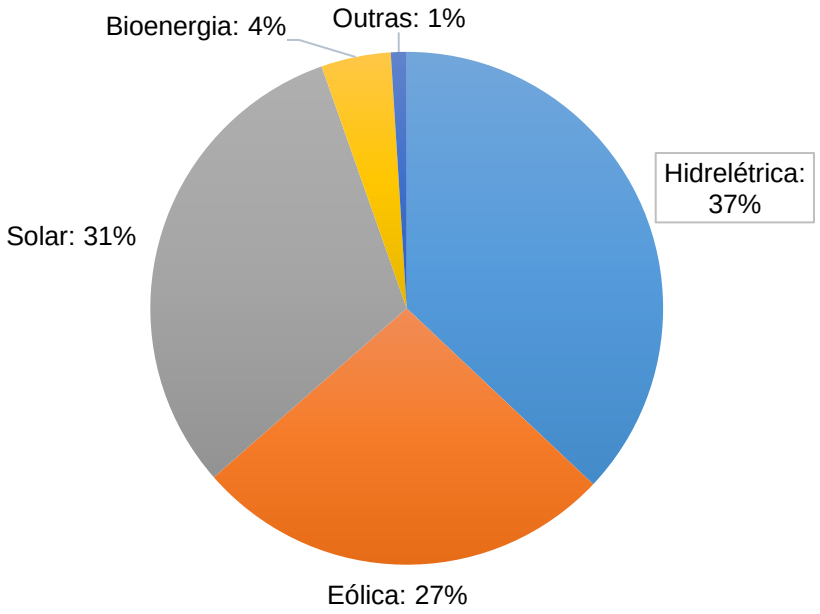

Fonte: IRENA (2023).

Figura 3 – Potência de geração centralizada e distribuída por fonte no Brasil.

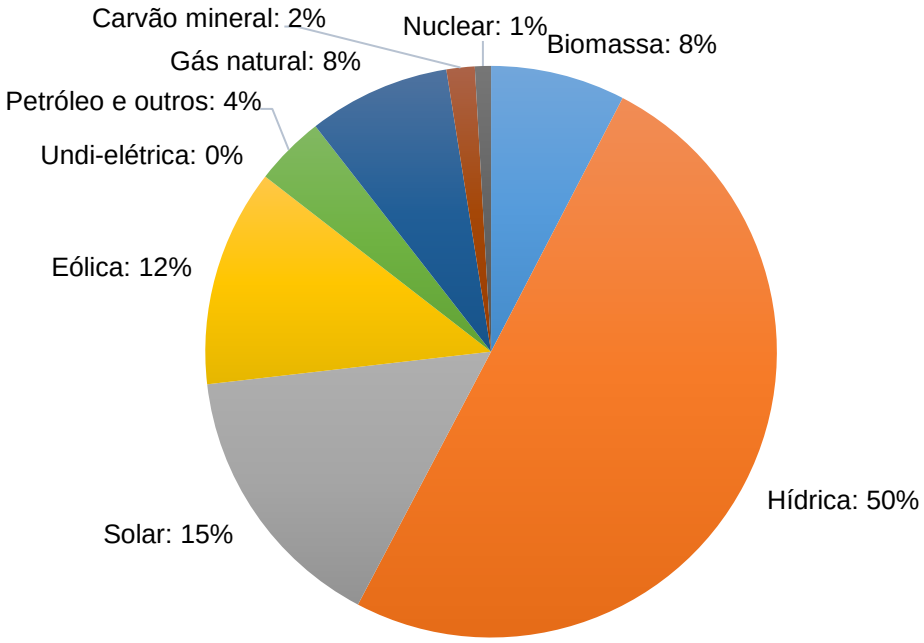

Fonte: ANEEL (2023a, 2023b).

Em geração distribuída (GD), o Brasil alcançou cerca de 23,5 GW de potência instalada até setembro de 2023, sendo 99% de fonte solar (ANEEL, 2023a). Portanto, a fonte solar é fundamental no contexto de GD no Brasil. A Figura 4 apresenta a

distribuição dos sistemas FV em GD por classe de consumo, de acordo com os dados da ANEEL (2023a). Cerca da metade da potência instalada dos sistemas FV de GD corresponde somente à classe residencial, enquanto que as classes comercial e rural somam 43% da potência instalada.

Figura 4 – Distribuição de sistemas FV em GD por classe de consumo no Brasil.

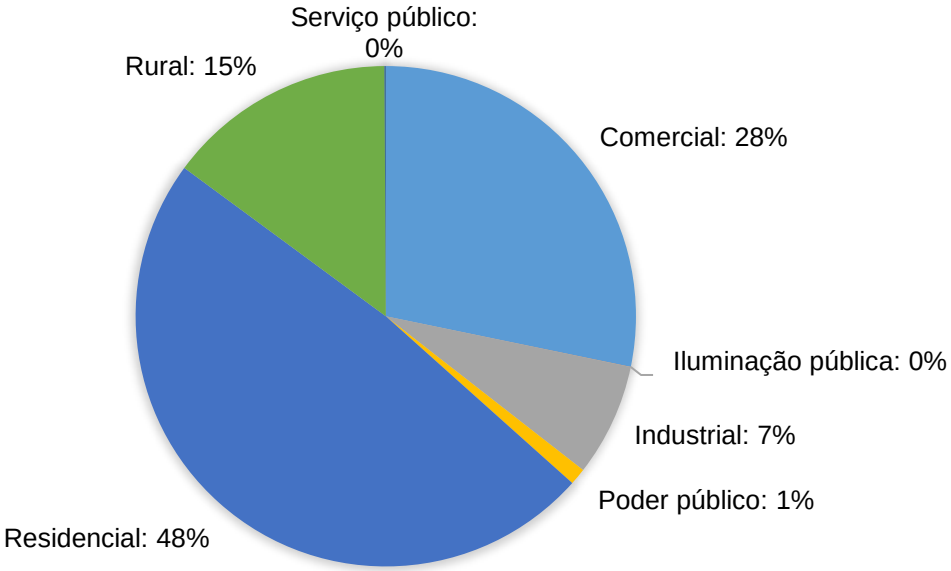

Fonte: ANEEL (2023a).

Diversos fatores influenciam o desempenho de sistemas FV, tais como o ângulo de inclinação e o azimute dos módulos FV, a poeira acumulada sobre os módulos e o sombreamento parcial. Sistemas FV de GD são, geralmente, instalados no telhado de uma edificação ou no solo. Muitos desses sistemas estão localizados em região urbana, estando mais suscetíveis a sombreamentos causados por elementos do entorno, tais como edificações vizinhas, vegetação próxima e elementos construtivos da própria edificação. Os efeitos do sombreamento parcial dependem de diversos fatores, como o número e a distribuição dos diodos de desvio (*bypass*), o número de células FV sombreadas e a fração de sombreamento das células em um módulo FV, por exemplo (DOLARA et al., 2013; TRZMIEL; GŁUCHY; KURZ, 2020).

Projetistas de sistemas FV comumente utilizam *softwares* comerciais para realizar o dimensionamento e a estimativa da energia produzida por esses sistemas, além da análise financeira. Wijeratne *et al*. (2019) analisaram e compararam diversas ferramentas computacionais disponíveis para projeto FV, listando vantagens e

desvantagens. Muitas dessas ferramentas apresentam opções de modelos simples para cálculo de sombreamento, uma vez que quanto mais detalhada é a análise de sombreamento, mais informações de entrada são necessárias e maior tempo de simulação é demandado. Além disso, algumas apresentam diferentes opções de cálculo de sombreamento disponíveis para escolha do usuário (MACALPINE; DELINE, 2015; MERMOUD; LEJEUNE, 2010). Rigo *et al*. (2022) realizaram uma pesquisa com 548 empresas brasileiras que trabalhavam com instalação fotovoltaica, distribuídas nas cinco regiões do país. Embora as perdas causadas pelo sombreamento parcial possam impactar significativamente o desempenho do sistema FV, eles verificaram que cerca de 25% dessas empresas não realizavam o serviço de análise de sombreamento.

As perdas por sombreamento em um sistema FV podem ser estimadas por meio de equações simplificadas de energia (MARTÍNEZ-MORENO; MUÑOZ; LORENZO, 2010). Por outro lado, uma análise mais detalhada dos efeitos do sombreamento costuma ser importante em alguns casos, sendo de interesse acadêmico principalmente. Para isso, as curvas I-V e P-V de um módulo ou sistema FV sombreado podem ser medidas ou simuladas (AYOP *et al*., 2020; HANIFI *et al*., 2019). A complexidade das análises aumenta de acordo com o nível de detalhamento da modelagem.

Nesse contexto, podem-se verificar algumas questões em relação à modelagem de sistemas FV parcialmente sombreados que este trabalho tem como foco. Existem programas comerciais que auxiliam na etapa de projeto FV, porém faltam metodologias para analisar as perdas por sombreamento de um sistema FV de maneira intuitiva e utilizando ferramentas disponíveis a todos. Além disso, a exatidão dos resultados simulados por programas da área de energia solar e quais modelos utilizados são mais precisos não são informações amplamente difundidas. A simulação de curvas I-V de módulos FV sombreados nem sempre é uma tarefa simples e precisa, portanto é importante haver um método simples e preciso para o cálculo das curvas I-V nessas condições. Por outro lado, os métodos simplificados de cálculo da energia produzida por sistemas FV parcialmente sombreados levam em consideração as perdas na radiação solar direta, negligenciando as perdas na radiação solar difusa, como o proposto por Martínez-Moreno, Muñoz e Lorenzo (2010), o que pode levar a importantes diferenças em comparação a dados medidos.

Esta tese visa preencher as lacunas discutidas e é composta por três artigos publicados.

1.1 Objetivo Geral

O objetivo geral desta tese é propor melhorias na modelagem da operação de instalações FV parcialmente sombreadas.

1.2 Objetivos Específicos

Os objetivos específicos do trabalho são:

a) desenvolver uma metodologia intuitiva para analisar sistemas FV parcialmente sombreados;
b) analisar a exatidão dos cálculos de sombreamento realizados por programas computacionais da área de energia solar;
c) propor uma metodologia simples e precisa para modelar curvas I-V de módulos FV parcialmente sombreados;
d) propor uma melhoria a um método simplificado de cálculo da energia produzida por sistemas FV parcialmente sombreados.

1.3 Estrutura da tese

A seção 2 desta tese apresenta os três artigos publicados. Na seção 3, é discutida a integração dos artigos publicados. As conclusões são analisadas na seção 4.

2 ARTIGOS PUBLICADOS

O primeiro artigo, intitulado "*A methodology for prediction and assessment of shading on PV systems*" (CHEPP; KRENZINGER, 2021), teve o objetivo de propor uma metodologia intuitiva e acessível para estimar perdas por sombreamento em instalações FV. A metodologia proposta foi desenvolvida na dissertação de mestrado da autora (CHEPP, 2018). Durante o doutorado, foi dada continuidade à pesquisa, que compreendeu uma extensa revisão da literatura da área, descrição da metodologia de forma mais detalhada e melhoria nos resultados, além da elaboração do artigo científico para publicação.

O segundo artigo, intitulado "*Accuracy investigation in the modeling of partially shaded photovoltaic systems*" (CHEPP; GASPARIN; KRENZINGER, 2021), teve o objetivo de analisar a exatidão dos resultados simulados por programas computacionais de um sistema FV parcialmente sombreado. Para isso, foram comparados dados experimentais de um sistema FV instalado no Laboratório de Energia Solar (LABSOL) da Universidade Federal do Rio Grande do Sul (UFRGS) com os resultados simulados para esse sistema utilizando os programas PVsyst e *System Advisor Model* (SAM). Foram comparados os diferentes modelos de cálculo de sombreamento disponíveis nos programas.

O terceiro artigo, "*Improvements in methods for analysis of partially shaded PV modules*" (CHEPP; GASPARIN; KRENZINGER, 2022), propôs uma metodologia para obtenção de curvas I-V de módulos FV parcialmente sombreados e uma melhoria em um método simplificado para estimativa da energia elétrica produzida por sistemas FV parcialmente sombreados. Foram medidas curvas I-V de módulos FV em diferentes condições de sombreamento parcial em um simulador solar. As curvas I-V foram analisadas e comparadas com curvas simuladas utilizando o método de modelagem proposto e outros dois métodos da literatura. Além disso, dados experimentais de potência do sistema FV parcialmente sombreado instalado no LABSOL foram comparados com os resultados estimados utilizando métodos simplificados encontrados na literatura e com a melhoria proposta no artigo.

Os artigos publicados estão listados na Tabela 1 e estão apresentados nesta seção de acordo com a ordem de publicação.

Tabela 1 – Dados dos artigos publicados (dados referentes ao ano de 2023).

Nº	Título do artigo	Ano de publicação	Revista			
			Nome	**Qualis**	***Impact Factor***	***CiteScore***
1	*A methodology for prediction and assessment of shading on PV systems*	2021	*Solar Energy*	A1	6,7	13,1
	https://doi.org/10.1016/j.solener.2021.01.002 https://www.sciencedirect.com/science/article/abs/pii/S0038092X21000050					
2	*Accuracy investigation in the modeling of partially shaded photovoltaic systems*	2021	*Solar Energy*	A1	6,7	13,1
	https://doi.org/10.1016/j.solener.2021.05.061 https://www.sciencedirect.com/science/article/pii/S0038092X2100431X					
3	*Improvements in methods for analysis of partially shaded PV modules*	2022	*Renewable Energy*	A1	8,7	16,1
	https://doi.org/10.1016/j.renene.2022.10.035 https://www.sciencedirect.com/science/article/pii/S0960148122015282					

Solar Energy 216 (2021) 537–550

Contents lists available at ScienceDirect

Solar Energy

journal homepage: www.elsevier.com/locate/solener

A methodology for prediction and assessment of shading on PV systems

Ellen David Chepp *, Arno Krenzinger

Universidade Federal do Rio Grande do Sul, Solar Energy Laboratory, Av. Bento Gonçalves, 9500, Agronomia, Porto Alegre, Rio Grande do Sul, Brazil

ARTICLE INFO

Keywords:
Photovoltaic
Losses
Partial Shading
Shading Effect
Power Output
Shadow prediction

ABSTRACT

Frequently, PV systems are affected by dirt, dust or shadowing from surrounding elements, such as trees and buildings. The shadows can cause partial shading conditions, when the irradiance is not uniform on PV installation, which lead to losses of power. Thus, the shadow prediction is primordial for a better output power estimation and to minimize its losses. The aim of this article is to propose a methodology using intuitive and available tools for shading prediction and losses assessment on PV installations. A study about the shadow pattern and module orientation (portrait and landscape) influence and an analysis of the shading losses on a PV plant were performed in order to demonstrate the applicability of the methodology. The shading effect is drastic when the shading is parallel to the short edge, whereas the effect is lower when it is parallel to the long edge. On the other hand, the losses due to shading and the difference in the position of the modules (landscape or portrait) have a lower impact on the photovoltaic plant case. It was concluded that the methodology is feasible and applicable for shading impact evaluation, despite limitations for large systems due to the simulation time.

1. Introduction

The output power of photovoltaic (PV) modules depends on the solar irradiance and cell temperature conditions. When a PV system is under uniform irradiance conditions, the electricity generated by each module is similar, thus the overall output power is the sum of modules power individually. On the other hand, the irradiance is non-uniform if the system is partially shaded, which lead to power losses. The partial shading can be caused by dirt and surrounding elements such as vegetation (trees) and neighbor buildings. Others conditions affect the PV system performance, such as wind, tilt angle and dust, which can also lead to partial shading sometimes (Zaihidee et al., 2016; Wang et al., 2017; Said et al., 2018; Babatunde et al., 2018; Maghami et al., 2016).

The assessment of shadows on PV system is important in order to avoid or reduce the effects and to improve the production estimation and performance (Rachchh et al., 2016). The first step for that assessment is the prediction of shadows on the PV installation, which is indispensable in order to know the shadow pattern and avoid the shading. In this step, the user can use 3D models of the PV installation and the neighbor and verify the shadings on system using drawing software. Some commercial software for photovoltaic design have shadings tools, and the user can draw or import a 3D model. After this, the shading fraction and the output power need to be estimated. The most of the works found in the literature are focused on methodologies for shading fraction estimation, for maximum power point tracking, to estimate and detect shading and to reconfigure the module, array and inverter to minimize these effects (Liu et al. 2015; Jordehi, 2016).

Methodologies for prediction of shading and shading fraction estimation have been proposed, such as SOMBRERO (Niewienda and Heidt, 1996) and SHADING (Shaviv and Yezioro, 1997). Sinapis et al. (2016) developed a yield model, which considered the shading effect. Regarding the shading prediction, an accurate representation of the installation and the obstruction elements was done in SketchUp and a Python script was developed to calculate a shading table for any given azimuth and elevation angle of the sun. The PV cell was modeled with a simplified double diode model. Melo et al. (2013) proposed a methodology to calculate the shading fraction and irradiation in a three-dimensional model, and developed a plug-in for SketchUp to test the methodology.

The impact of the PV module reconfiguration on energy and cost was analyzed by Baka et al. (2019) for three situations with different shadow patterns. They analyzed the conventional topology and two snake topologies: U-type and I-type. Under partial shading conditions, both topologies affect into energy gain; however, there are additional costs due the module reconfiguration. Thus, they concluded that the cost-benefit of the module reconfiguration is advantageous only for installations under partial shading conditions and depends on others factors such as the energy gain, location of the installation and price of electricity.

* Corresponding author.
E-mail address: ellen.chepp@gmail.com (E.D. Chepp).

https://doi.org/10.1016/j.solener.2021.01.002
Received 11 August 2020; Received in revised form 29 December 2020; Accepted 2 January 2021
Available online 6 February 2021

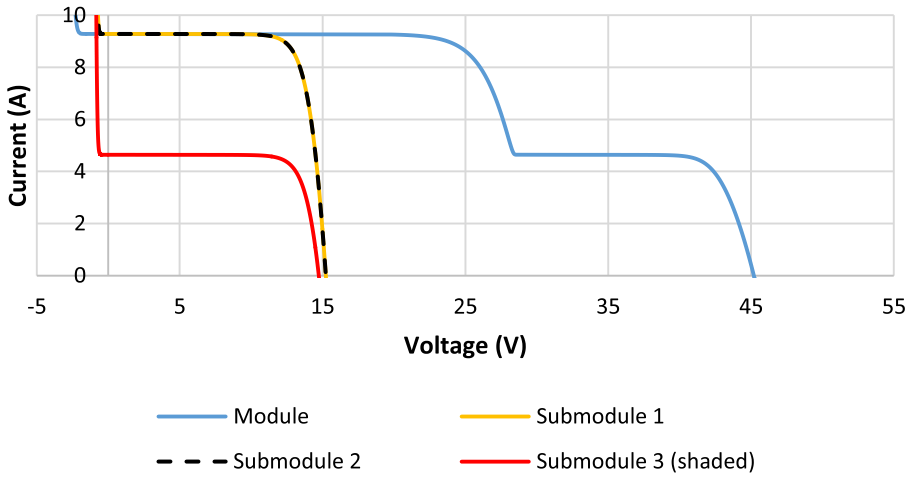

Fig. 1. Submodules and module I-V curves.

Moreover, the modification of the module configuration from series to parallel cells connections leads to lower shading losses (Lu et al., 2013). Furthermore, one bypass diode is connected in anti-parallel to a group of series cells conventionally, however modifications of the bypass circuit are also proposed in literature (Ghosh et al., 2019; Daliento et al., 2016).

In the array level, Tubniyom et al. (2018) studied the shading impact for three array configurations (3 × 3 array) under partial shading conditions using Matlab/Simulink: series–parallel (SP), bridge-linked (BL) and total cross-tied (TCT). They verified that the configurations BL and TCT were more suitable when the shaded area of module is less than 50%. These configurations increased the power up to 5% if the shading is greater. Belhachat and Larbes (2015) confirmed the shading losses depend on the configuration and shadow pattern. In their analysis, a comparison between S, P, SP, BL, TCT and Honey-Comb (HC) configurations (6 × 4 array) for different shadow patterns was performed, and the TCT configuration presented best performance (highest output power) when the system was shaded: (1) partially and unevenly, (2) completely and unevenly and (3) on the same row or column of array for high irradiance.

Reconfiguration techniques attempt to reduce the shading impacts through static or dynamic reconfiguration of PV array. In the dynamic reconfigurations, the electrical connections are altered, whereas the physical location is changed in the static techniques (Krishna and Moger, 2019a). In the literature, the improvement and comparison of the array reconfigurations techniques have been widely studied (Krishna and Moger, 2019b; Dhanalakshmi and Rajasekar, 2018; Yadav and Mukherjee, 2018; Iysaouy et al., 2019; El-Dein and Kazerani, 2013; Satpathy and Sharma, 2019; Tatabhatla et al., 2019; Deshkar et al., 2015). Krishna and Moger (2019a) presented a review about these strategies of reconfiguration, and a conclusion of this was that the dynamic techniques are more effective than static for improvement of the output power in partial shading conditions, despite being relatively expensive.

The inverter topology also influences the shadings losses, once the inverter is responsible for the Maximum Power Point Track (MPPT). Zheng et al. (2014) analyzed three inverters topologies (micro inverters, string inverter and central inverter) and the bypass diode configurations impact. The maximum power extraction without bypass diode was higher using micro inverter, whereas the central inverter leads to lower extraction. However, the central inverter became more efficient when the bypass diode is connected to cells groups. Ramli and Salam (2019) evaluated PV system under partial shadings with modules with dc power optimizer (DCPO), in the other words, a dc-dc converter with MPPT, and modules with dc-dc converter had higher output power compared to modules with bypass diode only. The conventional MPPT methods can fail in global maximum power point tracking because of the multiple local peaks in P-V curve. The most popular and used algorithm is the Perturb and Observe (P&O), which calculates the power and introduces perturbations in voltage based on the change of the power. In case of small voltage sweeps, this method can cause the system to have the power stuck in one of the peaks of the characteristic curve. Different MPPT methods have been proposed in the literature (Ahmed and Salam, 2014; Ram et al., 2017; Rezk et al., 2017).

Salem and Awadallah (2016) proposed a methodology for detection and assessment of shading conditions using artificial neural network. The partial shading condition could be detected, so the shading factor and number of shaded modules were determined using the methodology. Chaibi et al. (2019) developed a method to detect and diagnose failures and partial shading introducing three indicators (for voltage, current and power). Zhu et al. (2019) proposed a simplified model that compares the shaded cell area with I-V and P-V curves. Using this model, simulations in MATLAB were performed considering two situations: the shadow parallel to the long edge and parallel to the short edge. The shading effect had greater impact when the shadow reached parallel to the short edge, owing to simultaneous conduction of the three bypass diodes.

Shading effects on I-V curve behavior are also widely studied. Ahmad et al. (2017) analyzed the PV array under different partial shading patterns in order to guide researchers to explore these effects. Gallardo-Saaverda and Karlssom (2018) also studied different configurations of shading impact; however, these authors used a simulation program and validated the model with experimental analysis. The effect of different fraction of shading and number of shaded cells for the same diode and different diode were analyzed. These authors verified that: (1) when only one cell is shaded, a reduction of the maximum power occurs and a step in the I-V curve appears; (2) the effect will be independent of the number of shaded cells if there are more than one cell in same bypass diode with the same shaded area, however the curves will change if the shaded cells correspond to different bypass diode; (3) the current will be the same and the bypass diode will not be working when the shading configuration is the same for all bypass diode circuits; (4) and the curve has different steps when have different shading configuration on circuits.

This work does not focus on the minimization of the shading losses neither on the simulation nor estimation of power losses as some works cited. Most research focuses on just one aspect of the shading analysis, such as estimating the shading fraction or simulating the I-V curve. There is a lack of articles that propose methodologies that covers all stages from shading prediction to output power, using available and intuitive tools. In view of that, the aim of this article is to propose a methodology with intuitive tools, using software available to anybody for the prediction and evaluation of shading losses. The difference of this

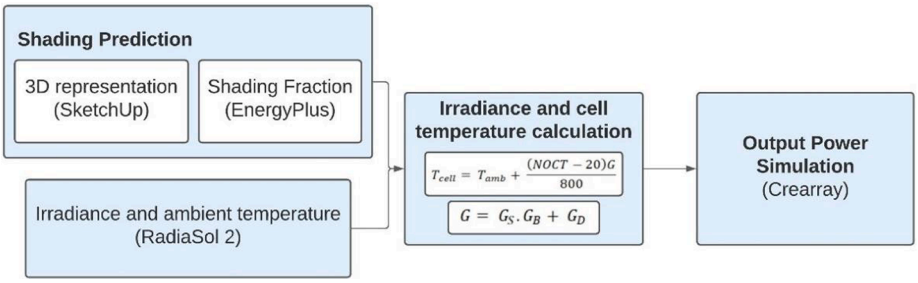

Fig. 2. Schematic diagram for the proposed methodology.

methodology, in comparison to the others, is that it makes it possible to view shadings, evaluate the shading fraction and estimate the output power of the installation under partial shading conditions.

The proposed methodology was demonstrated by studying the impact of different shadow patterns on a module. Shading losses in a photovoltaic plant located in Brazil and the impact for different module positions were also analyzed. Computer simulations were carried out, experimental analysis are not part of the scope of this article. The methodology is useful for shaded photovoltaic systems analysis; however, it has limitations for large systems, due to the simulation time.

In Section 2 of this article, the shading losses on a module are discussed. Then the methodology is proposed (Section 3) and its applicability is demonstrated for a study and a PV plant case (Section 4). Lastly, the main conclusions are presented in Section 5.

2. Shading effects

Since series connected cells have the same current, the current of all cells will be limited if one cell be shaded. Therefore, when at least one cell is shaded, the current of all series cells will be the same of the shaded cell (lowest current). The shaded cell starts to dissipate power and heat, which can lead to hotspot phenomenon. In order to avoid these losses, bypass diodes are connected in antiparallel to series cells groups, thus these diodes operate as an alternative way to current when the irradiance conditions are non-uniform (partial shading).

A module with 60 cells in series has three bypass diodes usually; each one is connected to 20 series cells. In partial shading condition, the overall module current is the sum of the current passing through the series cells and bypassed by diode, and the I-V curve presents multiple local MPP (maximum power points). In this sense, each section of a module with series cells and one bypass diode can be called a submodule, and a module can be seen as its submodules in series. Fig. 1 shows the shading effect on each submodule and the whole PV module I-V curves.

3. Materials and methods

The irradiance, temperature and system parameters are inputs to simulate the PV system power. Considering the irradiance is not uniform in partial shading conditions, it is necessary estimate the fraction of shaded area to simulate this behavior. In order to analyze the shading effect, each module should be divided into submodules according to bypass diodes, in other words, each submodule corresponds to a section with series cells and bypass diode connected in antiparallel. Since the most shaded cell will present the lowest current of submodule, the current of series cells is limited by this lowest current, so the most shaded cell will represent the whole submodule current.

Considering a module with all cells in series, the submodule open circuit and maximum power voltage are obtained by these parameters of the module divided by the number of submodules. On the other hand, the short circuit and maximum power current of the submodule are equal to these parameters of the module.

After that, the methodology proposed consists in three steps: (1) geometric representation and shadow prediction, (2) cell irradiance and temperature computation and (3) PV electric power estimation. The methodology scheme is shown in Fig. 2.

3.1. Geometric representation and shadow prediction

The first step of the methodology is the geometric representation and shadows prediction. SketchUp was chosen for this step, the drawing software has a shadow tool that permits a visual verification of the shading caused by surrounding elements on the external surfaces for a given date and time (Hernández-Callejo et al., 2019; Rodrigues et al., 2015).

The estimation of each cell shaded area can be visual or using the software EnergyPlus, for more precision and to automate the process. The second option makes it possible to perform the analysis for longer time interval and more complex systems. EnergyPlus is a program funded by the U.S. Department of Energy developed for energetic simulation of buildings and has the option “surface outside face sunlit fraction”, that evaluates the area fraction of external surfaces that receive beam radiation and saves the results in an output file. The software uses Polygon clipping based methods and solar position equations for sunlit area calculation (EnergyPlus, 2016; Rocha et al., 2017).

3.2. Irradiance and temperature computation

Considering that the modules in the PV systems are generally tilted, the irradiance incident on the tilted plane is an essential data. The Solar Energy Laboratory (LABSOL) of Universidade Federal do Rio Grande do Sul – UFRGS (Brazil) developed the software RadiaSol 2 (available for download on the laboratory’s web page: solar.ufrgs.br/#radiasol), which calculates the irradiance incident (beam, diffuse and global) for any tilt and azimuth deviation chosen by the user. Furthermore, the software has the capability of synthesizing hourly solar tilted radiation and ambient temperature data for Brazilian cities. The presented methodology can be applied using any source of meteorological data from that one can extract both hourly tilted radiation and ambient temperature. The calculation is based on Aguiar et al. (1988), Collares-pereira and Rabl (1979), Erbs et al. (1982) and Perez and Seals (1987) methods.

The most shaded cell receives less irradiance than others cells because the shaded area does not receive the beam irradiance (only the diffuse is incident).Therefore, the smallest fraction sunlit area of each submodule corresponds to the most shaded cell which will represent whole submodule. Thus, the submodule irradiance is calculated by Eq. (1), considering that G is the submodule irradiance, F_S is the shading fraction of most shaded cell (0 for completely shaded and 1 for non-shaded), G_B is the beam irradiance and G_D is the diffuse irradiance.

$$G = F_S.G_B + G_D \quad (1)$$

The cell temperature is calculated according to Eq. (2) (Ross and Smokler, 1986). NOCT, T_{amb} and T_{cel} are the Nominal Operation Cell Temperature, the ambient temperature and the cell temperature,

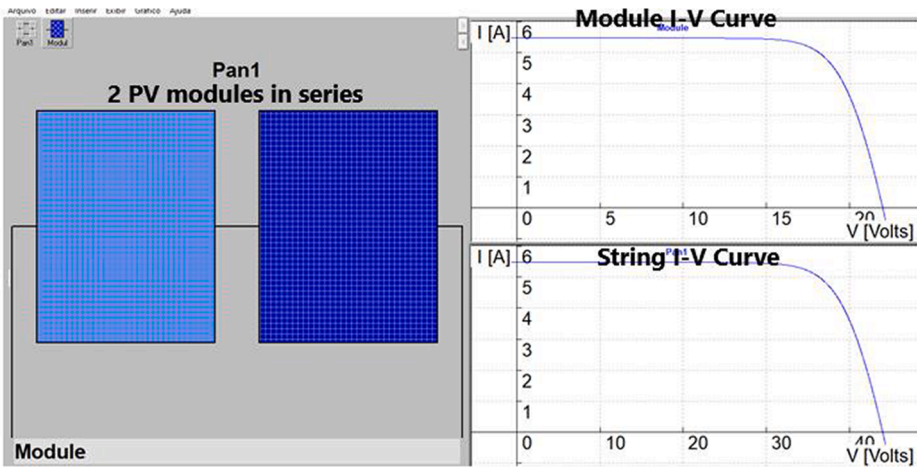

Fig. 3. I-V curves generated by Crearray.

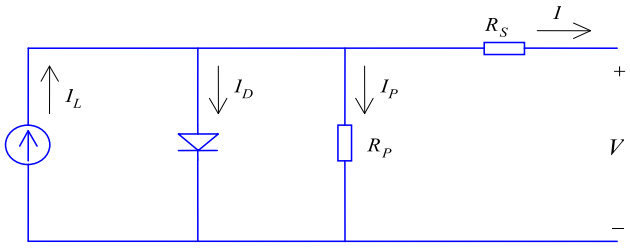

Fig. 4. Representation of one diode model.

respectively. The shaded cell heating was not considered in order to simplify the calculation.

$$T_{cel} = T_{amb} + \frac{(NOCT - 20)G}{800} \tag{2}$$

3.3. Output power estimation

The last step is the estimation of PV system electric power. The I-V curve is drawn and the maximum power point is obtained for each irradiance and temperature condition. The software Crearray, also developed at LABSOL, simulates the PV systems behavior and simulates the I-V curve for modules or cells arrays. The user adds modules or cells in series or parallel and the I-V curve is estimated from the irradiance and temperature data and electric parameters. An example of I-V curves of one module and string are seen in Fig. 3.

In the early versions, only catalog data from the modules were used in the software. However, the software has had some improvements and is in the third version developed. In this version, data from experimentally measured modules were inserted, in addition to the possibility of inserting new modules in the catalog.

This software allows inputting a data file containing irradiance and temperature data, and then calculates the maximum power point for each condition or the current for a fixed voltage and saves the results in an output file.

In order to simulate the PV system behavior in partial shading conditions, each module is previously divided into submodules, which are added in series in Crearray with their irradiance and temperature conditions. Thus, the module is equivalent to its submodules in series.

The association behavior is computed by Crearray using a numerical method. Firstly, after the input parameters are saved, the software computes the I-V curve of the module or cell according to the one diode model, as seen in Fig. 4, where I_L is the current photogenerated, I_D is the diode current and R_S and R_P are the series and parallel resistances, respectively. Moreover, the device current (I) and voltage (V) are computed using Eqs. (3)–(6), where I_P is the parallel resistance current, V_j is the PN junction voltage, I_0 is the reverse saturation current of diode, n is the ideality factor of diode, k is Boltzmann constant, T is the cell absolute temperature and N_s is the number of cells associated in series. The current of parallel resistance is computed using Eq. (7).

In order to draw the I-V curve, the I_L, R_S, I_0 and n parameters are necessary to compute I and V by Eqs. (3) and (4) for a given irradiance and temperature condition. Through numerical methods is possible find the values of these parameters. Therefore, the results of Eq. (3) match the experimental results. Considering only positive voltages and I_L equal to short circuit current, Eq. (8) can demonstrate the open circuit condition, where V_{OC} is the open circuit voltage.

$$I = I_L - I_D - I_P \tag{3}$$

$$V = V_j - I.R_S \tag{4}$$

$$I_D = I_0\left[\exp\left(\frac{V_j}{V_t}\right) - 1\right] \tag{5}$$

$$V_t = N_s\frac{nkT}{q} \tag{6}$$

$$I_P = \frac{V_j}{R_P} \tag{7}$$

$$I_0 = \frac{I_{SC} - \frac{V_{OC}}{R_P}}{\exp\left(\frac{V_{OC}}{V_t}\right) - 1} \tag{8}$$

Moreover, the derivative from power in relation to the voltage is zero in the maximum power point, and then the Eq. (9) can be demonstrated. The Eq. (10) is the derivative of current with respect to voltage. Therefore, the Eq. (10) is substituted in Eq. (9) and it results in Eq. (11). Finally, Eq. (11) can be substituted in Eq. (3) resulting in Eq. (12).

$$\left.\frac{\partial I(V)}{\partial V}\right|_{V=Vm} = \frac{-I_{mp}}{V_{mp}} \tag{9}$$

$$\frac{\partial I(V)}{\partial V} = \frac{\frac{I_0}{V_t}\exp\left\{\frac{V+I(V)Rs}{V_t}\right\} + \frac{1}{R_P}}{\frac{-I_0R_S}{V_t}\exp\left\{\frac{V+I(V)Rs}{V_t}\right\} - \frac{R_S}{R_P} - 1} \tag{10}$$

$$R_P = \frac{V_{mp} - I_{mp}R_S}{\frac{I_0}{V_t}\left[\left(I_{mp}R_S - V_{mp}\right)\exp\left(\frac{V_{mp}+I_{mp}R_S}{V_t}\right)\right] + I_{mp}} \tag{11}$$

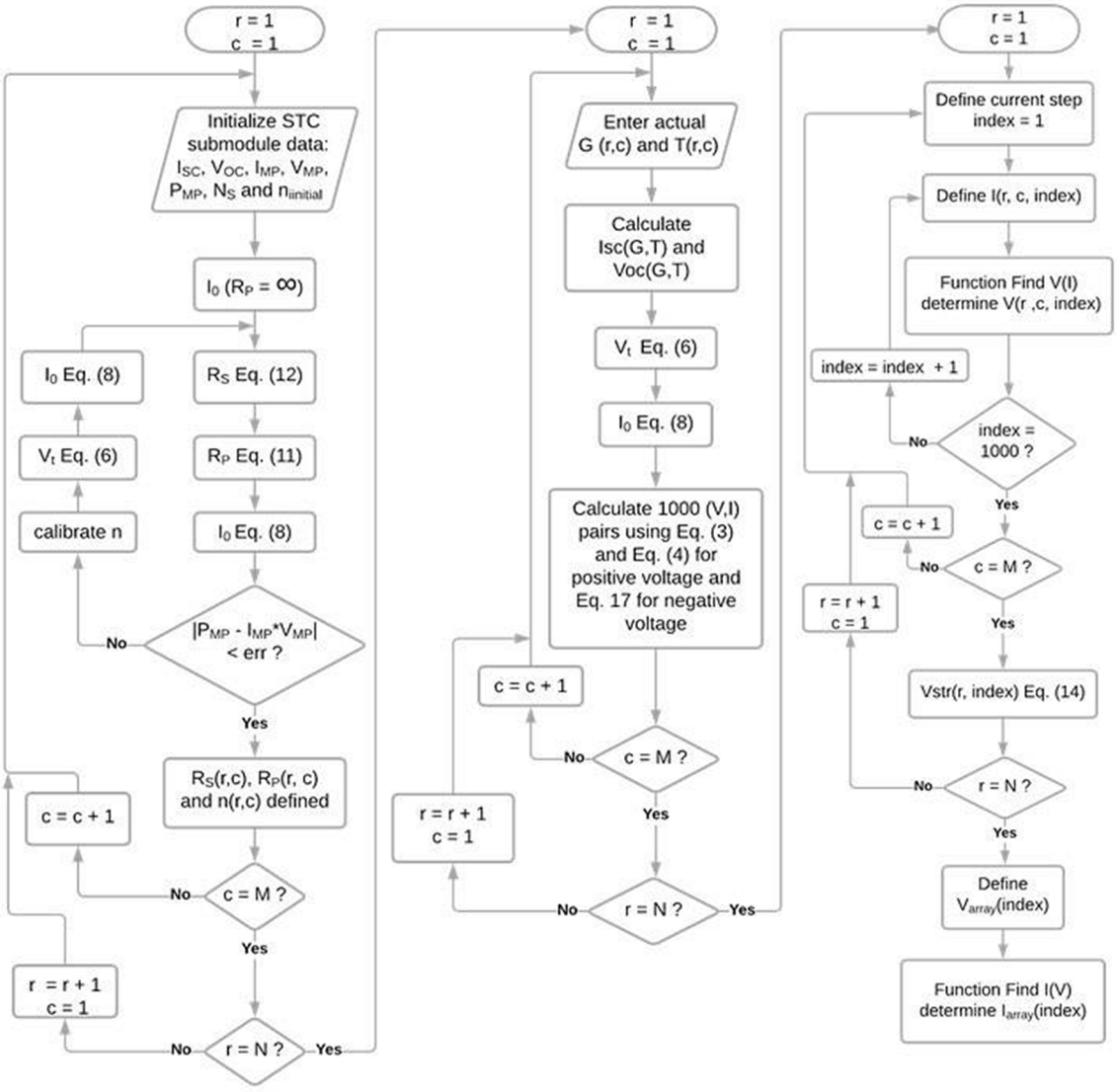

Fig. 5. Flowchart of the simulation.

$$R_S = \left\{ \frac{\left(\frac{V_{mp}}{I_{mp}}\right) - R_S}{\left[\frac{I_0}{V_t}\left(I_{mp}R_S\right)\right] \cdot \left[\exp\left(\frac{V_{mp}+I_{mp}\cdot R_S}{V_t}\right)\right] + I_{mp}} \right\} \cdot \left\{ I_L - I_{mp} - I_0 \cdot \left[\exp\left(\frac{V_{mp}+I_{mp}\cdot R_S}{V_t}\right) - 1\right] \right\} - \frac{V_{mp}}{I_{mp}} \quad (12)$$

Through an iterative process, the software considers the standard conditions firstly and, from the short circuit, open circuit and maximum power points, the R_S, R_P and n are computed. For that, Eqs. (8), (11) and (12) are repeated until the R_S, R_P and n values computed solve the Eq. (3) and the maximum power match the input. The negative voltage quadrant is solved using current values of the bypass diode.

When other temperature and irradiance condition are informed, new values of short circuit current and open circuit voltage are determined, however the R_S, R_P and n are kept invariable. The curve points (V, I) are computed using Eqs. (3) and (4).

The current of an association with N identical cells connected in series is the same of the one cell current, however the voltage increases N times. On the other hand, the current will be the same for whole string, even when the cells are not identical, and the voltage will be distributed. The association voltage will be the sum of individual voltages. Considering that voltages are function of current and the currents are function of voltage, the results can be computed using Eqs. (13) and (14).

$$\boldsymbol{I_{str}} = I_1(V_1) = I_2(V_2) = I_3(V_3) = \cdots = I_N(V_N) \quad (13)$$

$$\boldsymbol{V_{str}} = \sum_{i=1}^{N} \boldsymbol{V_i}(\boldsymbol{I_{str}}) \quad (14)$$

If M identical cells are connected in parallel, the voltage will be the

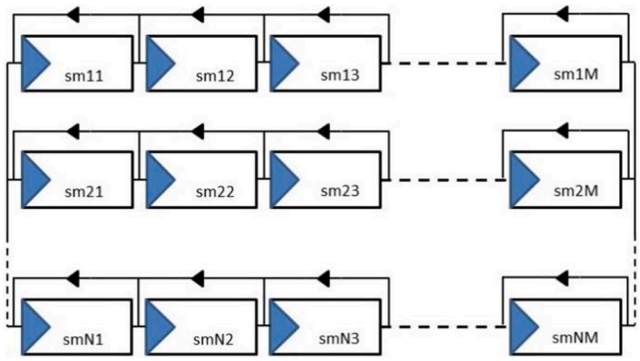

Fig. 6. Photovoltaic submodule array with N rows and M columns.

same of one cell and the current will increase M times. The behavior will be the same when the cells are not identical. The results can be computed using Eqs. (15) and (16).

$$V_{par} = V_1(I_1) = V_2(I_2) = V_3(I_3) = \cdots = V_M(I_M) \tag{15}$$

$$\boldsymbol{I_{par}} = \sum_{i=1}^{M} \boldsymbol{I_i}(\boldsymbol{V_{par}}) \tag{16}$$

From a set of points already computed and a polynomial interpolation, the software determinates a voltage as a function of a current or a current as a function of a voltage. Given a current I for which is required to find the voltage value V, the Find V(I) function search the first point of the set [Vp(j), Ip (j)] that fulfills the condition: Ip (j) > I. Then there are selected 3 points before and 3 points after the selected point and using this new set of 7 points it assembles a polynomial of degree 3 for interpolation. With this equation, the function finds the value of V for the given I. The same process is done to obtain the current as a function of the voltage. It is also possible input a set of points that was not calculated from the equations cited.

In view of the module can be divided into submodules, Crearray uses Eq. (17) to evaluate the reverse current for each submodule, where I_{OB} is the current of reverse saturation of bypass diode, V_B is the reverse voltage of submodule, n_b is the ideality factor of bypass diode and T_B is the temperature of bypass diode.

$$I = I_{SC} + I_{OB}\left[\exp\left(\frac{q(V_B)}{n_b k T_B}\right) - 1\right] \tag{17}$$

For example, if each photovoltaic module has 3 bypass diodes and 3 submodules, a string of 5 modules will be formed by 15 submodules in series, each with a particular irradiance and temperature. The irradiance considered for each submodule is the irradiance received by the photovoltaic cell that has the largest shadow coverage (minimum irradiance from the submodule). To determine the I-V curve, about 1000 current values are launched including negative values and values beyond the standard conditions short circuit current. For each current, the Find V(I) function determines the voltage of each element. The resulting voltage of the string is the sum of the voltages of each element. This procedure is repeated for all strings. In the next step, the characteristic curve of the array is calculated. For this, voltage values are launched from negative values to beyond the estimated standard condition open circuit voltage. Using the Find I(V) function for each voltage, a current value is found, thus forming the set of points that define the array characteristic curve. Fig. 5 shows the flowchart of Crearray simulation, and Fig. 6 shows a submodule array.

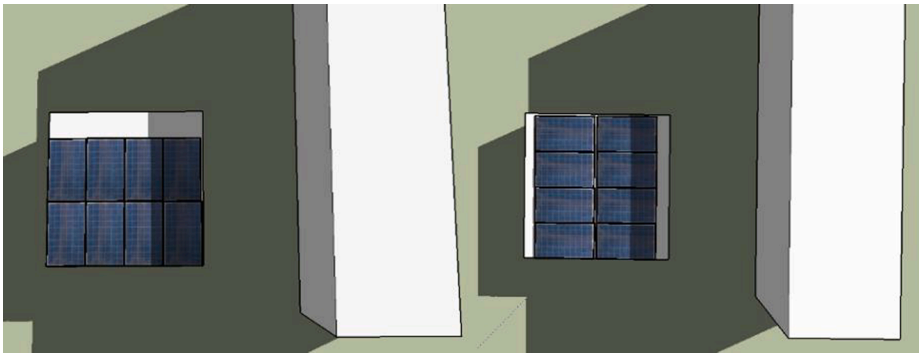

Fig. 7. Representation of two shadow patterns.

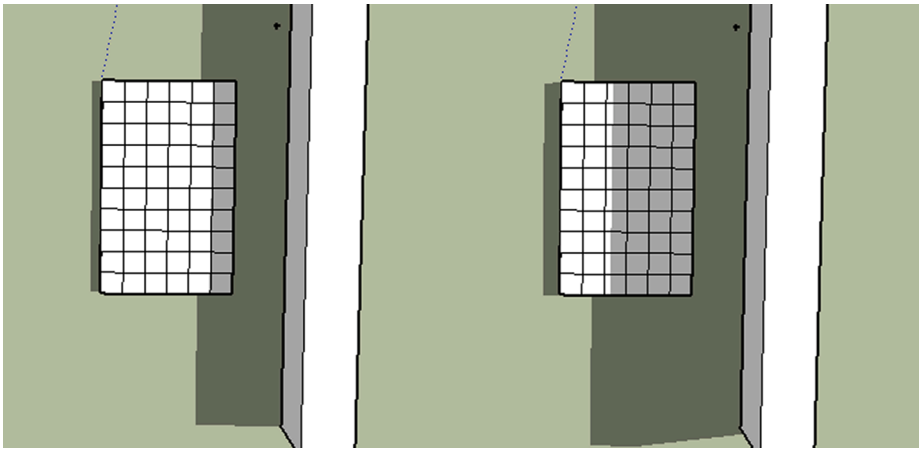

Fig. 8. Shadow parallel to the long edge (portrait orientation).

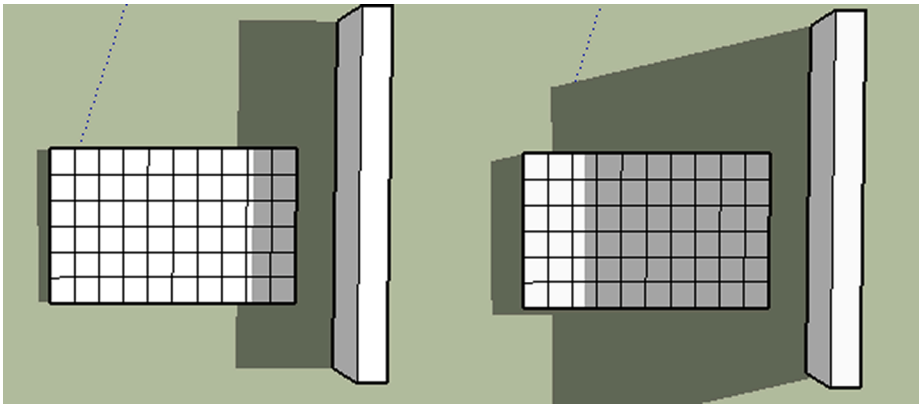

Fig. 9. Shadow parallel to the short edge (landscape orientation).

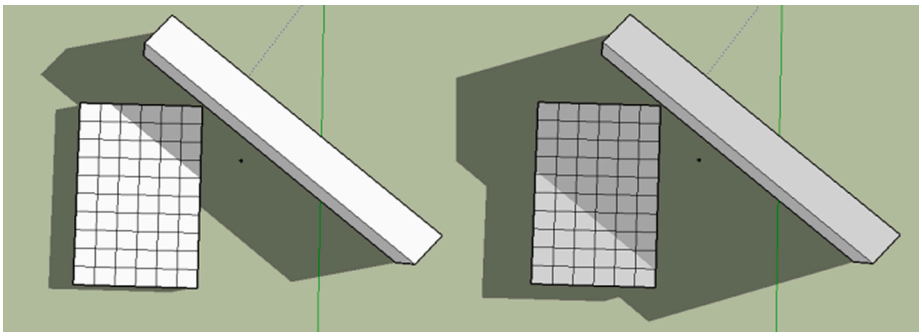

Fig. 10. Shadow transversal to the module (portrait orientation).

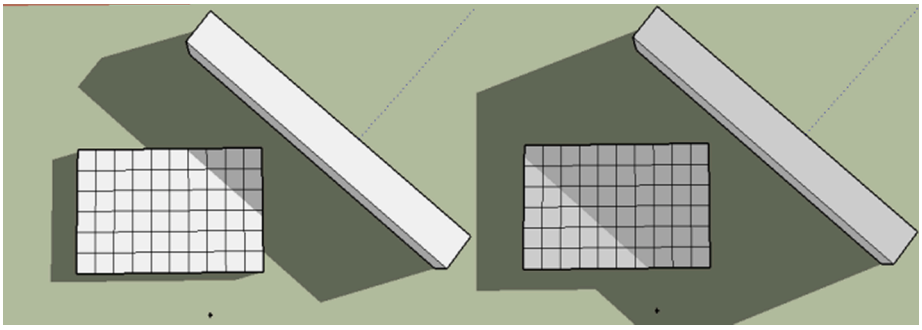

Fig. 11. Shadow transversal to the module (landscape orientation).

The application of the proposed methodology is demonstrated in two cases: a study of the module orientation influence in the shading losses and an estimation of shading losses of a PV plant.

4. Methodology feasibility

The application of the proposed methodology is demonstrated and the shading losses are analyzed in this section. First, the influence of the shadow pattern and module orientation on losses is analyzed. Then the methodology was performed to evaluate the shading losses of a PV plant case.

4.1. Shadow pattern analysis

The modules can be installed in landscape or portrait orientation and the choice depends on the available area conditions mainly. However, this position causes different impacts on partial shaded systems, once the shaded area, number of shaded modules and the shaded region of module changes with the orientation, as illustrated in Fig. 7. In order to analyze this situation, a comparison of shading effects on one module in both orientations for two shadow patterns was performed.

The first case studied was a situation when the shadow is parallel to the long edge (portrait position) and the short edge (landscape position). After this, a situation when the shadow reaches transversally the module was analyzed. The shading effect in portrait and landscape was compared for both situations.

Firstly, a module and shading elements were drawn using the SketchUp (with the cells), and the shading fraction of each cell was obtained by EnergyPlus 8.6. For each submodule, the cell with the smallest sunlit fraction (most shaded) was representative for entire submodule. Then, the irradiance and temperature of each submodule were estimated. The output power was evaluated by Crearray, and the shading effect was estimated using these data. The representations in SketchUp are seen in Figs. 8–11.

The irradiance considered was 1000 W/m^2 (800 W/m^2 correspondent to beam) and the cell temperature was 25 °C. The impact of the

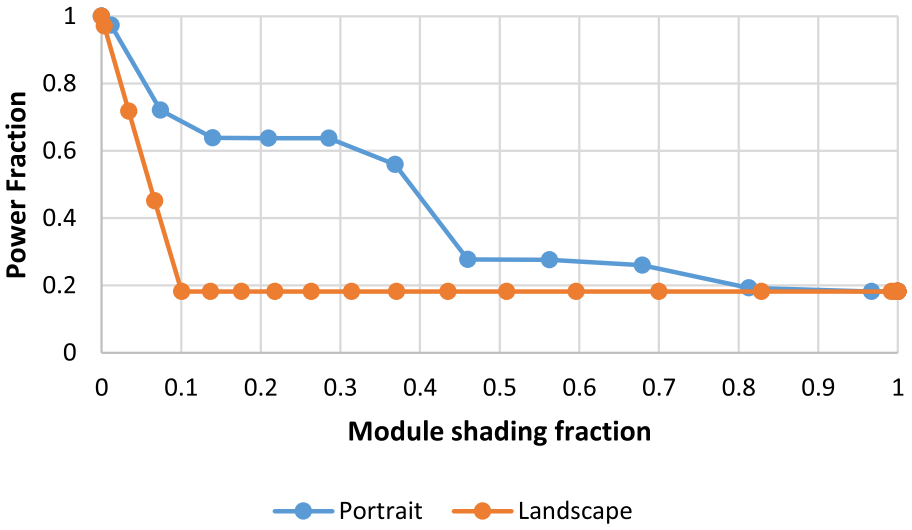

Fig. 12. Impact on power of the shadow parallel to the long edge and short edge.

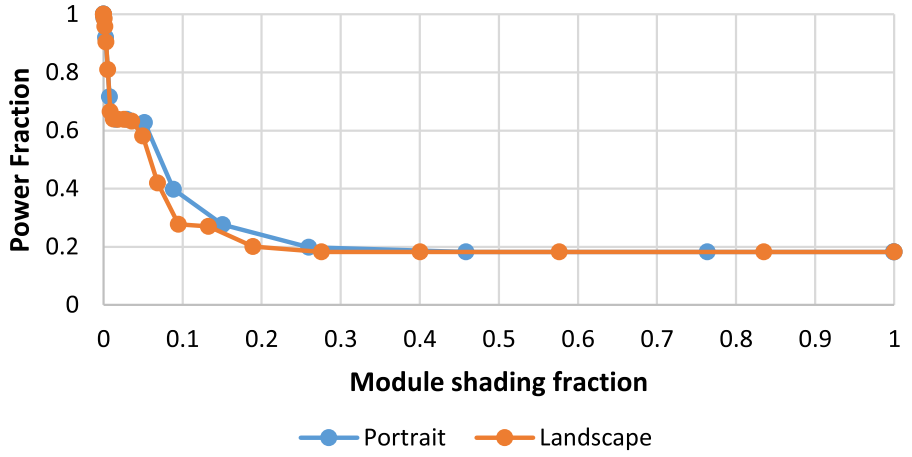

Fig. 13. Impact on power of the shadow traversal to the module.

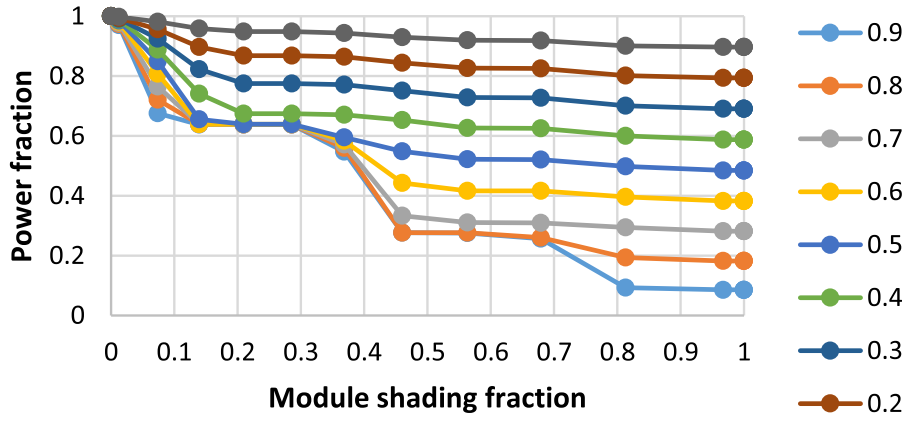

Fig. 14. Beam irradiance fraction impacts on the shading losses.

shaded area on output power of module is presented in Figs. 12 and 13 for both situations and orientations. An analysis varying the beam irradiance fraction was performed, and the Fig. 14 shows the effects of the beam irradiance on the shading losses. Table 1 summarizes the findings about the impact of the module orientation.

When the shadow is parallel to the short edge (landscape position illustrated in Fig. 9), the shading progresses row by row of the module, reaching all submodules equally. The power fraction decreases as increases the shading fraction of the first row cells. When the shading reaches from 10% of the module area, the border cells of all submodules are entire shaded, so the effect is the same as the module completely shaded and the power fraction remains the same as the shading area

Table 1
Module orientation impact.

Shading Pattern	Orientation	Shadow direction	Effect
Parallel	Landscape (parallel to the short edge)	Advances row by row, reaching all submodules equally.	The power decreases as the shading fraction of the first row increases, reaching all submodules equally. When the first row is completely shaded, the border cells of all submodules are shaded and the effect is the same as the entire shaded module.
	Portrait (parallel to the long edge)	Advances column by column, reaching the submodules sequentially.	The power decreases as the shadow reaches the first column of each submodule. When the first column is completely shaded, the effect is the same as the entire submodule completely shaded and remains the same until the first column of next module begins to be shaded.
Transversal	Landscape/Portrait	Advances by cells, reaching the submodules sequentially.	The power decreases as the shading fraction increases until a cell of each submodule be completely shaded. When a cell is completely shaded, the effect is the same as entire shaded submodule. The effect is similar for the both orientations.

Table 2
Module data.

Maximum Power	335 W
Maximum Power Voltage	38.2 V
Maximum Power Current	8.77 A
Open Circuit Voltage	45.7 V
Short Circuit Current	9.28 A
Cells Number	72
Cell type	Polycrystalline
Dimensions	2000 × 992 × 40 mm
Nominal Module Operating Temperature	43 ± 2 °C

increases. On the other hand, the shading effect is lower when shadow is parallel to the long edge (module is in portrait position, Fig. 8). In this position, the shading advances column by column. As soon as the shadow reaches completely the first column of each submodule, the effect is the same as submodule completely shaded and the power fraction remains the same until it reaches the first column of the next submodule. This effect justify the three steps in the curve for portrait position in Fig. 12.

For the second shadow pattern, which the shadow reaches the module transversally, the effect is similar in the both positions. The power decreases as the shading fraction increases until a cell be completely shaded for each submodule. When the shading reaches about 30% of the module area, at least one cell is shaded of all submodules, thus the effect is the same as entire module shaded.

Fig. 14 confirms that as bigger as the beam irradiance participation, higher shading effects on the module power.

Dolara et al. (2013) and Hanifi et al. (2019) obtained experimental results very similar to those summarized in Table 1, only with the difference that the shadow totally blocked the radiation in their studies. Therefore, it was possible to confirm the validity of the results obtained through this methodology. The results could also be confirmed experimentally similarly to the works cited, with a module and a shading element. Experimental analysis is not part of the scope of this article.

4.2. PV plant case

The shading loss on a PV plant, which is part of a project of P&D program of Agência Nacional de Energia Elétrica (ANEEL) developed by Companhia Estadual de Energia Elétrica – CEEE-D (RS, Brazil) with Universidade Federal do Rio Grande do Sul (UFRGS), is evaluated in this section. The PV plant, located in Porto Alegre (Brazil), has 1680 modules and 10 inverters, which each inverter is connected to an array with 12 parallel strings with 14 modules in series. The modules were oriented in landscape, 10° of tilt and facing north with azimuth deviation of 6° to the east. The modules data are presented in Table 2. Each module was divided into 3 submodules with 24 series cells.

4.2.1. Shadow prediction

The PV plant and the surrounding elements were represented in SketchUp, and the shadows were evaluated. The PV plant representation is seen in Fig. 15.

This plant was divided into 10 arrays with 168 modules according to the inverters to simplify the analysis, as seen in Fig. 16. After a visual analysis of shadows during a year, it was verified that the arrays 1 and 4 are equivalents, as well as the 2 and 5 and the arrays 3, 6 and 8. Therefore, only the arrays 1, 2 and 3 were analyzed. The others (7, 9 and 10) have different comportments and were analyzed singly.

The modules were arranged to reduce the shadings by the neighbor building, however shading among strings occurs in the early morning and the late afternoon. Each string of the arrays 1, 2 and 3 has only 3 modules of east and 2 of west boundary with shading fraction which can be different of the others (central). Beside these, all strings of each array are shaded equally. An example of shading on PV plant can be seen in Fig. 17.

The arrays 7, 9 and 10 have no shading on the last string (north). Only the last string (north) of array 10 is shaded by a neighbor building in some days of June around noon, as seen in Fig. 18. The others strings have the same behavior than the arrays 1, 2 and 3 (5 boundary modules different of central).

4.2.2. Simulation

For this case, it was used the simulation option of the software Crearray, so the next step was to prepare an input file with submodules conditions (temperature and irradiance). The shading fraction was obtained by EnergyPlus 8.6 every 15 min. along one year, then the irradiance of each submodule was calculated considering the shading fraction of submodule (corresponding to the most shaded cell) and the transmittance fraction of glass (F_τ), which depends on the angle between the beam irradiance and the normal of glass. These fractions were multiplied by beam irradiance, and then summed to the diffuse, according to Eq. (18). The submodule temperature was estimated using Eq. (2).

$$G = F_S.F_\tau.G_B + G_D \tag{18}$$

The transmittance of the glass depends on the incident angle of beam radiation, according to the Eqs. (19)–(22) (Duffie and Beckman, 2013). The transmittance fraction is the ratio between the transmittance of incident angle and the transmittance of normal angle, as seen in Eq. (23).

$$r_\perp = \frac{\text{sen}^2(\theta_1 - \theta_2)}{\text{sen}^2(\theta_1 + \theta_2)} \tag{19}$$

$$r\| = \frac{\tan^2(\theta_1 - \theta_2)}{\tan^2(\theta_1 + \theta_2)} \tag{20}$$

$$r = \frac{r_\perp + r\|}{2} \tag{21}$$

$$n_1 \text{sen}\theta_1 = n_2 \text{sen}\theta_2 \tag{22}$$

$$F_\tau = \frac{1 - r_{\theta_i}}{1 - r_{0^\circ}} \tag{23}$$

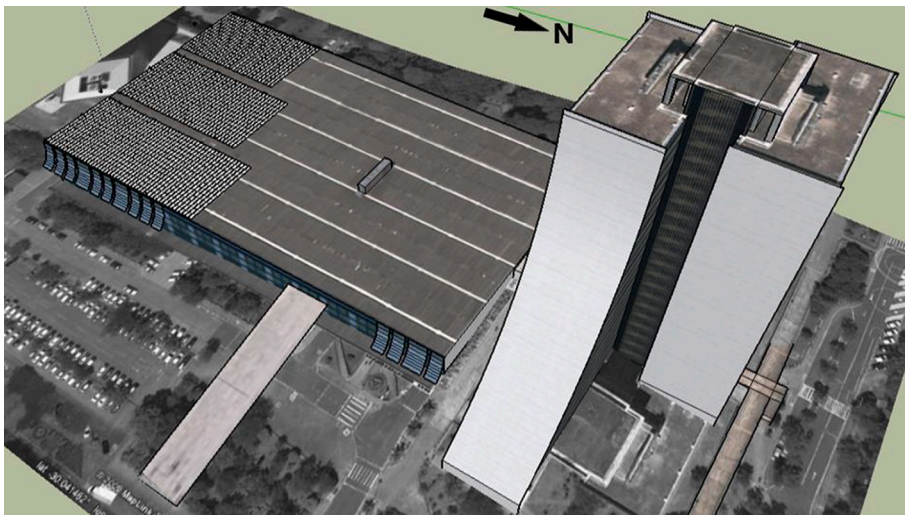

Fig. 15. PV plant representation.

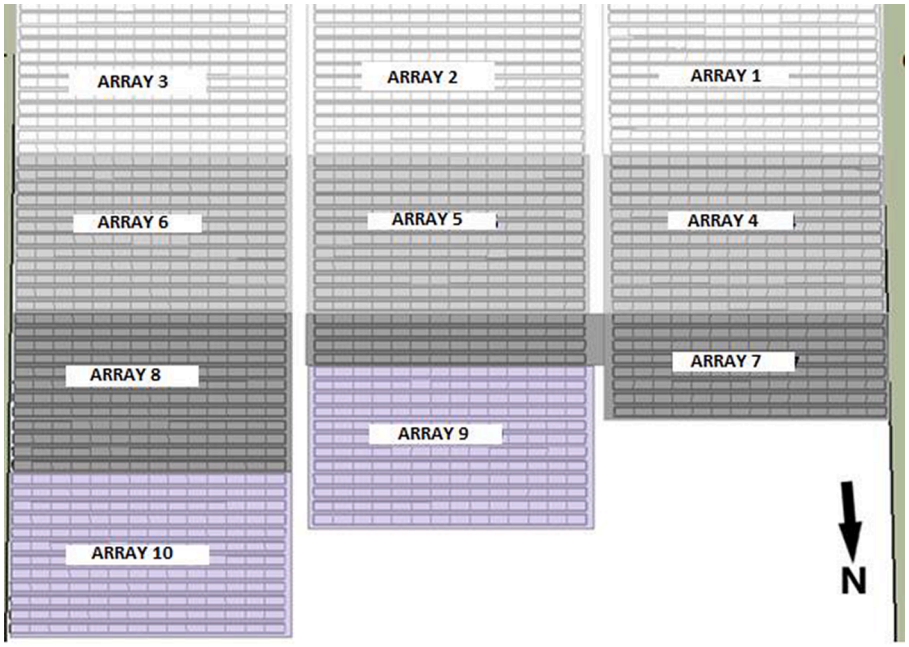

Fig. 16. Arrays distribution.

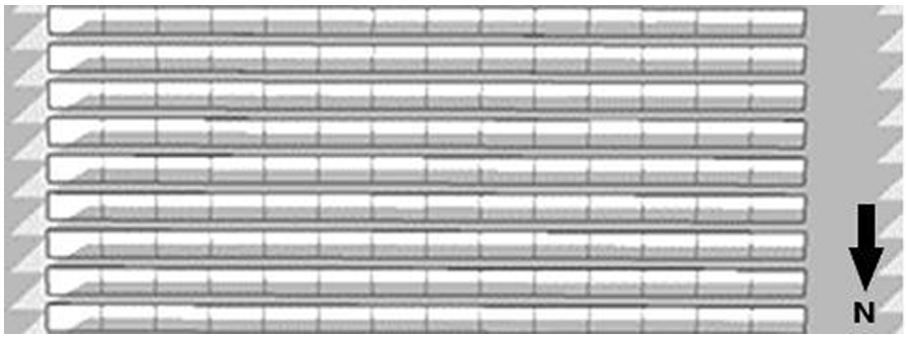

Fig. 17. Shading on central array on May 22 at 07:25 am.

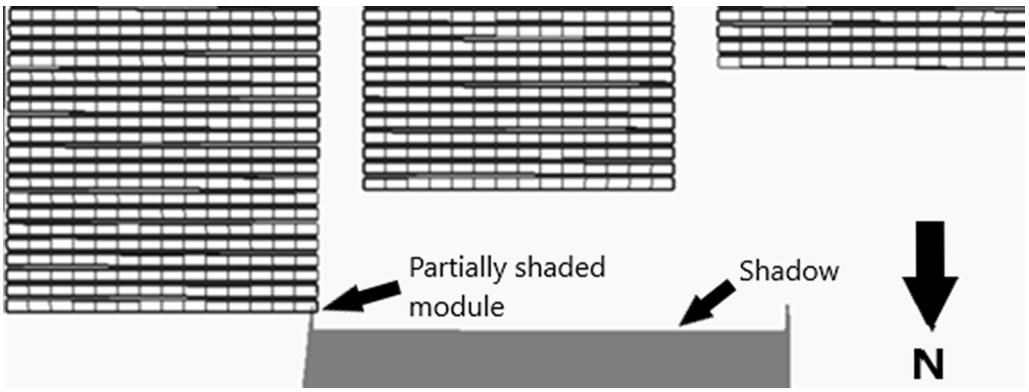

Fig. 18. Shading on June 24 at 11:50 am.

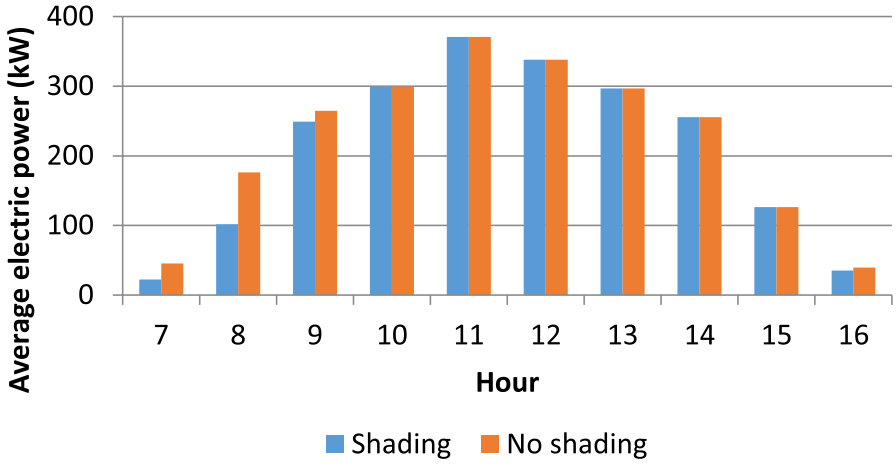

Fig. 19. Average hourly output power (dc) on June25th.

Table 3
Results of PV plant (dc).

Annual Production	869.7 MWh
Shading losses	0.50%
Annual Yield	1545 kWh/kWp
Capacity factor	17.64%

The global, beam and diffuse irradiance and ambient temperature were estimated by RadiaSol 2 every hour during a year. These data were considered constant along the whole hour to calculate the submodule irradiance and temperature every 15 min.

Then the input file (with submodule irradiance and temperature) was prepared, the arrays were represented in Crearray and the simulations were performed.

For the arrays 1, 2 and 3, six modules of each string can present different shading fraction (3 of the east boundary, 2 of the west boundary and 1 central), therefore 18 submodules were analyzed for these arrays. In Crearray, 18 submodules were inserted forming a string with 42 submodules. The string power obtained was multiplied by 12 in order to estimate the array power, since all strings were equivalent.

For the others (7, 9 and 10) there is one submodule pattern more that

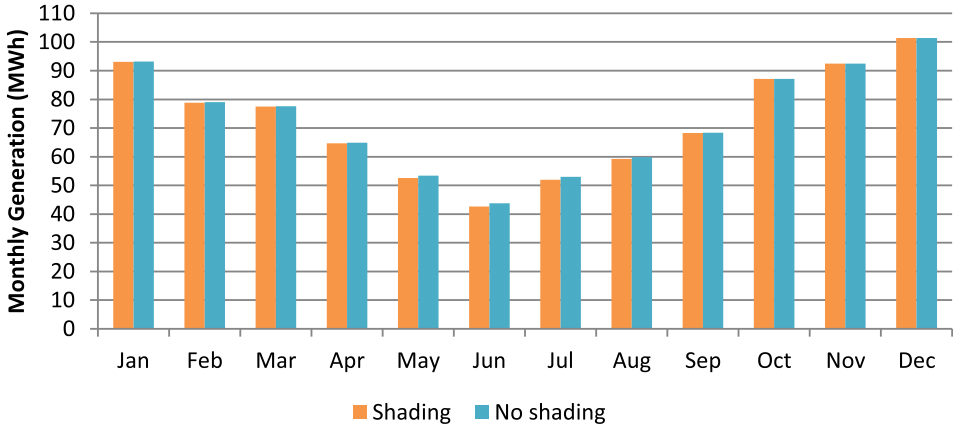

Fig. 20. Monthly production with shading and no shading (dc).

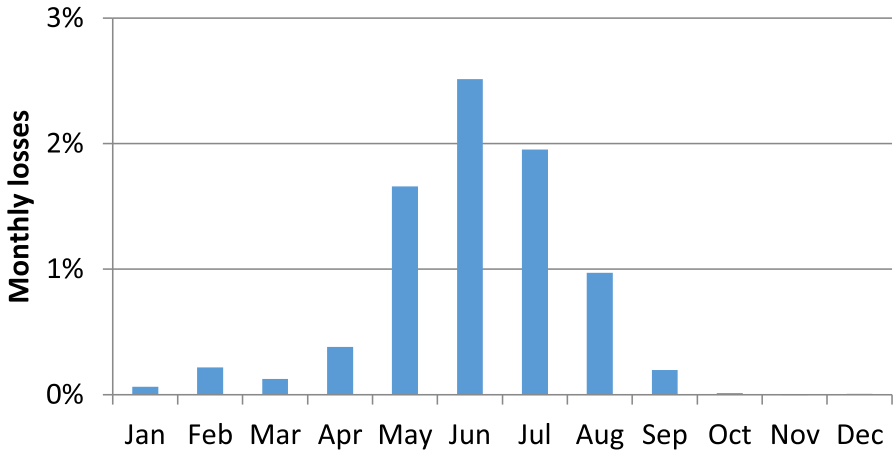

Fig. 21. Monthly shading losses.

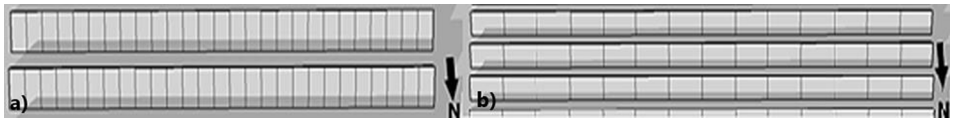

Fig. 22. Shading on May 22 at 07:50 am in orientation. (a) portrait; (b) landscape.

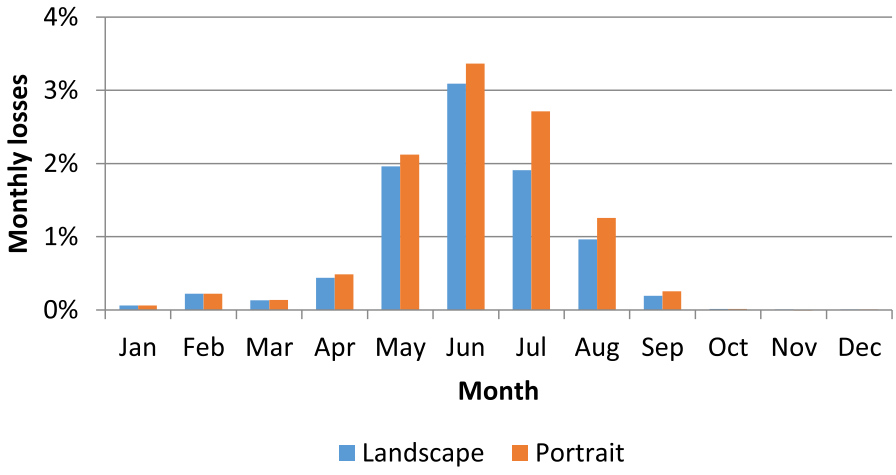

Fig. 23. Module monthly shading losses in landscape and portrait orientation.

is never shaded (north string), the shading on the last string of array around noon on June 10th was not considered in order to simplify the analysis. In this case, the strings were not equal, thus these 19 submodules were added in the Crearray to form an array of 12 strings with 14 modules in series. Therefore, the overall array power was obtained in this case.

4.2.3. Shading effects analysis

The shading losses in direct current (dc) were analyzed. The PV plant power with shading and no shading are compared in Fig. 19 on June 25th. It is evident that in the early morning and late afternoon the power is lower due to the shading.

The annual production, shading losses, annual yield and capacity factor in dc of PV plant are presented in Table 3. Capacity factor is the energy produced divided by the energy would be produced if the plant operate at nominal power over a period of time (1 year), which was about 18% in this case. During a year, the simulated plant production is about 870 MWh and the shading loss of energy (dc) is 0.50%. The annual yield was 1545 kWh per kWp. Shading losses were less than 1%, because shadows occur in the early morning and in the late afternoon in the winter months mainly, therefore, during the hours of less irradiance of the months with less irradiance. The energy injected on the grid could be estimated considering other losses such as the inverter efficiency.

The PV plant monthly energy with shading and no shading is presented in Fig. 20. The monthly losses due to shading are presented in Fig. 21. The summer months present the highest production and the period between May and August present lowest production. However, the highest losses occur in winter months due to the shadings in this period.

A comparison of shading losses with modules in portrait orientation was performed. The comparison of shadings on the arrays in both situations (portrait and landscape) is seen in Fig. 22. Comparing the central modules in Fig. 22, when the shading reaches one submodule in landscape (reaches columns), it reaches three submodules in portrait position (reaches rows). In portrait position, all submodules have the same shading fraction and as soon as the shadow reaches the first row completely, the effect is the same of entire module shaded. The shading losses in both situations were quantified and compared (case similar to

studied in Section 4.1).

The shading losses of a central module in portrait position were about 0.65% and in landscape position about 0.54% during a year. In Fig. 23, the monthly losses are presented for both positions. Thus, the landscape position leads to lower shading losses in this case.

5. Conclusions

This article proposed a methodology to analyze shading effects on photovoltaic systems. The methodology feasibility was demonstrated in two cases: a study of module position and shadow pattern impact on the shading losses and an analysis of shading losses on PV plant. It was proposed that the module should be divided into submodules according to the bypass diode, so each module was represented by its submodules in series. SketchUp and EnergyPlus were used to obtain the shading fraction, Radiasol 2 was used for radiation estimative and Crearray simulated the power output.

According to the study of shading pattern impact on losses, the shading effect is drastic when the shading is parallel to the module short edge because reaches all submodules simultaneously. The effect is minimized when it is parallel to the long edge and the shadow reaches the submodules sequentially. On the other hand, the effect is the same for both orientations (portrait or landscape) when the shadow reaches the module tranversally.

For the PV plant case, the methodology made it possible to evaluate the annual shading losses. Moreover, it was possible perform a comparison of the losses depending on the module orientation. The annual shading loss was 0.54% for landscape position (shading parallel to the long edge) and 0.65% for portrait position (shading parallel to the short edge). Simplifications were necessary to simulate the PV plant in Crearray because of the complexity of the system, nevertheless the analysis was feasible using the methodology.

It was concluded that the methodology proposed is useful and suitable to analyze shading losses on PV installations. Furthermore, the methodology differential is the use of intuitive tools available to anyone. The methodology may have limitations for large photovoltaic plants due to the complexity of the system, increasing the simulation time.

Declaration of Competing Interest

The authors declare that they have no known competing financial interests or personal relationships that could have appeared to influence the work reported in this paper.

Acknowledgements

This study was financed in part by the Coordenação de Aperfeiçoamento de Pessoal de Nível Superior – Brasil (CAPES) – Finance Code 001, by the Conselho Nacional de Desenvolvimento Científico e Tecnológico - Brasil, (CNPq) and by the Companhia Estadual de Energia Elétrica (CEEE).

References

Aguiar, R.J., Collares-Pereira, M., Conde, J.P., 1988. Simple procedure for generating sequences of daily radiation values using a library of markov transition matrices. Sol. Energy 40, 269–279.

Ahmad, R., Murtaza, A.F., Sher, H.A., Shami, U.T., Olalekan, S., 2017. An analytical approach to study partial shading effects on PV array supported by literature. Renew. Sustain. Energy Rev. 74, 721–732.

Ahmed, J., Salam, Z., 2014. A Maximum Power Point Tracking (MPPT) for PV system using Cuckoo Search with partial shading capability. Appl. Energy 119, 118–130. https://doi.org/10.1016/j.apenergy.2013.12.062.

Babatunde, A.A., Abbasoglu, S., Senol, M., 2018. Analysis of the impact of dust, tilt angle and orientation on performance of PV Plants. Renew. Sustain. Energy Rev. 90, 1017–1026.

Baka, M., Manganiello, P., Soudris, D., Catthioor, F., 2019. A cost-benefit analysis for reconfigurable PV modules under shading. Sol. Energy 178, 69–78.

Belhachat, F., Larbes, C., 2015. Modeling, analysis and comparison of solar photovoltaic array configurations under partial shading conditions. Sol. Energy 120, 399–418.

Chaibi, Y., Malvoni, M., Chouder, A., Boussetta, M., Salhi, M., 2019. Simple and efficient aproach to detect and diagnose electrical faults and partial shading in photovoltaic systems. Energy Convers. Manage. 196, 330–343.

Collares-pereira, M., Rabl, A., 1979. The average distribution of solar radiation–correlations between diffuse and hemispherical and between daily and hourly insolation values. Sol. Energy 22, 155–164.

Daliento, S., Di Napoli, F., Guerriero, P., d'Alessandro, V., 2016. A modified by-pass circuit for improved hot spot reliability of solar panels subject partial shading. Sol. Energy 134, 211–218.

Deshkar, S.N., Dhale, S.B., Mukherjee, J.S., Babu, T.S., Rajasekar, N., 2015. Solar PV array reconfiguration under partial shading conditions for maximum power extraction using genetic algorithm. Renew. Sustain. Energy Rev. 43, 102–110.

Dhanalakshmi, B., Rajasekar, N., 2018. A novel Competence Square based PV array reconfiguration technique for solar PV maximum power extraction. Energy Convers. Manage. 174, 897–912.

Dolara, A., Lazaroiu, G.C., Leva, S., Manzolini, G., 2013. Experimental investigation of partial shading scenarios on PV (photovoltaic) modules. Energy 55, 466–475. https://doi.org/10.1016/j.energy.2013.04.009.

Duffie, J.A., Beckman, W.A., 2013. Wiley: Solar Engineering of Thermal Processes, 4th Edition - John A. Duffie, William A. Beckman.

El-Dein, M.Z.S., Kazerani, M., 2013. Optimal photovoltaic array reconfiguration reduce partial shading losses. IEEE Trans. Sustain. Energy 4 (1).

EnergyPlus, 2016. EnergyPlus Engineering Reference.

Erbs, D.G., Klein, S.A., Duffle, J.A., 1982. Estimation of the diffuse radiation fraction for hourly, daily and monthly-average global radiation. Sol. Energy 28, 293–302.

Gallardo-Saaverda, S., Karlssom, B., 2018. Simulation, validation and analysis of shading effects on a PV system. Sol. Energy 170, 828–839.

Ghosh, S., Yadav, V.K., Mukherjee, V., 2019. Improvement of partial shading resilience of PV array though a modified bypass arrangement. Renew. Energy 143, 1079–1093.

Hanifi, H., Pander, M., Jaeckel, B., Schneider, J., Bakhtiari, A., Maier, W., 2019. A novel electrical approach to protect PV modules under various partial shading situations. Sol. Energy 193, 814–819. https://doi.org/10.1016/j.solener.2019.10.035.

Hernández-Callejo, L., Gallardo-Saavedra, S., Alonso-Gómez, V., 2019. A review of photovoltaic systems: Design, operation and maintenance. Sol. Energy 188, 426–440. https://doi.org/10.1016/j.solener.2019.06.017.

Iysaouy, L.E., Lahbabi, M., Oumnad, A., 2019. A novel magic square view topology of a PV system under partial shading condition. Energy Procedia 157, 1182–1190.

Jordehi, A.R., 2016. Maximum power point tracking in photovoltaic (PV) systems: a review of different approaches. Renew. Sustain. Energy Rev. 65, 1127–1138.

Krishna, G.S., Moger, T., 2019a. Reconfiguration strategies for reducing partial shading effects in photovoltaic arrays: State of the art. Sol. Energy 182, 429–452.

Krishna, G.S., Moger, T., 2019b. Improved SuDoKu reconfiguration technique for total-cross-tied PV array to enhance maximum power under partial shading conditions. Renew. Sustain. Energy Rev. 109, 333–348.

Liu, Y., Chen, J., Huang, J., 2015. A review of maximum power tracking techniques for use in partially shaded conditions. Renew. Sustain. Energy Rev. 41, 436–453.

Lu, F., Guo, S., Walsh, T.M., Aberle, A.G., 2013. Improved PV module performance under partial shading conditions. Energy Procedia 33, 248–255.

Maghami, M.R., Hizam, H., Gomes, C., Radzi, M.A., Rezadad, M.I., Hajighorbani, S., 2016. Power Loss Due to soiling on solar panel: a review. Renew. Sustain. Energy Rev. 59, 1307–1316.

Melo, E.G., Almeida, M.P., Zilles, R., Grimoni, J.A.B., 2013. Using a shading matrix to estimate the shading factor and the irradiation in a three-dimensional model of a receiving surface in an urban environment. Sol. Energy 92, 15–25. https://doi.org/10.1016/j.solener.2013.02.015.

Niewienda, A., Heidt, F.D., 1996. SOMBRERO: A PC-tool to calculate shadows on arbitrarily oriented surfaces. Sol. Energy 58, 253–263. https://doi.org/10.1016/S0038-092X(96)00088-6.

Perez, R., Seals, R., 1987. A new simplified version of the perez diffuse. Sol. Energy 39, 221–231.

Rachchh, R., Kumar, M., Tripathi, B., 2016. Solar photovoltaic system design optimization by shading analysis to maximize energy generation from limited urban area. Energy Convers. Manage. 115, 244–252.

Ram, J.P., Babu, T.S., Rajasekar, N., 2017. A comprehensive review on solar PV maximum power point tracking techniques. Renew. Sustain. Energy Rev. 67, 826–847.

Ramli, M.Z., Salam, Z., 2019. Performance evaluation of dc Power optimizer (SCPO) for photovoltaic (PV) system during partial shading. Renew. Energy 139, 1336–1354.

Rezk, H., Fathy, A., Abdelaziz, A.Y., 2017. A comparison of different global MPPT techniques based on meta-heuristic algorithms for photovoltaic system subjected to partial shading conditions. Renew. Sustain. Energy Rev. 74, 377–386.

Rocha, A.P.D.A., Oliveira, R.C.L.F., Mendes, N., 2017. Experimental validation and comparison of direct solar shading calculations within building energy simulation tools : Polygon clipping and pixel counting techniques. Sol. Energy 158, 462–473. https://doi.org/10.1016/j.solener.2017.10.011.

Rodrigues, J.M., Alves, A.J., Domingues, E.G., Calixto, W.P., 2015. A technical and economical study of a photovoltaic system installed on the rooftop of a public building. Renew. Energy Power Qual. J. 1, 380–385. https://doi.org/10.24084/repqj13.332.

Ross, R.G., Smokler, M.I., 1986. Flat-Plate Solar Array Project Final Report: Volume VI, Engineering sciences and reliability. United States: N. p., 1986.

Said, S.A.M., Hassan, G., Walwil, H.M., Al-Aqeeli, N., 2018. The effect of environmental factors and dust accumulation on photovoltaic modules and dust-accumulation mitigation strategies. Renew. Sustain. Energy Rev. 82, 743–760.

Salem, F., Awadallah, M.A., 2016. Detection and assessment of partial shading photovoltaic arrays. J. Electr. Syst. Inf. Technol. 3, 23–32.
Satpathy, P.R., Sharma, R., 2019. Power and mismatch losses mitigation by electrical reconfiguration technique for partially shaded photovoltaic arrays. Energy Convers. Manage. 192, 52–70.
Shaviv, E., Yezioro, A., 1997. Analyzing mutual shading among buildings. Sol. Energy 59, 83–88. https://doi.org/10.1016/S0038-092X(96)00103-X.
Sinapis, K., Tzikas, C., Litijens, G., Ven den Donker, M., Folkerts, W., van Sark, W.G.J.H. M., Smets, A., 2016. A comprehensive study on partial shading response of c-Si modules and yield modeling of string inverter and module level power electronics. Sol. Energy 135, 731–741. https://doi.org/10.1016/j.solener.2016.06.050.
Tatabhatla, V.M.R., Agarwal, A., Kanumuri, T., 2019. Improved power generation by dispersing the uniform and non-uniform partial shades in solar photovoltaic array. Energy Convers. Manage. 197.
Tubniyom, C., Jaideaw, W., Chatthaworn, R., Suksri, A., Wongwuttanasatian, T., 2018. Effect of partial shading patterns and degrees of shading on Total Cross Tied (TCT) photovoltaic array configuration. Energy Procedia 153, 35–41.
Wang, Z., Li, Y., Wang, K., Huang, Z., 2017. Environment-adjusted operational performance evaluation of solar photovoltaic power plants: A three stage efficiency. Renew. Sustain. Energy Rev. 76, 1153–1162.
Yadav, A.S., Mukherjee, V., 2018. Line losses reduction techniques in puzzled PV array configuration under different shading conditions. Sol. Energy 171, 774–783.
Zaihidee, F.M., Mekhilef, S., Seyedmahmoudian, M., Horan, B., 2016. Dust as an unalterable deteriorative factor affecting PV paneĺs efficiency: Why and how. Renew. Sustain. Energy Rev. 65, 1267–1278.
Zheng, H., Li, S., Challoo, R., Proano, J., 2014. Shading and bypass diode impacts to energy extraction of PV arrays under different converter configurations. Renew. Energy 68, 58–66.
Zhu, L., Li, Q., Chen, M., Cao, K., Sun, Y., 2019. A simplified mathematical model for power output predicting of Building Integrated Photovoltaic under partial shading conditions. Energy Convers. Manage. 180, 831–843.

Solar Energy 223 (2021) 182–192

Contents lists available at ScienceDirect

Solar Energy

journal homepage: www.elsevier.com/locate/solener

Accuracy investigation in the modeling of partially shaded photovoltaic systems

Ellen David Chepp *, Fabiano Perin Gasparin, Arno Krenzinger

Solar Energy Laboratory, Post-Graduation Program in Mining, Metallurgical and Materials Engineering (PPGE3M), Federal University of Rio Grande do Sul (UFRGS), Av. Bento Gonçalves, 9500 Agronomia, Porto Alegre, Rio Grande do Sul, Brazil

ARTICLE INFO

Keyword:
Photovoltaic
Shading
Simulation
Accuracy

ABSTRACT

Software for simulation of photovoltaic (PV) systems is widely used for dimensioning and forecasting electrical production. A factor of losses in PV installations is the partial shading caused by surrounding elements, and these software allow the user to estimate this effect. However, the accuracy of these simulated results for shaded PV systems is not widely studied. The purpose of this article is to investigate the accuracy and quantify the differences between simulated and measured data of partially shaded PV systems, obtained with the widely used tools SAM and PVSyst. Measured data from a PV installation were compared to results from simulations performed using the different shading calculation options available in both tools. The simulated outputs were both underestimated and overestimated in the shading situations. This variation was related to the use of an hourly fraction of shading and, in the case of SAM, due to the limitations of the 3D tools available for representation. Another source of differences between simulated and measured values was the use of uniform shading factors for diffuse and albedo. In addition, the simplification of the 3D model had a significant impact on the predicted energy, mainly on cloudy days. Both software overestimated the electricity production for the entire measurement period, reaching differences between the predicted and the measured energy varying from 9% to 24%. Shaded PV systems must be carefully analyzed, and the simulated results may differ from the measured values, which may even influence the decision on the feasibility of an installation.

1. Introduction

Photovoltaic (PV) conversion from solar energy has become increasingly used worldwide (Jäger-Waldau, 2020). Technological improvements, mainly related to the increase in efficiency, and the reduction in costs have driven this growth in recent years, a behavior that is expected to continue (Victoria et al., 2021). Others advantages that favor expansion are the PV modularity and shorter installation times compared to other sources (Victoria et al., 2021). In addition to these advantages, PV energy is a fundamental source for the transition to a 100% renewable electricity system (Bogdanov et al., 2019; Jacobson et al., 2017).

In this scenario of PV expansion, a good estimate of the available solar radiation and the electric energy produced by PV systems allows better use of this source. Thus, accurate models for estimating radiation and PV system performance considering loss factors are essential. Partial shading is a common loss factor mainly in PV systems installed in urban areas, and these losses should be considered when forecasting electrical production (Trzmiel et al., 2020). Therefore, the accuracy of shaded PV systems modeling for forecasting electricity production should be known.

The purpose of this article is to investigate the accuracy and quantify the differences between simulated and measured data of a partially shaded PV system. Detailed simulations were carried out to analyze a PV system's performance under partial shading. Electrical and climatic data as well measured I-V curves were employed to adjust the input parameters for the simulations and check the simulation accuracy. The software called Crearray (Chepp and Krenzinger, 2021) was used to perform the simulations with greater control of variables and for comparison with the results of the analyzed tools. Simulations with SAM and PVSyst were performed using a weather file with measured data and adjusted input parameters, allowing the comparison between the simulated and measured results.

The literature is reviewed in Section 2 of this article. Section 3 briefly describes how shading losses are estimated in the tools used, and the methodology used for the analysis is described in Section 4. I-V curves

* Corresponding author.
E-mail address: ellen.chepp@gmail.com (E.D. Chepp).

https://doi.org/10.1016/j.solener.2021.05.061
Received 25 February 2021; Received in revised form 14 May 2021; Accepted 17 May 2021
Available online 27 May 2021

were measured over a day to better analyze the PV system behavior and adjust the input parameters, as described in Section 5. The results of the simulations were compared to the measured data in Section 6. Finally, the conclusions are presented in Section 7.

2. Literature review

Simulation software for PV systems is widely used by designers to assist the step of dimensioning and estimating electrical production (Wijeratne et al., 2019). Among the most used tools, PVSyst has been used for solar potential assessment (Belmahdi and Bouardi, 2020), PV system performance analysis (Kumar et al., 2017), design and simulation (Kumar et al., 2020), and economic evaluation (Dey and Subudhi, 2020). Other tools such as PV*Sol (Sharma and Gidwani, 2017) and SAM (Shukla et al., 2016) have also been used for these analyzes. As in any simulation, the quality of the results depends on the input parameters used, so the greater the number of parameters provided by the user, the greater the complexity of the simulations and the results (Freeman et al., 2014).

The accuracy analysis of the results obtained by simulation from widely used tools is extremely important (Mondol et al., 2007), and some uncertainties in PV systems design have been verified by Quesada et al. (2011). Axaopoulos et al. (2014) compared experimental data from a 19.8 kW PV installation with simulated data using TRNSYS, Archelios, Polysun, PVSyst, PV*Sol and PVGIS software. They found that all tools underestimated the electricity generation for every month of the year, except PVGIS, which did not allow an input file with measured data; however, all investigated tools overestimated the radiation on the tilted plane. The results generated by the TRNSYS software were the closest to the measured ones. The biggest error was associated with the PV cell model. Freeman et al. (2014) also validated multiple tools (SAM, PVWatts, PVSyst and PV*Sol) for modeling PV systems, and all tools showed annual errors within ±8%. Palmero-marrero and Matos (2015) concluded that PVSyst and TRNSYS are accurate tools for forecasting annual production based on the comparison of measured data from a 124.2 kWp plant and software simulation. All accuracy analyzes mentioned above were performed considering PV systems under uniform radiation only. The work reported here focuses on the accuracy of shaded PV systems modeling. In addition to analyzing differences in the accumulated energy between measured and simulated results, the research reported in this article analyzes the input parameters and compares measured and simulated I-V curves from a partially shaded PV system.

PV systems partially shaded or installed in locations with many elements that obstruct the horizon are the ones that require greater attention for performance simulation (Trzmiel et al., 2020). The effects of partial shading on PV systems are widely known and investigated; however, the accuracy of the input variables involved in the simulation can lead to significant differences, which is the scope of this article. Some previous studies have focused on proposing simplified methods to simulate the I-V curve in shading situations (Bai et al., 2015; Deline et al., 2013; Kermadi et al., 2020), while others verify the impact of different shading patterns (Ahmad et al., 2017; Alonso-García et al., 2006; Gallardo-Saavedra and Karlsson, 2018). These shading effects can be reduced through different configurations of the PV module (Baka et al., 2019; Daliento et al., 2016; Ghosh et al., 2019) or the PV array (Karatepe et al., 2007; Mohammadnejad et al., 2016; Saiprakash et al., 2020). Sai Krishna and Moger (2019) reviewed the state of the art of techniques to reduce the effect of partial shading, which are the bypass diode, different configurations of PV array interconnections, distributed maximum power point tracking (MPPT) techniques, multilevel inverters and reconfiguration strategies. In addition, the power curve as a function of voltage has multiple peaks (local maximum and global maximum) during partial shading conditions. This situation can lead to failure in the MPPT, following a local maximum instead of the global maximum. Therefore, different methods for MPPT for partial shading situations have been proposed in the literature (da Rocha et al., 2020; Mohapatra et al., 2017; Verma et al., 2020). Ram et al. (2017) reviewed the state of the art of techniques for MPPT and compared conventional and unconventional (soft computing) methods.

To enable faster simulations, some commercial tools offer simplified models, and sometimes they have different options for shading calculation, which can affect the simulation accuracy. Previous studies on the accuracy of simulations comparing simulated and measured results rarely focus on shaded PV systems. Therefore, the simulation accuracy of partially shaded PV systems performed in widely used software packages and the quantitative effect of different options for shading calculation are not sufficiently investigated or reported. The knowledge gap discussed above is the purpose of the investigation reported here.

3. Estimation of shading losses

When a PV system is partially shaded, the shaded region receives less radiation than the non-shaded one, therefore the photogenerated current is less in the shaded cells. In addition to the loss of incident beam solar radiation in a shaded region, there are also diffuse radiation losses due to elements that obstruct the horizon and reduce the sky view factor. Therefore, the 3D representation of a system and its surroundings is an indispensable step in the simulation, and failure to consider one of these surrounding elements can result in an overestimated value of electrical production (Trzmiel et al., 2020). There are also electrical effects related to the configuration of PV cells which, because are usually in series, increase the losses (Mermoud and Lejeune, 2010).

The vast majority of crystalline silicon PV modules are composed of series-connected cells and bypass diodes connected in antiparallel to a set of cells. Dividing a PV module into submodules, with each submodule corresponding to a group of cells connected in series and a bypass diode, is effective to assess the impact of partial shading (Daliento et al., 2016; Mermoud and Lejeune, 2010; Mohammed et al., 2020). The electric current of the most shaded cell (lowest current) limits the current of all PV cells that are in series in the same submodule. Performing in cell level simulations is significantly wearing, so it is common for simulation tools to simplify the estimation of shading effects by submodule (Mikofski et al., 2018).

The PVSyst software version 7.1 (PVSyst, 2021) has three different methods for estimating the shading effects available for the user. To perform the shading analysis, it is necessary to build the 3D representation using the available tools or to import a 3D model generated in another software. The method called linear shading considers that the shading losses of the PV system are proportional to the shaded area. In this first model, only irradiance losses in the module plane are considered and it has two options: calculation through shading tables (faster) or simulation (slower). The second method assesses losses according to the strings and it considers that as soon as the shadow reaches a string of modules, all modules become unproductive; the user can determine the fraction of the electrical effect. According to the software manual, this model represents the maximum loss limit. In the detailed model (third option), the modules are divided into submodules according to the bypass diodes. The fraction of linear shading for each submodule is calculated, and the I-V curve is generated. The resulting curve is obtained by adding the voltages of the curves of the submodules in series and adding the currents of the curves of the submodules in parallel.

The System Advisor Model (SAM) software version 2020.2.29 was developed by NREL (National Renewable Energy Laboratory) and has two options for shading losses (SAM, 2020). The first option considers a linear loss (irradiance loss), and the second, called partial shading model, consists of dividing the module into submodules. SAM has the option to perform 3D representation; however, the tools are limited and it is not possible to import files generated in another software. Nevertheless, it allows the user to import shading tables that can be generated in PVSyst, SunEye or Solar Pathfinder software. Macalpine and Deline (2015) described the shading calculation method.

It is expected that the methods that divide the PV modules into submodules are more accurate than the others for crystalline silicon PV modules. However, it is important to analyze the simulated results for the other calculation options, considering that, although there is an explanation about the methods in the software manuals, a user can choose any of the options to perform the simulation. Therefore, simulated results for each calculation option of both software are compared to measured data in this work to evaluate the differences expected according to the available options.

4. Methodology

The studied PV system is located in Porto Alegre (southern Brazil, coordinates 30°S 51°W) and consists of a string with 10 multicrystalline silicon PV modules of 245 Wp connected to a grid-connected inverter with 2500 W. The array is tilted at 50° and facing north. The PV modules dimensions are 1650 mm × 990 mm, they have 60 cells and one bypass diode for every 20 cells, which makes a submodule. The PV modules were installed in a plane respecting the architectural characteristics of the building, and the tilt is not ideal for maximizing annual electricity production considering the site latitude. The system was installed for analysis and testing under non-ideal conditions, such as high tilt and partial shading.

A pyranometer (EKO, MS60) was used to measure the global horizontal solar irradiance. Another pyranometer (Kipp & Zonen, CM-11) installed under a shadow ring was used to measure the diffuse horizontal solar irradiance. A crystalline silicon reference cell measures the solar irradiance on the plane of the PV modules. The ambient temperature and the central PV module temperature were measured with Pt100 temperature sensors. Data acquisition and recording equipment (SMA, Sunny Boy SBCOP02) register 20 min average values from each variable. Fig. 1 shows the PV system and some details of the positioning of instruments and sensors.

Simulated results of the PV system were performed using the Crearray software, developed at LABSOL (Solar Energy Laboratory at UFRGS), which generates I-V curves for given temperature and irradiance conditions. The software also calculates the maximum power point (MPP) from an input file with irradiance and temperature data. The PV modeling based on the single diode model and the operation of Crearray were described by Chepp and Krenzinger (2021). This software allows a detailed analysis of the I-V curve for any condition, making possible a better adjustment of input variables that are shared with the simulations performed in PVSyst and SAM later on.

Fig. 2 shows the system surroundings which consist of trees, a wall (the white wall on the right of Fig. 1), and another PV system. The PV array with each PV module divided into submodules, the wall, the neighboring PV modules and some trees were modeled in the SketchUp software. The shading fraction for each submodule was obtained with the EnergyPlus software. The shading fraction of the submodule when the shadow reaches a complete cell was determined, which is the same effect as if the entire submodule to which it belongs were shaded.

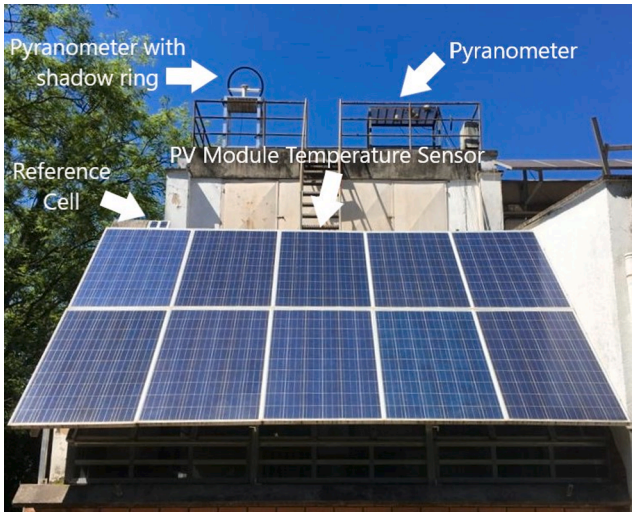

Fig. 1. Studied PV system.

The effective incident irradiance on a PV module on the tilted plane ($G_{T,eff}$) was calculated according to Eq. (1), by adding beam (G_B), diffuse (G_D) and the reflected radiation on the ground, considering the global horizontal radiation (G), albedo (ρ), angle of incidence (θ), zenith angle (θ_Z) and slope (β) (Duffie and Beckman, 2013). Moreover, the losses due to the shading fraction (F_S), effective view factor (EVF), soiling (L_S), angular reflection of the glass ($K\tau\alpha$) and air mass modifier (M_{am}) were considered. F_S is 0 for completely shaded and 1 for non-shaded. The effective irradiance is the input for the Crearray software, while SAM and PVSyst apply their methods to calculate the effective irradiance on a PV module. Snell's law, Eq. (2), relates the refractive index of medium 1 (n_1) and medium 2 (n_2) to the incidence (θ_1) and refraction (θ_2) angles. Eq. (3) gives the reflection of the glass as a function of the angle of incidence, $r(\theta_1)$, and Eq. (4) gives the angular reflection coefficient of the glass (De Soto et al., 2006; Duffie and Beckman, 2013). The air mass (AM_a) was calculated from Eq. (5) and depends on the altitude (h) and solar zenith (θ_Z) (King et al., 1998). Eq. (6) gives the air mass modifier, in which the polynomial coefficients used are: $a_0 = 0.918093$; $a_1 = 0.086257$; $a_2 = -0.024459$; $a_3 = 0.002816$; $a_4 = -0.000126$ (Fanney et al., 2003).

$$G_{T,eff} = G_B\left(\frac{\cos\theta}{\cos\theta_z}\right)K_{\tau\alpha}M_{am}F_sL_S + \left[G_D\left(\frac{1+\cos\beta}{2}\right) + G\rho\left(\frac{1-\cos\beta}{2}\right)\right]L_SEVF \quad (1)$$

$$n_1\sin\theta_1 = n_2 sin\theta_2 \quad (2)$$

$$r(\theta_1) = \frac{1}{2}\left(\frac{sin^2(\theta_2-\theta_1)}{sin^2(\theta_2+\theta_1)} + \frac{tan^2(\theta_2-\theta_1)}{tan^2(\theta_2+\theta_1)}\right) \quad (3)$$

$$K_{\tau\alpha} = \frac{1-r(\theta_1)}{1-r(0^\circ)} \quad (4)$$

$$AMa = \frac{\exp(-0.0001184h)}{cos\theta_z + 0.5057(96.080-\theta_z)^{-1.634}} \quad (5)$$

$$M_{am} = a_0 + a_1AMa + a_2AMa^2 + a_3AMa^3 + a_4AMa^4 \quad (6)$$

Several I-V curves of the PV system were measured (using an I-V curve tracer PVE, PVPM 1100C) over a clear day and they were compared to the I-V curves simulated in Crearray for the same conditions. The I-V curves are essential for an extensive analysis of the system behavior, checking the pattern of shadows, and for a better adjustment of input parameters for the simulations. After adjusting the input parameters, the system performance in direct current (DC) was obtained for the entire measurement period (approximately 2 months) from Crearray, SAM and PVSyst. The simulated results were analyzed and compared with the measured ones.

The hourly average values of the measured irradiance from the pyranometers and ambient temperature data were used for simulations in PVSyst and SAM as parameters of the input weather file. PVSyst allows the user to make a geometric model using drawing tools or import a model (the model created in SketchUp was imported), and average values for diffuse and albedo shading factors are calculated. Two simulations were done with SAM: one using a shading table exported from PVSyst and another with the simplified 3D model generated in SAM, which has quite simple and limited drawing tools.

Fig. 2. PV System surroundings.

5. Analysis of the PV system over a clear day and adjustment of the input parameters

Some variables are difficult to estimate due to the complexity of the PV installation surrounding, such as the albedo and therefore, the reflected radiation incident on the PV plane, which can vary over time, and the effective view factor (EVF) of the PV modules. In addition, the PV system performance simulations used hourly averages, and the shadows vary significantly within that time interval. In order to verify the behavior of the PV system and to better adjust the input parameters for the simulation, I-V curves were measured over a clear day with a time interval of 20 min.

Several I-V curves of the PV system were simulated in Crearray using the effective irradiance on the PV array calculated from measured global and diffuse solar irradiance and measured PV module temperature. Shading fractions in the submodule level were visually determined by inspecting photos taken at the same time that the I-V curve was measured. An albedo of 0.4 was considered to estimate the radiation reflected by the ground and surroundings and 5% of radiation losses due to soiling on the PV modules. The simulated I-V curves were compared with the measured ones.

Initially, uniform diffuse and albedo shading factors calculated by PVSyst were used for all PV modules. However, the measured I-V curve showed visible differences compared to the simulated one. Fig. 3 (a) shows that the measured curve has a higher current and a larger slope in the short circuit region. The measured current of the I-V curve around higher voltages (~300 V) has a slightly lower current than the simulated curve. These results indicate that the shaded modules have a lower EVF since the wall causes shade and also reduces the EVF for the diffuse radiation. Because of this behavior, different EVF were estimated for the modules, considering lower for the modules closer to the wall and increasing as they move away from the wall. The curve was simulated again considering non-uniform EVF. The comparison with the measured curve is in Fig. 3 (b), showing that a non-uniform EVF improves the accuracy of the simulated I-V curve.

The system is partially shaded by the neighboring trees in the morning, as shown in Fig. 4 (a). This type of shadow is difficult to reproduce with models as seen in Fig. 4 (b) because it is irregular and changes fast. Another visible issue in the I-V curve is the effect of the white wall reflection indicated in Fig. 4 (b), where the measured array short circuit current is higher than the simulated one. The variable characteristic of this non-uniform shading and the high radiation reflection in the early morning introduces extra complexity to the modeling.

During the moments without shading, the simulated and measured curves are considerably close, as shown in Fig. 5 (a) and (b). The short-circuit current of the measured curve is greater than that simulated one at 10 am, as indicated in Fig. 5 (a), and also at 9:20 am as indicated in Fig. 4 (b). This effect occurs because part of the solar radiation is being reflected by the white wall (which has an albedo greater than 0.4), increasing the current of the modules closer to the wall. Although this reflection increases the short circuit current, it does not affect the array's maximum power. This reflection effect does not happen at solar noon (12:10 pm), and both curves overlap as shown in Fig. 5 (b).

The wall and PV modules of the neighboring PV system begin to shade the studied PV system at 12:20 pm. Fig. 6 shows the PV system with two shaded submodules and the corresponding I-V curves at 1 pm. From this time on, a voltage difference between the curves is also verified, related to the temperature difference between the shaded modules and those that are not shaded, which was not considered in the simulation. This effect is also reported previously by Mohammed et al. (2020).

From 3 pm, the measured curve has a higher current than the simulated one, as shown in Fig. 7, as a result of the solar radiation that is reflected by the tree leaves located to the east of the PV system and affects the modules that are not shaded. Moreover, the MPP of the curve moves to voltages below 224 V (minimum voltage of the inverter MPPT) between 3 pm and 4 pm as indicated in Fig. 7. Therefore, the PV system

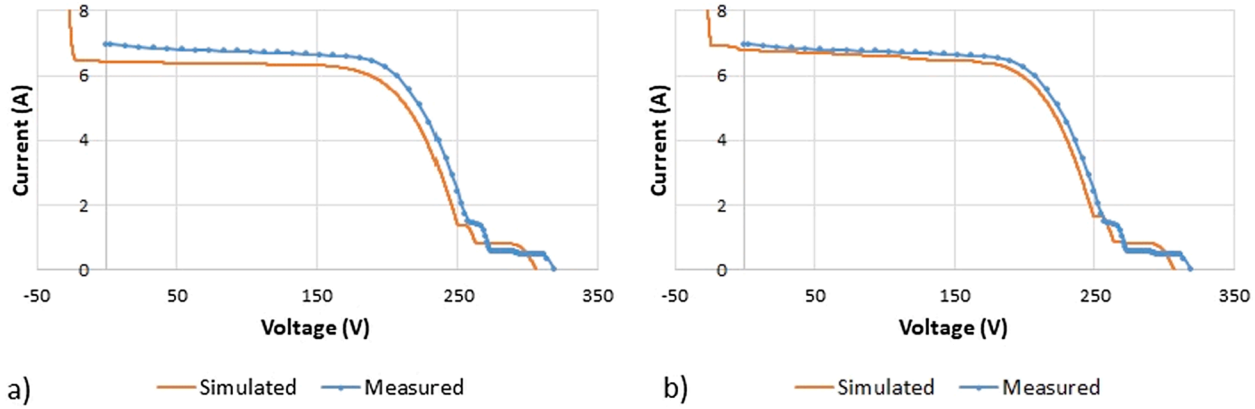

Fig. 3. I-V curves measured and simulated at 2 pm; (a) using uniform diffuse and albedo shading factors; (b) using non-uniform EVF for the PV modules.

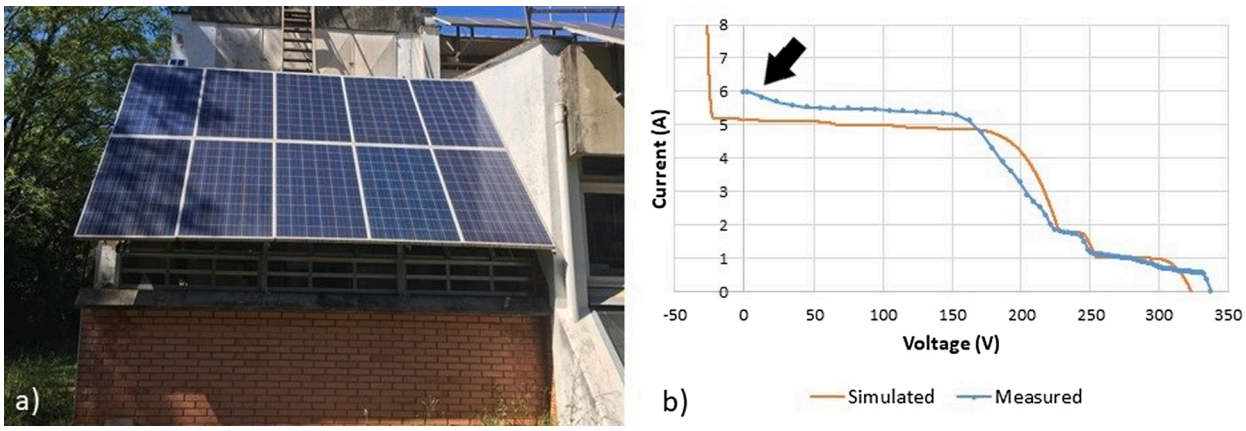

Fig. 4. (a) The PV system at 9:20 am showing irregular shadows; (b) The I-V curves where the white wall reflection effect is indicated.

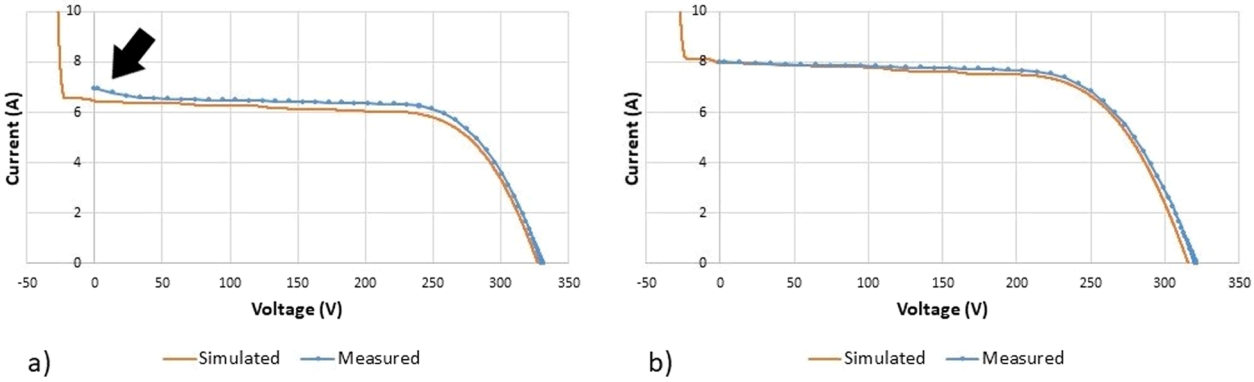

Fig. 5. (a) I-V curves at 10 am with the white wall reflection effect indicated. (b) Overlapping I-V curves at 12:10 pm.

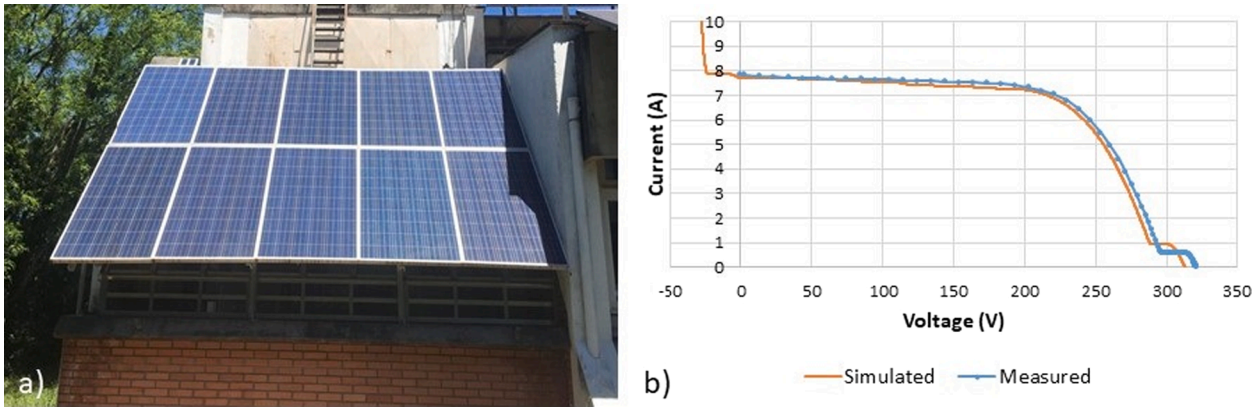

Fig. 6. (a) Partially shaded system photo at 1 pm; (b) corresponding I-V curves at 1 pm.

does not operate at maximum power during these shading periods.

The effect of the reference cell shading in the morning and the leaves reflection in the afternoon can be confirmed in Fig. 8, which compares the hourly average values of the irradiance measured by the reference cell and the effective one calculated from the pyranometers measurements (without shading and soiling effects). The effective irradiance is greater than that of the reference cell in the early morning, between 7 am and 9 am, due to the reference cell being shaded sometimes. The solar irradiance measured by the reference cell and the calculated one is very close from 10 am to 12 pm. The reflection effect of the leaves of the trees begins to occur from 1 pm, when the difference between both radiation values begins to increase.

From this analysis, the reflection caused by the wall in the early morning and by the trees in the afternoon contributes to the measured current being greater than the simulated one. The temperature difference between the PV modules leads to voltage differences between the simulated and measured curves. The use of non-uniform EVF for the PV modules leads to a simulation closer to measurement results. The shadows caused by the trees in the early morning are irregular, making it difficult to reproduce both the shadows and the effect on the I-V curve. Therefore, the non-uniform EVF was employed and the albedo of 0.4 and 5% of soiling loss was set for the simulations in Crearray, since the curves overlapped at times close to the solar noon (without shadow and reflection of the wall and trees).

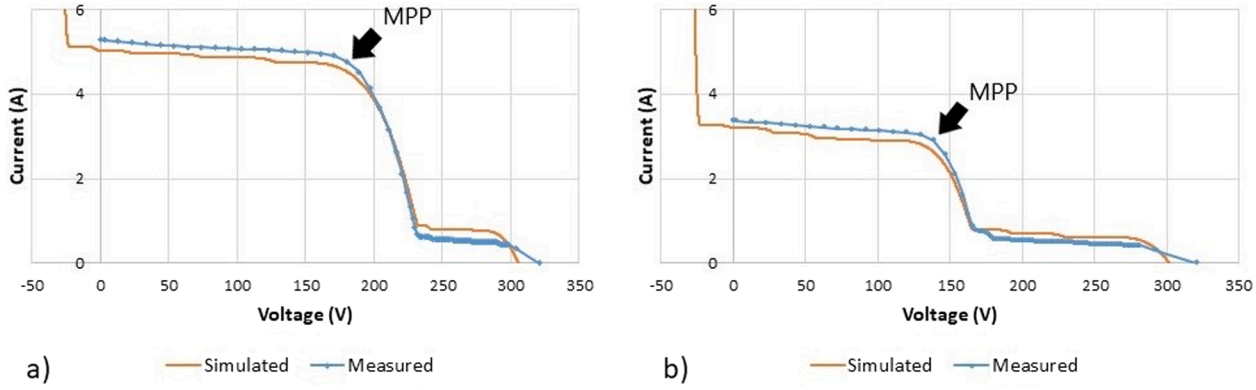

Fig. 7. I-V curves measured and simulated with the MPP indicated (a) at 3 pm; and (b) at 4 pm.

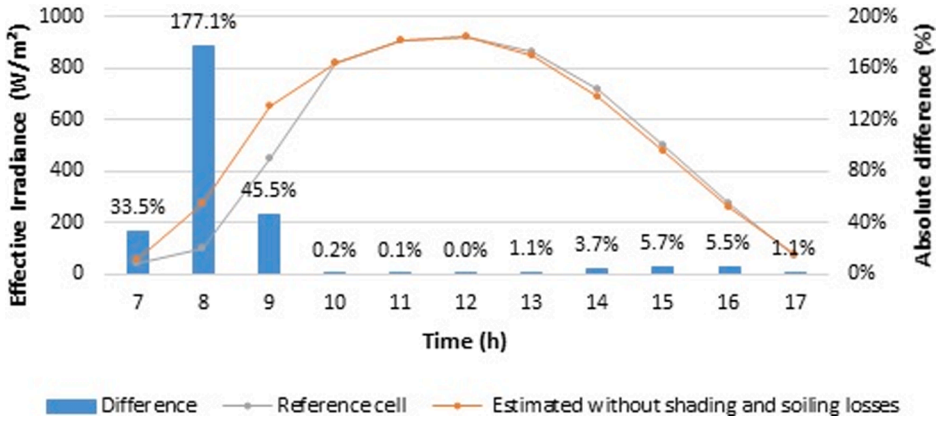

Fig. 8. Solar irradiance measured by the reference cell, the effective solar irradiance calculated from pyranometers measurements without shading and soiling effects and the absolute difference between them.

6. Comparison between simulated and measured values

The data measured between August 27 and October 31, 2020, were compared with the results simulated by Crearray, PVSyst and SAM. In PVSyst, the 3D model generated in SketchUp was imported and the following shading options were considered: detailed, linear (table), linear (simulation) and losses according to string (with fractions of electrical effect set to 60% and 100%). A simplified geometric model was made in SAM, considering the studied PV system, the wall and the trees, with the partial shading option selected. The neighboring PV system was not considered, as SAM has limited set tools for accurate 3D modeling. Another simulation was performed using a shading loss table generated by PVSyst (linear loss) for beam solar radiation considering the sun path over a day. It is expected that the partial shading models of PVSyst (detailed calculation option) and SAM (3D shade calculator) will show results closer to those measured, but all available options were analyzed.

All PV modules used in the system had their I-V curves measured

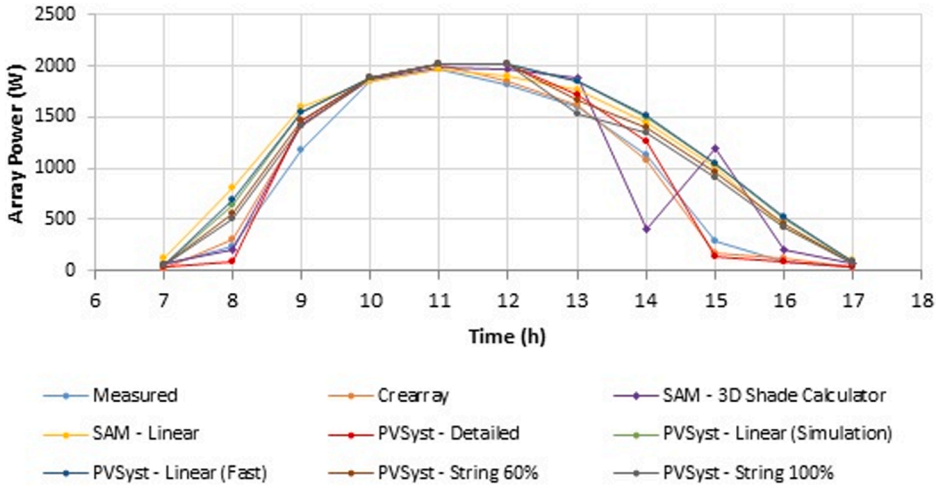

Fig. 9. PV system power (DC) measured and simulated by all tools over a clear day.

with a solar simulator (PASAN, Sunsim 3C), and the mismatch was estimated in the Crearray software. In the simulations, soiling losses of 5%, mismatch losses of 0.7% and ohmic losses of 0.21% were considered. The albedo was considered constant over the period with a value set to 0.4. All analyzes were performed using DC values.

6.1. Comparison of results on a clear day and a cloudy day

Fig. 9 shows the measured and simulated hourly average power over a clear day. On this day, Crearray, PVSyst with detailed model and SAM with 3D model reproduce the effect of tree shadows in the early morning, approaching the measured power, while the other models showed higher average power. In the afternoon, SAM with the geometric model shows a power reduction in the shadow hours but does not coincide with the measured values, while the detailed model of PVSyst and Crearray had results closer to the measured values. The difference showed by SAM with the 3D model is related to the geometric modeling difficulties, where some details were not considered. The other models showed fewer shading effects and greater differences compared to the measured values.

Fig. 10 shows the hourly differences for Crearray, PVSyst (detailed) and SAM (3D shade calculator) in comparison to measured values. The differences between 10 am and 1 pm are lower than the others, times when the system is not shaded (at 10 am and 11 am) or is poorly shaded (at 12 am and 1 pm). The differences vary at other times when there is shading, with both overestimated and underestimated average hourly power. Moreover, the simulated daily energy production is greater than the measured by 5% for PVSyst (detailed) and 10% for SAM (3D shade calculation) for this specific day.

Fig. 11 shows that the shadows predicted by SketchUp and PVSyst are similar to the shadow observed on the PV system. The differences are related to inaccuracies in the 3D representation. However, the software performs hourly calculations, and, as shown in Section 5, shadows vary significantly over an hour. Therefore, although the shadow prediction is close to that visually verified, the use of an hourly shading value may affect the results. The power estimated by Crearray, SAM (3D shade calculator) and PVSyst (detailed) are lower than the measured at some times and higher at other times under shading conditions.

Fig. 12 shows the measured and simulated hourly average power over a cloudy day. Crearray results are considerably close to those measured since it was employed a non-uniform EVF. The EVF varies significantly according to the PV module position in the PV system for this case study. SAM and PVSyst use average values for shading losses in diffuse radiation and albedo. The difference is more significant on cloudy days since they have a greater fraction of diffuse solar radiation. This effect was evident with the influence of the EVF in the analysis of the curves performed in Section 5 and with the similarity between the results obtained by Crearray and those measured. Throughout the day, the electricity simulated by PVSyst (detailed) and SAM (3D shade calculator) was about 7% and 35% higher than the measure one, respectively. All PVSyst models had the same results and the plots overlapped.

6.2. Analysis of the results over the entire measurement period

Fig. 13 shows the difference between the simulated and measured results for 11 am (non-shaded PV system) every day as a function of effective solar irradiance on PV modules. It is verified that the greater the irradiance, the lower the differences calculated for all software. The differences are larger and vary more when the solar irradiance is less than 500 W/m^2. Except for cases of low irradiance (<200 W/m^2), PVSyst and SAM tend to estimate greater production than the measured in situations without shading. However, the hourly differences were less than 10% for solar irradiance above 700 W/m^2 (clear days). Unlike the results of PVSyst, the simulated results in SAM vary with the chosen shading model, the difference that can be related to the surrounding elements not considered in the 3D model.

Table. 1 shows the DC electric energy (kWh) produced over the entire period, which shows that the electricity generated was less than that simulated by all software. Crearray results have the least difference between simulated and measured outputs, as it was used as a comparison standard and to adjust the input parameters. The detailed model of PVSyst had the lowest difference (9%) compared to the other models of PVSyst and SAM. The SAM partial shading calculation had a significant difference between simulated and measured values of 20%, a value close to the difference obtained with the linear loss option. This result for SAM can be associated with the limitations of the 3D modeling.

PVSyst and SAM have different options to perform the simulations that lead to significant differences in the results obtained, reaching a difference of up to 15% between the linear and detailed shading models in PVSyst. These significant differences show that an inappropriate choice of the model by the user can lead to results that are far from those obtained experimentally.

The clear days produced the largest part of the accumulated energy. Among 62 measurement days, 22 were cloudy days (irradiance does not exceed 400 W / m^2 over the day) that produced about 10% of the energy accumulated during the entire measurement period. Table. 2 shows the impact of the difference between the simulated ($E_{S,\ Clear\ day}$) and measured ($E_{M,\ Clear\ day}$) accumulated energy on clear days on the total energy accumulated over the entire measurement period ($E_{M,\ total}$), calculated according to Eq. (7).

$$Difference\ \ in\ \ weight = \frac{(E_{S,Clear\ \ day} - E_{M,Clear\ \ day})}{E_{M,total}} \times 100\% \quad (7)$$

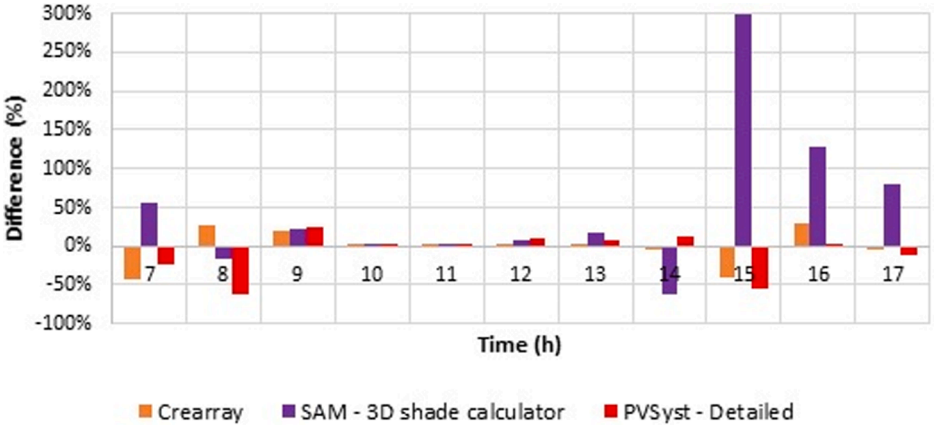

Fig. 10. Differences between simulated and measured hourly average power over a clear day.

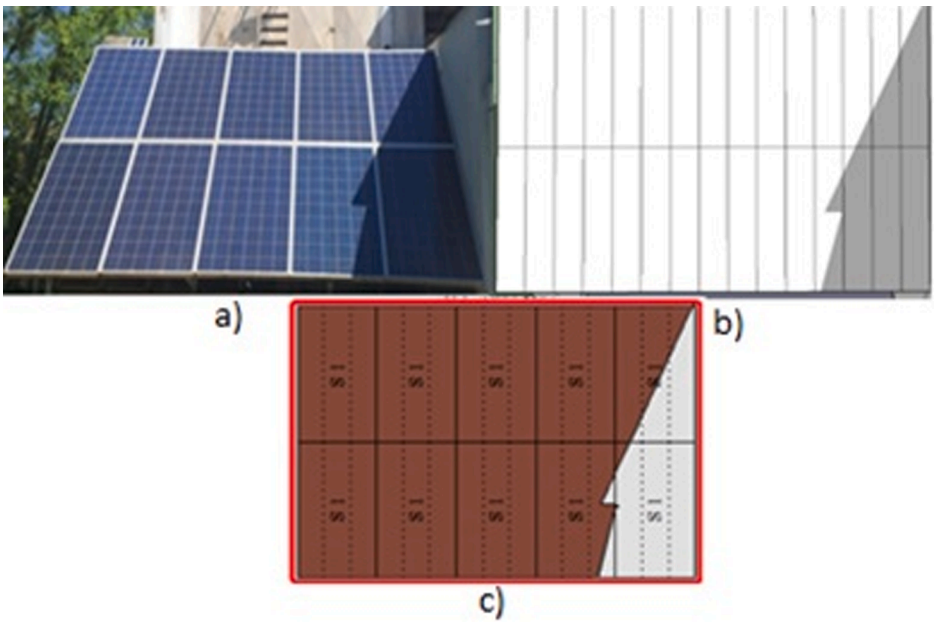

Fig. 11. Comparison between shadow patterns for October 19 at 2:46 pm. (a) system photo; (b) prediction by SketchUp where the lines represent submodules; (c) prediction by PVSyst showing module and submodule divisions.

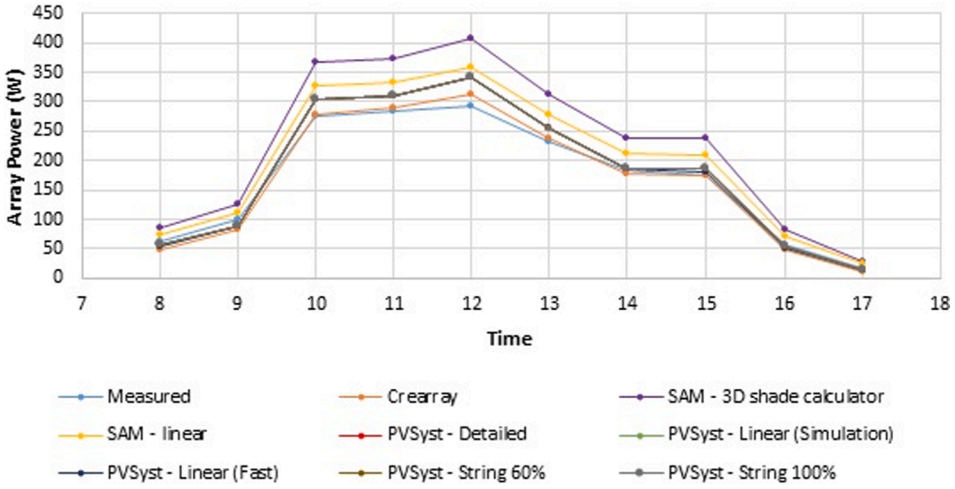

Fig. 12. Simulated and measured PV system power (DC) by all tools over a cloudy day.

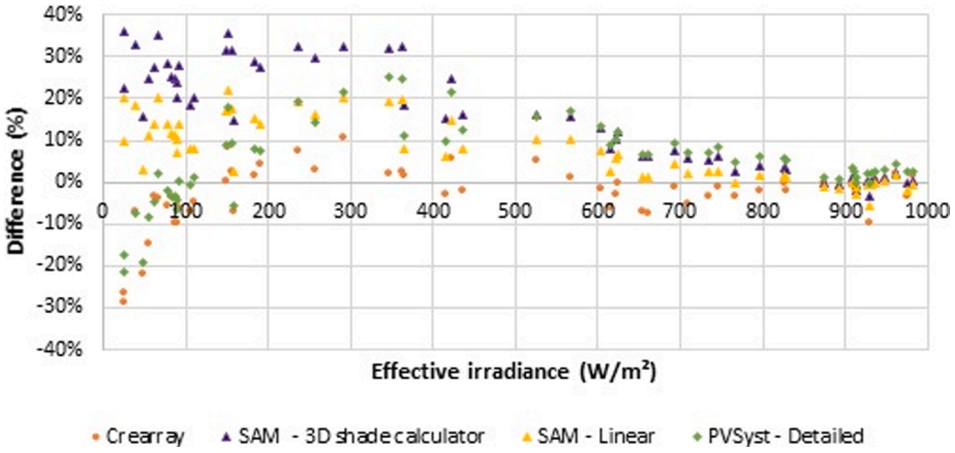

Fig. 13. Difference between simulated and measured results as a function of solar irradiance at 11 am of every measured day.

Table 1
Simulated and measured electricity generated (DC) throughout the entire measurement period.

	Energy (kWh)	Difference (kWh)	Difference %
Measured	309.5	–	–
Crearray	313.7	4.2	1%
SAM - 3D shade calculator	371.3	61.8	20%
SAM - Linear	379.5	70.0	23%
PVSyst - Detailed	338.4	28.9	9%
PVSyst - Linear (Slow)	384.4	74.8	24%
PVSyst - Linear (Fast)	384.1	74.6	24%
PVSyst - String 60%	371.7	62.2	20%
PVSyst - String 100%	363.2	53.7	17%

Table 2
Ratio of the difference between simulated and measured energy for clear days by the energy measured over the entire measurement period.

Model	Simulated energy (kWh)	Difference from the measured value (kWh)	Difference in weight (%)
Crearray	282.6	4.7	2%
SAM - 3D shade calculator	329.3	51.4	17%
SAM - Linear	341.8	63.9	21%
PVSyst - Detailed	305.4	27.5	9%
PVSyst - Linear (Slow)	350.2	72.3	23%
PVSyst - Linear (Fast)	350.1	72.2	23%
PVSyst - String 60%	337.6	59.8	19%
PVSyst - String 100%	329.3	51.4	17%

Table 3 shows these values for cloudy days, showing the impact of the measured ($E_{M,\ Cloudy}$) accumulated energy and the simulated ($E_{S,\ Cloudy}$) one for cloudy days on the total accumulated energy, calculated according to Eq. (8). These values show that the differences between simulated and measured values for cloudy days have a lower effect on accumulated energy, although the daily differences are greater than those obtained for clear days. The lower influence of cloudy days is related to less solar irradiance and less production on these days.

$$Difference\ \ in\ \ weight = \frac{(E_{S,Cloudy\ \ day} - E_{M,Cloudy\ \ day})}{E_{M,total}} \times 100\% \quad (8)$$

Table 3
Ratio of the difference between simulated and measured energy for cloudy days by the energy measured over the entire measurement period.

Model	Simulated energy (kWh)	Difference from the measured value (kWh)	Difference in weight (%)
Crearray	31.1	−0.5	0%
SAM - 3D shade calculator	42.0	10.4	3%
SAM - Linear	37.7	6.0	2%
PVSyst - Detailed	33.0	1.4	0%
PVSyst - Linear (Slow)	34.2	2.6	1%
PVSyst - Linear (Fast)	34.1	2.4	1%
PVSyst - String 60%	34.1	2.4	1%
PVSyst - String 100%	34.0	2.3	1%

6.3. Effect of the surrounding elements on the 3D representation

Considering that the detailed geometric representation with all the surrounding elements is a wearing step, some simulations were made using a more simplified geometric representation. Considering only two trees that shade the system in the morning (the other trees that influence the EVF were not considered), the differences between the simulated and measured accumulated energy were around 22% (for the detailed model) and 35% (linear model) in the PVSyst and around 24% (partial shading) and 32% (linear) in SAM for the entire period considered. In addition, differences would vary between 26% and 37% in PVSyst and between 28% and 33% in SAM if no trees were considered in the 3D model. Therefore, the fewer elements of the surroundings are considered, the greater the difference between the forecasted and measured energy.

Fig. 14 shows the simulated power over a cloudy day considering the detailed model (PVSyst) and partial shading (SAM) for the three surrounding scenarios. It is confirmed that the more detailed the 3D representation is, the closer to accurate the simulations will be, and the elements that do not cause a shadow, but obstruct the horizon, can significantly affect the results.

7. Conclusions

This article analyzed the accuracy and the differences between measured and forecasted power when modeling partially shaded PV systems. Measured DC power was compared to simulations performed using the Crearray, SAM and PVSyst software. Crearray was used to better adjust the input parameters of the simulation to match the measured results. Although the differences between simulated and measured values obtained by the detailed calculation option of PVSyst and the partial shading option of SAM (with 3D representation) were expected to be the smallest, the other options were simulated to analyze the differences for all options available to the user.

Over a clear day, the simulated power was overestimated and underestimated in shading situations, which can be related to the use of hourly shading fractions. The accuracy of the shadow prediction in SketchUp and PVSyst was confirmed. In uniform irradiance conditions, the tools tend to overestimate the power of the PV system.

When performing an analysis of a cloudy day, the surrounding elements that do not cause shadow significantly influence the diffuse solar radiation, since they reduce the effective view factor. The more elements that were considered in the 3D model, the closer to the experimental results was the simulation. Both software use average and uniform shading factors for diffuse radiation (from sky and albedo), which was verified as a possible source of differences between simulated and measured energy values, mainly in cloudy days.

In terms of electricity produced in the entire measurement period, the results obtained by PVSyst with the detailed calculation differ 9% from measured values, which was the smallest difference, as expected. The other options available in PVSyst showed differences of around 20%. The difficulty found in SAM is related to the limited drawing tools, influencing the accuracy of the 3D model, which led to errors in predicting shadows. Although there is an option to import a shading table from PVSyst, this one also showed significant differences. Both the partial shading model and the linear model in SAM had differences of around 20%.

Therefore, partially shaded PV systems should be simulated carefully, and the results can substantially differ from the measured values. In addition, the different options for shading losses calculation lead to significant differences in results, and a wrong choice of the calculation option can lead to results that are far from those obtained experimentally. The differences can also affect the decision of the viability of a given PV system.

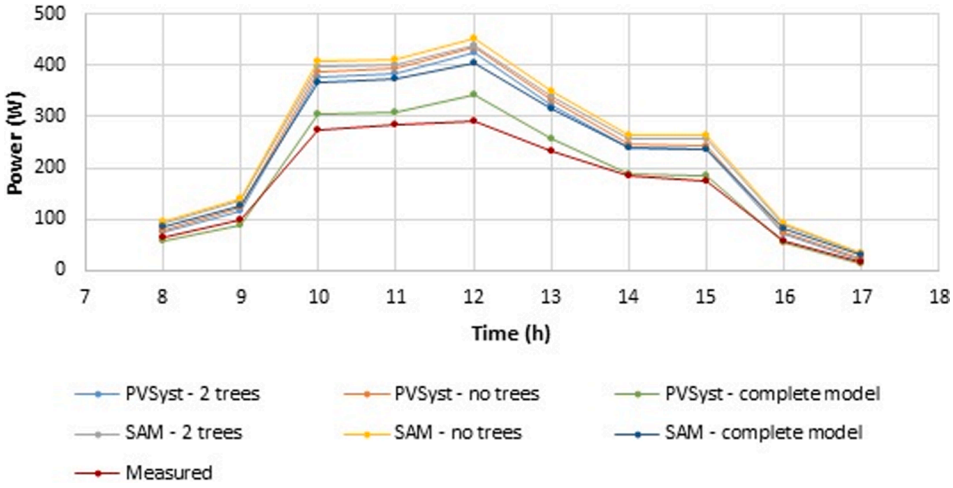

Fig. 14. Simulated power (DC) over a cloudy day for different elements of surroundings.

Declaration of Competing Interest

The authors declare that they have no known competing financial interests or personal relationships that could have appeared to influence the work reported in this paper.

Acknowledgements

This study was financed in part by the Coordenação de Aperfeiçoamento de Pessoal de Nível Superior – Brasil (CAPES) – Finance Code 001 and by the Conselho Nacional de Desenvolvimento Científico e Tecnológico – Brasil.

References

Ahmad, R., Murtaza, A.F., Ahmed Sher, H., Tabrez Shami, U., Olalekan, S., 2017. An analytical approach to study partial shading effects on PV array supported by literature. Renew. Sustain. Energy Rev. 74, 721–732. https://doi.org/10.1016/j.rser.2017.02.078.

Alonso-García, M.C., Ruiz, J.M., Herrmann, W., 2006. Computer simulation of shading effects in photovoltaic arrays. Renew. Energy 31, 1986–1993. https://doi.org/10.1016/j.renene.2005.09.030.

Axaopoulos, P.J., Fylladitakis, E.D., Gkarakis, K., 2014. Accuracy analysis of software for the estimation and planning of photovoltaic installations. Int. J. Energy Environ. Eng. 5, 1–7. https://doi.org/10.1186/2251-6832-5-1.

Bai, J., Cao, Y., Hao, Y., Zhang, Z., Liu, S., Cao, F., 2015. Characteristic output of PV systems under partial shading or mismatch conditions. Sol. Energy 112, 41–54. https://doi.org/10.1016/j.solener.2014.09.048.

Baka, M., Manganiello, P., Soudris, D., Catthoor, F., 2019. A cost-benefit analysis for reconfigurable PV modules under shading. Sol. Energy 178, 69–78. https://doi.org/10.1016/j.solener.2018.11.063.

Belmahdi, B., Bouardi, A.E., 2020. Solar potential assessment using PVsyst software in the Northern Zone of Morocco. Procedia Manuf. 46, 738–745. https://doi.org/10.1016/j.promfg.2020.03.104.

Bogdanov, D., Farfan, J., Sadovskaia, K., Aghahosseini, A., Child, M., Gulagi, A., Oyewo, A.S., de Souza Noel Simas Barbosa, L., Breyer, C., 2019. Radical transformation pathway towards sustainable electricity via evolutionary steps. Nat. Commun. 10, 1–16. https://doi.org/10.1038/s41467-019-08855-1.

Chepp, E.D., Krenzinger, A., 2021. A methodology for prediction and assessment of shading on PV systems. Sol. Energy 216, 537–550. https://doi.org/10.1016/j.solener.2021.01.002.

da Rocha, M.V., Sampaio, L.P., da Silva, S.A.O., 2020. Comparative analysis of MPPT algorithms based on Bat algorithm for PV systems under partial shading condition. Sustain. Energy Technol. Assessments 40, 100761. https://doi.org/10.1016/j.seta.2020.100761.

Daliento, S., Di Napoli, F., Guerriero, P., d'Alessandro, V., 2016. A modified bypass circuit for improved hot spot reliability of solar panels subject to partial shading. Sol. Energy 134, 211–218. https://doi.org/10.1016/j.solener.2016.05.001.

De Soto, W., Klein, S.A., Beckman, W.A., 2006. Improvement and validation of a model for photovoltaic array performance. Sol. Energy 80, 78–88. https://doi.org/10.1016/j.solener.2005.06.010.

Deline, C., Dobos, A., Janzou, S., Meydbray, J., Donovan, M., 2013. A simplified model of uniform shading in large photovoltaic arrays. Sol. Energy 96, 274–282. https://doi.org/10.1016/j.solener.2013.07.008.

Dey, D., Subudhi, B., 2020. Design, simulation and economic evaluation of 90 kW grid connected Photovoltaic system. Energy Rep. 6, 1778–1787. https://doi.org/10.1016/j.egyr.2020.04.027.

Duffie, J.A., Beckman, W.A., 2013. Wiley: Solar Engineering of Thermal Processes, 4th Edition - John A. Duffie, William A. Beckman.

Fanney, A.H., Dougherty, B.P., Davis, M.W., 2003. Short-term characterization of building integrated photovoltaic panels. J. Sol. Energy Eng. Trans. ASME 125, 13–20. https://doi.org/10.1115/1.1531642.

Freeman, J., Whitmore, J., Blair, N., Dobos, A.P., 2014. Validation of multiple tools for flat plate photovoltaic modeling against measured data. In: 2014 IEEE 40th Photovolt. Spec. Conf. PVSC 2014 1932–1937. https://doi.org/10.1109/PVSC.2014.6925304.

Gallardo-Saavedra, S., Karlsson, B., 2018. Simulation, validation and analysis of shading effects on a PV system. Sol. Energy 170, 828–839. https://doi.org/10.1016/j.solener.2018.06.035.

Ghosh, S., Yadav, V.K., Mukherjee, V., 2019. Improvement of partial shading resilience of PV array though modified bypass arrangement. Renew. Energy 143, 1079–1093. https://doi.org/10.1016/j.renene.2019.05.062.

Jacobson, M.Z., Delucchi, M.A., Bauer, Z.A.F., Goodman, S.C., Chapman, W.E., Cameron, M.A., Bozonnat, C., Chobadi, L., Clonts, H.A., Enevoldsen, P., Erwin, J.R., Fobi, S.N., Goldstrom, O.K., Hennessy, E.M., Liu, J., Lo, J., Meyer, C.B., Morris, S.B., Moy, K.R., O'Neill, P.L., Petkov, I., Redfern, S., Schucker, R., Sontag, M.A., Wang, J., Weiner, E., Yachanin, A.S., 2017. 100% clean and renewable wind, water, and sunlight all-sector energy roadmaps for 139 countries of the world. Joule 1, 108–121. https://doi.org/10.1016/j.joule.2017.07.005.

Jäger-Waldau, A., 2020. Snapshot of photovoltaics-February 2020. Energies 13. https://doi.org/10.3390/en13040930.

Karatepe, E., Boztepe, M., Metin, C., 2007. Development of a suitable model for characterizing photovoltaic arrays with shaded solar cells 81, 977–992. https://doi.org/10.1016/j.solener.2006.12.001.

Kermadi, M., Jack, V., Mekhilef, S., Salam, Z., 2020. A fast and accurate generalized analytical approach for PV arrays modeling under partial shading conditions. Sol. Energy 208, 753–765. https://doi.org/10.1016/j.solener.2020.07.077.

King, D.L., Kratochvil, J.A., Boyson, W.E., 1998. Field Experience With a New Performance Characterization Procedure for Photovoltaic Arrays. world Conf. Exhib. Photovolt. Sol. energy conversion, Vienna (AT), 07/06/1998–07/10/1998.

Kumar, N.M., Kumar, M.R., Rejoice, P.R., Mathew, M., 2017. Performance analysis of 100 kWp grid connected Si-poly photovoltaic system using PVsyst simulation tool. Energy Procedia 117, 180–189. https://doi.org/10.1016/j.egypro.2017.05.121.

Kumar, R., Rajoria, C.S., Sharma, A., Suhag, S., 2020. Materials Today: Proceedings Design and simulation of standalone solar PV system using PVsyst Software: A case study. In: Materials Today: Proceedings. Elsevier Ltd. https://doi.org/10.1016/j.matpr.2020.08.785

Macalpine, S., Deline, C., 2015. Simplified method for modeling the impact of arbitrary partial shading conditions on PV array performance. In: 2015 IEEE 42nd Photovolt. Spec. Conf. PVSC 2015. https://doi.org/10.1109/PVSC.2015.7355938.

Mermoud, A., Lejeune, T., 2010. Partial shadings on PV arrays: By-pass diode benefits analysis. Eur. Photovolt. Sol. Energy Conf. 6–10.

Mikofski, M.A., Lynn, M., Byrne, J., Hamer, M., Neubert, A., Newmiller, J., 2018. Accurate performance predictions of large PV systems with shading using submodule mismatch calculation. In: 2018 IEEE 7th World Conf. Photovolt. Energy Conversion, WCPEC 2018 - A Jt. Conf. 45th IEEE PVSC, 28th PVSEC 34th EU PVSEC 3635–3639. https://doi.org/10.1109/PVSC.2018.8547323.

Mohammadnejad, S., Khalafi, A., Ahmadi, S.M., 2016. Mathematical analysis of total-cross-tied photovoltaic array under partial shading condition and its comparison with other configurations. Sol. Energy 133, 501–511. https://doi.org/10.1016/j.solener.2016.03.058.

Mohammed, H., Kumar, M., Gupta, R., 2020. Bypass diode effect on temperature distribution in crystalline silicon photovoltaic module under partial shading. Sol. Energy 208, 182–194. https://doi.org/10.1016/j.solener.2020.07.087.

Mohapatra, A., Nayak, B., Das, P., Mohanty, K.B., 2017. A review on MPPT techniques of PV system under partial shading condition. Renew. Sustain. Energy Rev. 80, 854–867. https://doi.org/10.1016/j.rser.2017.05.083.

Mondol, J.D., Yohanis, Y.G., Norton, B., 2007. Comparison of measured and predicted long term performance of grid a connected photovoltaic system. Energy Convers. Manag. 48, 1065–1080. https://doi.org/10.1016/j.enconman.2006.10.021.

Palmero-marrero, A., Matos, J.C., 2015. Comparison of software prediction and measured performance of a grid-connected photovoltaic power plant. J. Renew. Sustain. Energy. doi 10 (1063/1), 4935376.

PVSyst, 2021. PVSyst 7 Help.

Quesada, B., Sánchez, C., Cañada, J., Royo, R., Payá, J., 2011. Experimental results and simulation with TRNSYS of a 7.2kWp grid-connected photovoltaic system. Appl. Energy 88, 1772–1783. https://doi.org/10.1016/j.apenergy.2010.12.011.

Ram, J.P., Babu, T.S., Rajasekar, N., 2017. A comprehensive review on solar PV maximum power point tracking techniques. Renew. Sustain. Energy Rev. 67, 826–847. https://doi.org/10.1016/j.rser.2016.09.076.

Sai Krishna, G., Moger, T., 2019. Reconfiguration strategies for reducing partial shading effects in photovoltaic arrays: state of the art. Sol. Energy 182, 429–452. https://doi.org/10.1016/j.solener.2019.02.057.

Saiprakash, C., Mohapatra, A., Nayak, B., Ghatak, S.R., 2020. Analysis of partial shading effect on energy output of different solar PV array configurations. Mater. Today Proc. https://doi.org/10.1016/j.matpr.2020.08.307.

SAM, 2020. SAM Help.

Sharma, R., Gidwani, L., 2017. Grid connected solar PV system design and calculation by using PV SOL premium simulation tool for campus hostels of RTU Kota. In: Proc. IEEE Int. Conf. Circuit, Power Comput. Technol. ICCPCT 2017 1–5. https://doi.org/10.1109/ICCPCT.2017.8074315.

Shukla, A.K., Sudhakar, K., Baredar, P., 2016. Design, simulation and economic analysis of standalone roof top solar PV system in India. Sol. Energy 437–449.

Trzmiel, G., Głuchy, D., Kurz, D., 2020. The impact of shading on the exploitation of photovoltaic installations. Renew. Energy 153, 480–498. https://doi.org/10.1016/j.renene.2020.02.010.

Verma, P., Garg, R., Mahajan, P., 2020. Asymmetrical interval type-2 fuzzy logic control based MPPT tuning for PV system under partial shading condition. ISA Trans. 100, 251–263. https://doi.org/10.1016/j.isatra.2020.01.009.

Victoria, M., Haegel, N., Peters, I.M., Sinton, R., Jäger-Waldau, A., del Cañizo, C., Breyer, C., Stocks, M., Blakers, A., Kaizuka, I., Komoto, K., Smets, A., 2021. Solar photovoltaics is ready to power a sustainable future. Joule 1–16. https://doi.org/10.1016/j.joule.2021.03.005.

Wijeratne, W.M.P.U., Yang, R.J., Too, E., Wakefield, R., 2019. Design and development of distributed solar PV systems: do the current tools work? Sustain. Cities Soc. 45, 553–578. https://doi.org/10.1016/j.scs.2018.11.035.

Renewable Energy 200 (2022) 900–910

Contents lists available at ScienceDirect

Renewable Energy

journal homepage: www.elsevier.com/locate/renene

Improvements in methods for analysis of partially shaded PV modules

Ellen David Chepp *, Fabiano Perin Gasparin, Arno Krenzinger

Universidade Federal Do Rio Grande Do Sul, Solar Energy Laboratory, Brazil

ARTICLE INFO

Keywords:
Photovoltaic
Modeling
Shading
Mismatch

ABSTRACT

Several methods for analyzing photovoltaic (PV) systems under partial shading conditions (PSC) can be found in the literature. However, the simplest methods are not very accurate. This article presents (1) a simple and accurate method to model I–V curves for PSC and (2) an improvement of a simplified method, without calculating the I–V curves, to accurately estimate the energy generated by PV systems under PSC. The I–V curves of two PV modules under PSC were measured. The measured curves were compared with modeled curves using two methods from the literature and a new proposed method. Four simplified methods from the literature for estimating the energy generated by PV systems were analyzed. The accuracy of these methods was investigated by comparing the calculated values with measured data from a PV system. For modeling the I–V curves, the new method showed a mean absolute percentage error of 1.5% and proved to be accurate. For the evaluated PV system, using a monthly database and the proposed diffuse shading factor resulted in differences between the measured and modeled results of up to 10% per month and 5% for the entire measurement period. The two proposed methods are simple and accurate.

1. Introduction

Given the growing concern about environmental issues, renewable energy sources are increasingly being used around the world. Photovoltaics (PV) has gained prominence in this context, about 126 GW of power was installed worldwide in 2020 [1,2]. Total installed PV capacity was 710 GW by 2020, representing 25.3% of the global installed capacity from renewable sources [2].

PV modules in urban environments are often subject to partial shading conditions (PSC), which leads to losses in incident solar radiation and consequently in PV module output [3,4]. Since these are important losses in PV systems, there are several works in the literature dealing with the analysis of partial shading effects [5–7], ways of mitigating losses [8,9], and modeling of shaded PV systems [10,11].

PV systems under PSC are often analyzed in detail using modeled or measured I–V and P–V curves [12–14]. However, modeling these curves is not always straightforward because many input data and calculation steps are required. For less detailed analyzes, there are simplified equations to calculate the energy generated by the PV system under PSC for a given time period, which is particularly useful for PV designers [15, 16].

There are methods to facilitate the modeling of the I–V curve of PV modules and simplified methods to calculate the maximum power of PV systems under non-uniform partial shading. For example, it is possible to consider as a hypothesis only the condition of the most shaded cell per submodule [17], but this may affect the accuracy of the results, with differences especially in the open-circuit region of the I–V curve. Furthermore, simplified methods for energy calculation only consider the effects of shading on the beam component of solar radiation and ignore the effects on diffuse radiation, which can lead to differences in the comparison of modeling and measurements [18].

Therefore, in this article, the effects of PSC on measured I–V curves were evaluated and a simple and accurate method for modeling the I–V curves was proposed. An improvement of a simplified method found in the literature for energy calculation was proposed to increase the accuracy of the results and was used to analyze a PV system under PSC. The methods found in the literature were also analyzed and compare with the proposed method. The study presented in this article can be divided into two parts: (1) proposing an accurate and simple method for modeling the I–V curves of PV modules under PSC, and (2) proposing an improvement of a simplified method for accurately estimating the generated energy (without modeling the I–V curve) in PV systems under PSC.

This article is structured as follows. The effect of shading and some modeling methods for shaded PV systems found in the literature are discussed in Section 2. The methodology is described in Section 3. In

* Corresponding author.
E-mail address: ellen.chepp@gmail.com (E.D. Chepp).

https://doi.org/10.1016/j.renene.2022.10.035
Received 31 May 2022; Received in revised form 1 September 2022; Accepted 8 October 2022
Available online 12 October 2022

Section 4, the results are shown and discussed. Limitations of the proposed methods are provided in Section 5. Finally, the conclusions are presented in Section 6.

2. Modeling of partially shaded PV modules

A PV module generally consists of cells connected in series. When a PV cell in a series is shaded, the current generated by that cell is less than the current generated by the other cells, limiting the current of the entire series. The shaded cell is reverse biased, dissipating power and heating up, which can lead to overheating and hot spots. To prevent this overheating, bypass diodes are connected antiparallel to a group of cells connected in series to serve as an alternative path for current in the event of cell failure or shading. Each group of cells connected in series and then antiparallel to a bypass diode is called a submodule.

The effect of partial shading on a PV module with three bypass diodes can be analyzed in Fig. 1, which shows the I–V curves of three submodules, two of which are partially shaded, and the resulting I–V curve of the module. The resulting I–V curve was divided into three voltage regions (R1, R2, and R3) corresponding to the highlighted short-circuit points of the submodules. In R1, the PV module current is larger than the short-circuit currents of submodules 2 and 3 (I_{sc2} and I_{sc3}), so both submodules are reverse biased. In R2, the current is greater than I_{sc3}, so only submodule 3 is reverse biased. From the point where the current is less than I_{sc3}, in R3, the three submodules are forward biased. Therefore, if the module current is greater than the I_{sc} of a submodule, this submodule is reverse biased so that the current flows through the bypass diode.

Accurate modeling of PV modules is important for performance analysis and estimation of energy generation over time. A review of

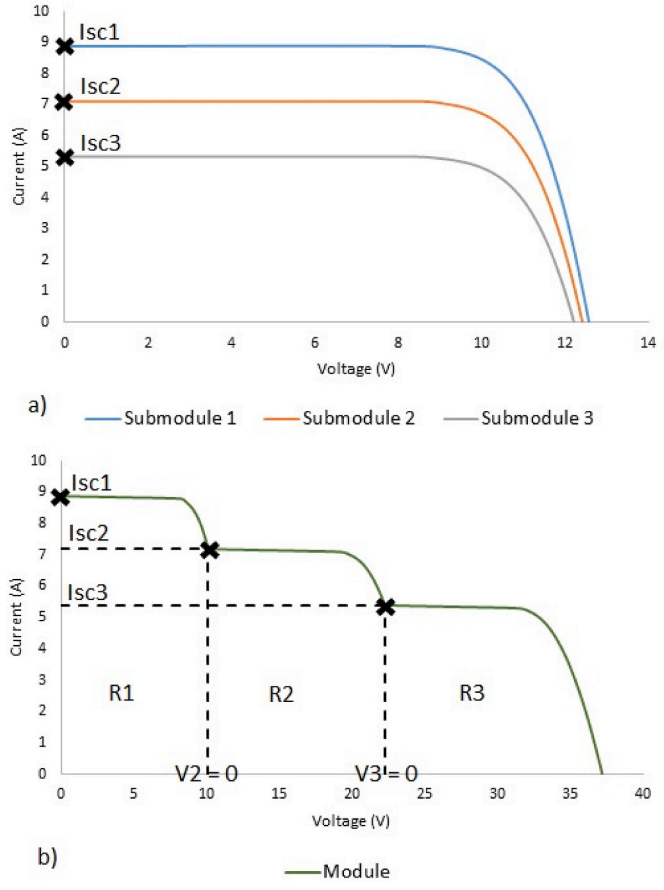

Fig. 1. (a) I–V curves of three submodules under different irradiance conditions and (b) I–V curve of the PV module.

techniques for modeling uniform and non-uniform conditions was provided by Jena and Ramana [19]. PV modules are often modeled accurately based on the I–V curve of the PV cell using the single diode model or the two-diode model [11,20]. In the case of a PV module under uniform conditions, the cell model can be easily scaled to a module, since the I–V curves of the cells can be considered identical. When a PV module is partially shaded, the cells are not under the same conditions, so the I–V curves of the shaded and unshaded cells are different. There are situations where PV modules are uniformly shaded, when the modules have the same shading fraction, which can occur, for example, due to inter-rows shading. In these cases, the performance of the PV systems can be analyzed using equations such as those proposed by Deline et al. [21] and Thakkar et al. [22]. However, the PV cells may have different shading fractions when the shading is non-uniform. Therefore, the modeling of the PV system becomes more complex as the number of PV modules and shading fractions increase.

Given the complexity associated with modeling PV systems with non-uniform partial shading, some considerations and simplifications can be made to model the I–V curve. One way to reduce the simulation steps is to perform submodule simulations, an approach analyzed by Qing et al. [23] and MacAlpine et al. [24]. Since partial shading mainly reduces the current of the shaded cell and this current limits the current of the other cells connected in series, one option is to consider the whole submodule under the same conditions as the most shaded cell, as suggested by Mikofski et al. [17]. Some authors, such as Ayop et al. [25], Kermadi et al. [26] and Zhang et al. [27], proposed adjustments in modeling the I–V curve for PSC to simplify the modeling and reduce the simulation time.

Designers and some computer programs for PV system design use simplified methods to estimate shading losses, since the main goal is to estimate energy production rather than the exact behavior of the PV system at a given time. These methods have advantages such as the small number of input parameters about the cells and bypass diodes, in addition to the shorter simulation time, which are very useful for estimating the performance of PV systems [16]. On the other hand, may occur different electrical losses for the same fraction of a shaded area with different shading patterns [6,28]. Furthermore, PV system configuration and inverter characteristics also affect the losses [29–31]. All these factors are not considered in these simplified methods.

Estimation of shading losses without modeling the I–V curve can be achieved by assuming that the electrical losses are directly proportional to the solar radiation losses or the shading fraction since the short-circuit current is directly proportional to the incident solar irradiance [15,24]. Following this approach, Martinez-Moreno et al. [15] proposed an empirical method to calculate the effective shading fraction, considering the fraction of shaded area and the number of shaded submodules. This fraction was applied only to beam solar radiation in the proposed calculation. Zomer and Rüther [32] proposed to estimate the electricity production of a shaded PV system based on the average annual shaded area, which would correspond to the shading losses in the annual yield. Macalpine and Deline [33] proposed a database for shading losses as a function of the shading fraction and the diffuse radiation fraction and verified that this method gives accurate results. However, the difficulty in applying this simplification is the size of the required database.

Many simplified methods found in the literature consider shading losses only for the beam component of solar radiation, without considering the complete surroundings of the PV installation. However, the surroundings can significantly affect diffuse shading fractions in some cases [34]. Chepp et al. [18] modeled a PV system in the software PVSyst and System Advisor Model (SAM), compared the results with the values measured on site and discussed the importance of considering the surrounding elements.

3. Methodology

The methodology was divided into two parts: (1) experimental

analysis of the I–V curve under different PSC configurations to identify the behavior of the I–V curve and show where the proposed improvement in modeling is achieved; and (2) analysis of the limitations of simplified methods for estimating the energy generated by a PV system under PSC to improve the accuracy.

3.1. Analysis and modeling of I–V curves of PV modules under PSC

An experimental analysis of different configurations of PSC in I–V curves was performed. The measured I–V curves were modeled using two different calculation methods and a new method proposed here. These modeling methods were implemented using the Python programming language. Finally, the measured and modeled I–V curves for different PSC were compared. In this article, NS1 represents the number of shaded cells in submodule 1, NS2 represents the number of shaded cells in submodule 2, FS1 represents the shading fraction (percentage of a cell area covered) in submodule 1, and FS2 has the same meaning for submodule 2.

3.1.1. Experimental analysis of I–V curves of PV modules under PSC

The I–V curves of two PV modules under different PSC were measured in a solar simulator (PASAN, SunSim 3C). The electrical characteristics of the two PV modules for the standard test conditions are shown in Table 1.

First, the I–V curves of Module A with only one covered cell (NS1 = 1) were measured with different shaded area fractions (FS): 25%, 50%, 75% and 100%. To verify the detailed behavior of the I–V curve under shading, the I–V curves of Module A were measured under other conditions varying the shading fraction and shading pattern as follows.

I. Submodule 1: only one cell is covered by a shading net (attenuation 25%). Submodule 2: 50% of a cell area is covered by an opaque material. In the results section, this configuration is shown as NS1 = 1, NS2 = 1, FS1 = 25%, FS2 = 50%.
II. All cells of submodule 1 were uniformly shaded by a shading net (50%). In the results section, this condition is shown as NS1 = 20, FS1 = 50%.
III. Only one cell of submodule 1 was 25% shaded by an opaque material; all cells of submodule 2 were uniformly shaded by a shading net (50%). This condition is presented as NS1 = 1, NS2 = 20, FS1 = 25%, FS2 = 50%.
IV. Submodule 1: all cells were uniformly shaded by a shading net (30%). Submodule 2: all cells were uniformly shaded by a shading net (50%). In the results section, this case is presented as NS1 = 20, NS2 = 20, FS1 = 30%, FS2 = 50%.

Similar tests were performed with Module B, varying the shading fraction and the number of shaded cells to confirm the behavior verified in Module A.

3.1.2. Modeling of I–V curves using cell-by-cell method

In the cell-by-cell method, the I–V curve of each cell is modeled individually. The single diode model was used to calculate the I–V curve, according to Eq. (1), for positive voltages. For negative voltages, a term corresponding to the avalanche breakdown is added to the equation, according to Eq. (2) proposed by Bishop [35].

$$I = I_L - I_o\left[exp\left(\frac{q\,(V+IR_s)}{nkT}\right)-1\right]-\frac{V+IR_s}{R_{sh}} \tag{1}$$

$$I = I_L - I_o\left[exp\left(\frac{q\,(V+IR_s)}{nkT}\right)-1\right]-\frac{V+IR_s}{R_{sh}}\left\{1+a\left(1-\frac{V+IR_s}{V_{br}}\right)^{-m}\right\} \tag{2}$$

To use these equations, five parameters of the PV cells must first be determined: shunt resistance (R_{sh}), series resistance (R_s), ideality factor (n), reverse saturation current of the diode (I_0), and photogenerated current (I_L). These five parameters were determined according to the method proposed by Villalva et al. [36] using the I–V curve measured under standard test conditions. The shunt and series resistances were corrected according to the irradiance using Eqs. (3) and (4) proposed by De Soto et al. [37] and Ruschel et al. [38], respectively. The parameters used for the avalanche breakdown are the fraction of ohmic current involved in the avalanche breakdown (a), the breakdown voltage (V_{br}), and the avalanche breakdown exponent (m), which were experimentally determined by Peroza et al. [39]. In addition, the device current (I) is calculated considering the device voltage (V), electron charge (q), Boltzmann constant (k) and temperature (T).

$$R_{sh} = R_{sh0}\left(\frac{G_0}{G}\right) \tag{3}$$

$$R_s = \left(10.361\ G^{-0.342}\right)R_{s0} \tag{4}$$

The I–V curve of the submodule is obtained by summing the voltages of the I–V curves of the individual cells at constant current values, since the cells are connected in series. To simplify this, the I–V curves were modeled for different irradiance conditions. Then the voltages of each I–V curve were multiplied by the number of cells under the same conditions. Each submodule has a bypass diode, so the equation of the bypass diode is considered for the negative currents of each submodule after adding the curves of cells. Eq. (5) is the equation for bypass diode current (I_B), which depends on the bypass diode reverse saturation current (I_{OB}), the submodule reverse voltage (V_B), the bypass diode ideality factor (m_B) and the bypass diode temperature (T_B). Finally, the I–V curves of the submodules are summed to calculate the module I–V curve of the whole PV.

$$I_B = I_{OB}\left[exp\left(\frac{q\,V_B}{m_B k T_B}\right)-1\right] \tag{5}$$

3.1.3. Modeling of I–V curves using worst cell condition (WCC) for each submodule

In this method of modeling the I–V curve of a partially shaded PV module, it is assumed that the entire submodule is under the worst cell conditions, the so-called WCC method. Thus, if the most shaded cell (worst cell) of the submodule receives 50% of the solar radiation incident on the other unshaded cells, it is assumed that the entire submodule receives 50% of the solar radiation. In this way, the I–V curve of the submodule was modeled as if it were uniformly shading. The five parameters of Eq. (1) were determined for a submodule from the I–V curve measured experimentally under uniform radiation conditions, following the method proposed by Villalva et al. [36]. Eq. (6) was used for positive voltages, where N is the number of cells connected in series in the submodule, and $I = I_B$, given in Eq. (5), was used for negative voltages. The series and shunt resistances were also corrected according to Eqs. (3) and (4). After modeling the I–V curves of each submodule, these curves are summed.

$$I = I_L - I_o\left[exp\left(\frac{q\,(V+IR_s)}{nkTN}\right)-1\right]-\frac{V+IR_s}{R_{sh}} \tag{6}$$

Table 1
Electrical characteristics of PV modules used in this work.

	Module A	Module B
Maximum power (P_{mp})	260 Wp	270 Wp
Maximum power voltage (V_{mp})	30.4 V	31.12 V
Maximum power current (I_{mp})	8.56 A	8.71 A
Open-circuit voltage (V_{oc})	37.5 V	38.21 V
Short-circuit current (I_{sc})	9.12 A	9.25 A
Module efficiency	16.16%	16.60%
Number of cells	60	60
Number of bypass diodes	3	3

3.1.4. Proposed improvement for modeling I–V curves for PSC

For a shaded submodule, the I–V curve of this submodule was modeled under unshaded conditions and then adjusted for PSC. The current (I_{adj}) was adjusted by calculating the short-circuit current for the most shaded cell, taking into account that the current varies linearly with incident irradiance and that the smallest current limits the entire string. In addition, the shunt resistance affects the slope of the I–V curve in the short-circuit region. Therefore, the I–V curve was limited to the short-circuit current of the worst cell considering the slope caused by the shunt resistance according to Eq. (7).

$$I_{adj} = I_{sc} - \frac{1}{R_{sh}} V \tag{7}$$

The I–V curve voltage (V_{adj}) was fitted starting from the open-circuit voltage of the I–V curve under uniform conditions (V_{oc}), according to Eq. (8), taking into account that the open-circuit voltage varies logarithmically with the irradiance. The number of shaded cells (N_{SC}), ideality factor (n), Boltzmann constant (k), temperature (T), electron charge (q), irradiance of the most shaded cell (G_S) and irradiance of the unshaded cells (G) were considered in the calculation.

$$V_{adj} = V_{oc} + N_{SC} \frac{nkT}{q} ln \frac{G_S}{G} \tag{8}$$

Then, the I–V curves of the submodules were summed. Eqs. (3)–(6) were used to correct the shunt and series resistances and to calculate the current for positive and negative voltages. The five parameters of the submodule were also determined according to the method proposed by Villalva et al. [36].

3.2. Estimation of the energy generated by a PV system under PSC

The energy generated by a PV system was measured in direct current (DC). The shading losses were estimated using the five methods described in Sections 3.2.2 and 3.2.3 and compared with measurements. Analyzes were performed using two databases: an hourly database and a monthly database for the measurement period. Only losses due to shading, dust (5%) and spectral reflectance of the glass of the PV modules were considered.

3.2.1. Description of the PV system under PSC

The PV system under study is installed in Porto Alegre (30°4′28.4″S 51°7′31.8″W) at Universidade Federal do Rio Grande do Sul (UFRGS), in southern Brazil. It consists of 10 PV modules of 245 Wp tilted at 50° to the north and is connected to the grid through a 2500 W inverter. This system is partially shaded in the early morning and afternoon by trees and a neighboring PV system. The PV system power, solar irradiance and temperature of a PV module were measured, and the average values were stored every 15 min for the period from August 27, 2020 to January 31, 2021. The PV system and measurement equipment can be seen in Fig. 2, and the surrounding are shown in Fig. 3. Chepp et al. [18] have described this PV system and the measurement equipment used in detail.

3.2.2. Simplified methods for the analysis of PV systems under PSC

Martínez-Moreno et al. [15] proposed Eq. (9) to calculate the effective shading fraction (F_{ES}), which is used to calculate the shaded system power (P_S) according to Eq. (10). The proposed effective shading fraction considers the shaded area fraction of the PV system (F_S), the number of shaded submodules (N_{SM}) and the total number of submodules (N_T). The power of the shaded system is calculated from the estimated power for the unshaded PV system (P_{Un}), taking into account the beam (B), diffuse (D), reflected (R) and total (G) solar irradiance incident on the PV module plane.

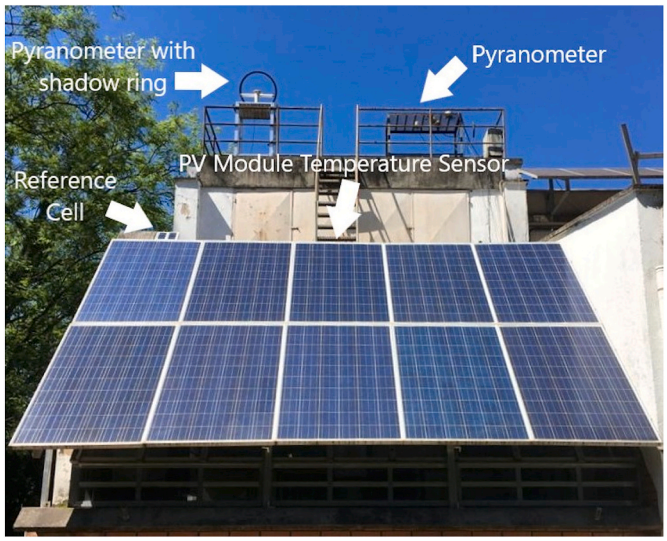

Fig. 2. Photo of the PV system with the indicated measurement equipment. Source: Chepp et al. [18].

$$(1 - F_{ES}) = (1 - F_S)\left(1 - \frac{N_{SM}}{N_T + 1}\right) \tag{9}$$

$$P_S = P_{Un}\left(\frac{B\,(1 - F_{ES}) + D + R}{G}\right) \tag{10}$$

Three other simplified methods were analyzed by Martínez-Moreno et al. [15] and also used for comparison in this article. The effective shading fractions calculated by these three methods were also used in Eq. (10) to calculate the PV power.

In Simplified Method 1 (SM 1), the effective shading fraction is equated to the fraction of the shaded area, according to Eq. (11).

$$F_{ES} = F_S \tag{11}$$

Simplified Method 2 (SM 2) assumes that any shadow that reaches the PV system causes a loss of 100% of the beam solar radiation, according to Eq. (12). This consideration leads to a more pessimistic estimate of the losses.

$$F_S > 0 \rightarrow F_{ES} = 1 \tag{12}$$

Simplified Method 3 (SM 3) only considers the number of shaded submodules, according to Eq. (13).

$$F_{ES} = \frac{N_{SM}}{N_T} \tag{13}$$

3.2.3. Proposed improvement for a simplified method of PV systems under PSC

Martínez-Moreno et al. [15] assumed that shading only reduces incident beam solar radiation, while losses related to diffuse and reflected solar radiation are considered insignificant. In this article, a diffuse shading factor (F_{DS}) is proposed. Therefore, the power of the shaded PV system was calculated according to Eq. (14) with the proposed improvement. The F_{ES} is also calculated according to Eq. (9) in this case.

$$P_S = P_{Un}\left(\frac{B\,(1 - F_{ES}) + D\,(1 - F_{DS}) + R}{G}\right) \tag{14}$$

For the automatic analysis of shading, the PV system under study and the elements of its surroundings were modeled in the software SketchUp. The shading fractions and the number of shaded submodules were determined using EnergyPlus software. The factor by which the diffuse solar radiation is multiplied (1 – F_{DS}) was determined using an

Fig. 3. Photo of the surroundings of the PV system. Source: Chepp et al. [18].

extension of SketchUp software, Sky View Analysis, which calculates the sky view factor for a given point in the 3D model. The sky view factor for a central point of the PV modules determined by this extension was 0.7, which is close to the value estimated by PVSyst software and validated by Chepp et al. [18] with experimental I–V curves for the same PV system. This factor can also be determined using other software that provides a 3D representation of the PV system and its surroundings, and in some cases, a visual estimate can also be made at the PV system site.

4. Results and discussion

4.1. Comparison between measured and modeled I–V curves

In this section, the measured I–V curves of two PV modules under PSC are analyzed and the effects of PSC are described. Modeled and measured I–V curves are compared. Finally, the differences in the maximum power point are calculated and presented.

4.1.1. Analysis of experimental I–V curves under PSC

Fig. 4 shows the I–V curves of Module A measured with only one shaded cell (NS = 1) and under different shading fractions (FS). When one cell is shaded, the current of the entire submodule decreases proportionally to the shading fraction of that cell, as shown in Fig. 4.

The effect of the number of shaded cells and the shading fraction in the I–V curve is shown in Fig. 5. Comparing the I–V curve of Module A for a 25% shaded cell of submodule 1 and a 50% shaded cell of submodule 2 (NS1 = 1 and NS2 = 1; FS1 = 25% and FS2 = 50%) with the I–V curve for two uniformly shaded submodules with fractions of 30% and 50% (NS1 = 20 and NS2 = 20; FS1 = 30% and FS2 = 50%) in Fig. 5, it can be seen that the two curves in the highlighted region 2 have the same current level. This region corresponds to the forward bias of the submodule with a shading fraction of 50% (submodule 2). When only one cell of submodule 2 is 50% shaded, the slope of the I–V curve in the short-circuit region of this submodule increases due to the electrical

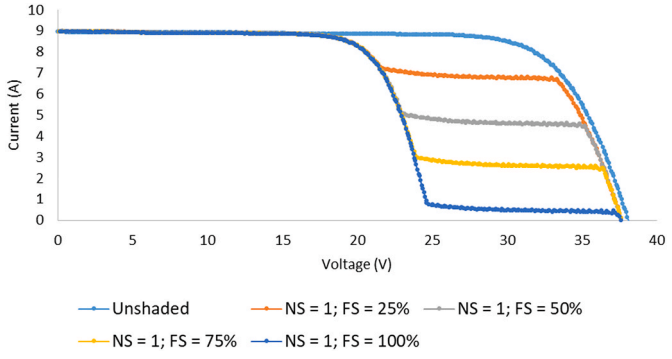

Fig. 4. I–V curves of Module A measured with only one shaded cell (NS = 1) under different shading fractions (FS).

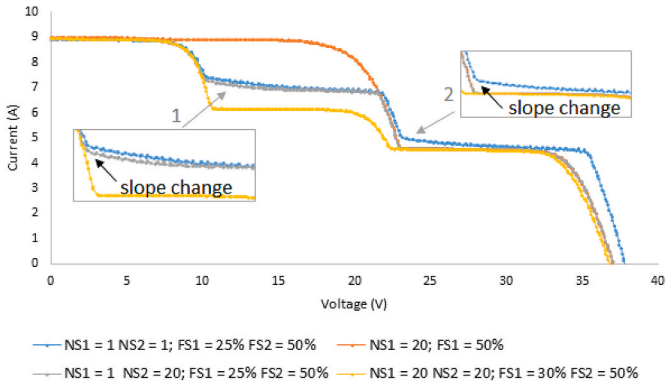

Fig. 5. I–V curves of Module A measured for different shading fractions (FS) and varying the number of shaded cells (NS). The electrical mismatch effect is highlighted.

mismatch of the cells, as shown in Fig. 5. The same effect can be seen in the highlighted region 1. In the cases where all cells of a submodule are uniformly shaded, this effect of electrical mismatch does not occur. In addition, the number of shaded cells also affects the open-circuit voltage of the submodule, which decreases as the number of shaded cells increases, since the voltage also varies with irradiance.

The effect of the electrical mismatch can be understood by analyzing Fig. 6, which shows the I–V curve of a shaded cell, the I–V curve of the remaining cells of the same submodule reflected in the current axis and the I–V curve of the submodule. The highlighted intersection point corresponds to the short-circuit current of the submodule ($I_{sc\ sm}$), which occurs when the sum of the voltages of the shaded cell and the other cells equals zero at the same current. In the indicated region of the

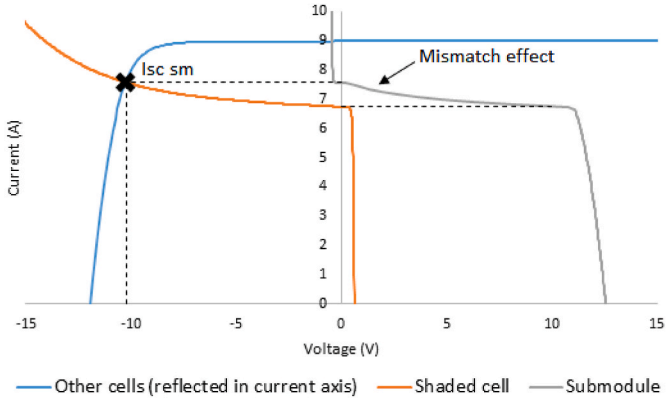

Fig. 6. I–V curve of a cell with 25% shaded area, I–V curve of the remaining unshaded cells reflected in the current axis and I–V curve of the submodule. Short circuit current and mismatch effect are highlighted.

submodule's I–V curve, there is a change in slope due to the reverse bias of the shaded cell, which is characteristic of cell mismatch.

4.1.2. Modeling of I–V curves

The I–V curve of each unshaded PV module was measured, and the five parameters of the cells and submodules were determined, as shown in Table 2. The measured I–V curves and the curves modeled using the three methods described in Section 3.1 are shown in Figs. 7 and 8. The modeled I–V curves overlap with the measured I–V curves, demonstrating the accuracy of the modeling under uniform conditions.

Figs. 9–12 show the measured and modeled I–V curves of Module A under different PSC. The I–V curves were divided into voltage regions according to the current levels. The modeled and measured I–V curves of Module B for a single cell with 25% shaded area are shown in Fig. 13.

The I–V curves generated by the cell-by-cell method are significantly close to the measured curves and show the same behavior due to the electrical mismatch (indicated in the figures). In Fig. 9, the modeled I–V curve of Module A had a larger slope in the short-circuit region of the shaded submodule, in region 2 (R2), compared to the measured curve. On the other hand, the modeled I–V curve of Module B under the same PSC does not show this difference and overlaps with the measured I–V curve in Fig. 13. As can be seen in Fig. 6, the submodule short-circuit current depends significantly on the slope of the I–V curve of shaded cell, which is related to the shunt resistance, when the cell is reverse biased. The five parameters of Eq. (1) were determined using a numerical method, so there are different sets of values that can be used to solve the equations. The shunt resistance determined for Module A is small, which resulted in a larger slope in R2 of the modeled I–V curve of PV Module A in Figs. 9 and 11. This does not occur in the I–V curve of PV Module B, since the shunt resistance calculated for this PV module is larger.

The change in shunt resistance is inversely proportional to irradiance, so this parameter increases with increasing shaded area. In this way, the difference between the modeled and measured I–V curves decreases and the curves overlap when the shading fraction of Module A is larger, as shown in Fig. 10.

The I–V curves generated by the WCC and proposed methods do not reproduce the effect of electrical mismatch. However, the shaded submodule current in the modeled I–V curves is at the same level as in the measured curves. The most significant difference between the measured I–V curves and the I–V curves modeled using the WCC method is in the voltage, especially in the open-circuit region. The WCC method assumes that all cells are under the conditions of the most shaded cell, but the unshaded cells operate at a higher voltage than the shaded cells. On the other hand, the proposed method considers the voltage of the unshaded submodule and makes an adjustment proportional to the number of shaded cells, so that the modeled open-circuit voltage approaches the measured value. Therefore, the proposed method is more accurate than WCC in the open-circuit region of the I–V curve.

4.1.3. Analysis of differences between modeled and measured maximum power point

Figs. 14–17 show the power curves (P–V) of Module A under the same conditions as in Figs. 9–12. The global maximum power (GMP) of the P–V curves modeled using the WCC method is smaller than the measured GMP in Figs. 14 and 16. In Fig. 15, the difference occurs in the local maximum power (LMP) of the P–V curve. This difference at a local maximum is also important because the PV module can operate in this region of the P–V curve depending on the operating voltage range of the inverter. These differences in power are caused by voltage differences in the open-circuit region of P–V curve. All methods are accurate when all cells of a submodule are uniformly shaded, as shown in Fig. 17.

Tables 3 and 4 show the differences in GMP and LMP values between the modeled and measured P–V curves of modules A and B, respectively. The differences between the modeled ($P_{modeled}$) and measured ($P_{measured}$) power were calculated according to Eq. (15). Absolute differences

Table 2
Five parameters calculated for PV cells.

Cell parameters	Module A	Module B
R_{sh} (Ω)	22.47	55.83
R_s (Ω)	0.0032	0.0047
I_0 (A)	9.85E-08	1.7E-10
I_L (A)	8.96	9.078
n	1.38	1.036

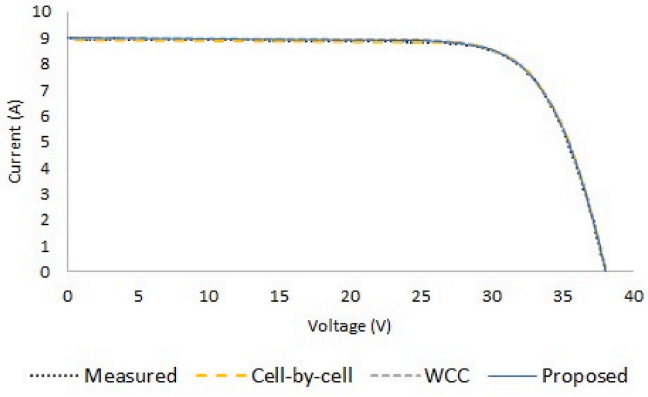

Fig. 7. I–V curves measured and modeled under uniform conditions of Module A.

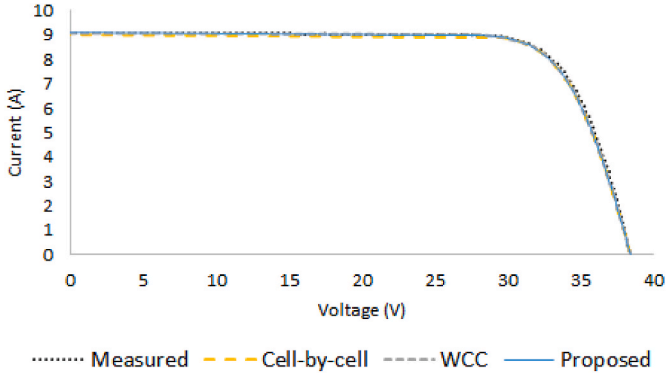

Fig. 8. I–V curves measured and modeled under uniform conditions of Module B.

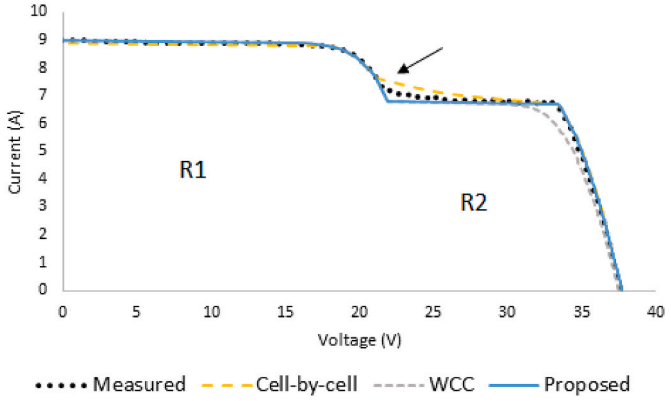

Fig. 9. Measured and modeled I–V curves of Module A with a cell 25% shaded (NS1 = 1 FS1 = 25%). The mismatch effect is highlighted.

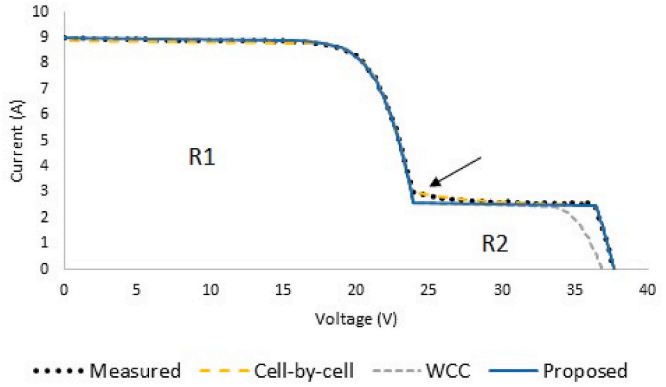

Fig. 10. Measured and modeled I–V curves of Module A with a cell 75% shaded (NS1 = 1 FS1 = 75%). The mismatch effect is highlighted.

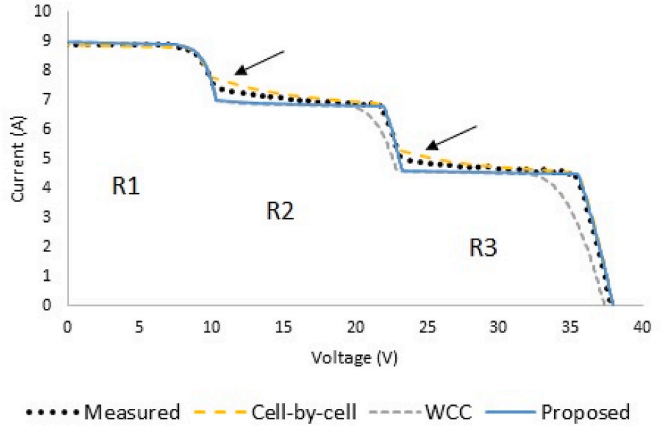

Fig. 11. Measured and modeled I–V curves of Module A with one cell 25% shaded of submodule 1 and a cell 50% shaded of submodule 2 (NS1 = 1 NS2 = 1; FS1 = 25% FS2 = 50%). The mismatch effect is highlighted.

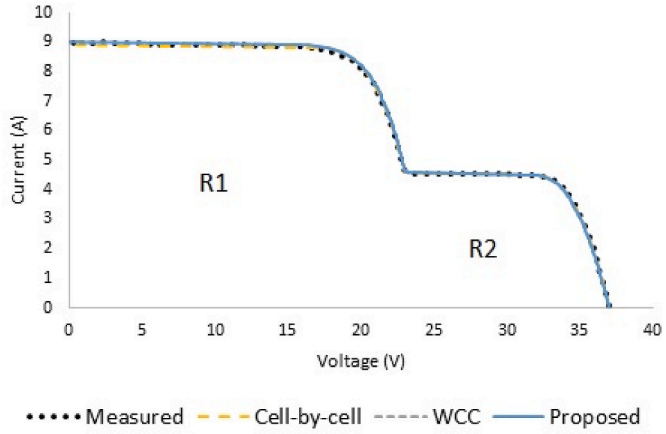

Fig. 12. Measured and modeled I–V curves of Module A with all cells of submodule 1 50% shaded (NS1 = 20; FS1 = 50%).

greater than or equal to 7% are highlighted in the tables. The proposed method resulted in values that were close to the cell-by-cell method, and both methods had a mean absolute percentage error (MAPE) of 1.5%. The WCC method had the largest differences in power compared to the measured P–V curve, with a MAPE of 4.7%.

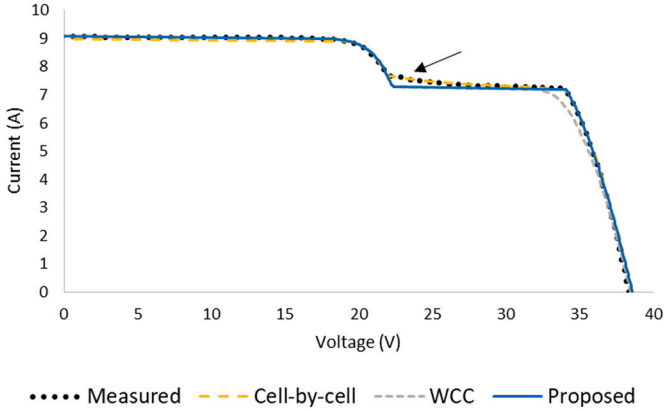

Fig. 13. Measured and modeled I–V curves of Module B with a 25% shaded cell (NS1 = 1; FS1 = 25%). The mismatch effect is highlighted.

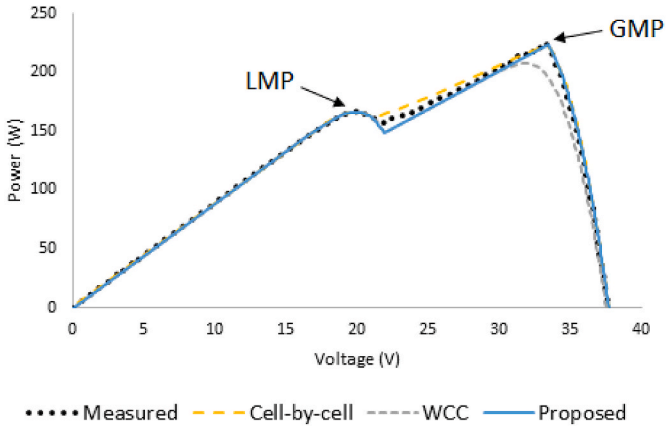

Fig. 14. Measured and modeled P–V curves of Module A with a cell 25% shaded (NS1 = 1; FS1 = 25%).

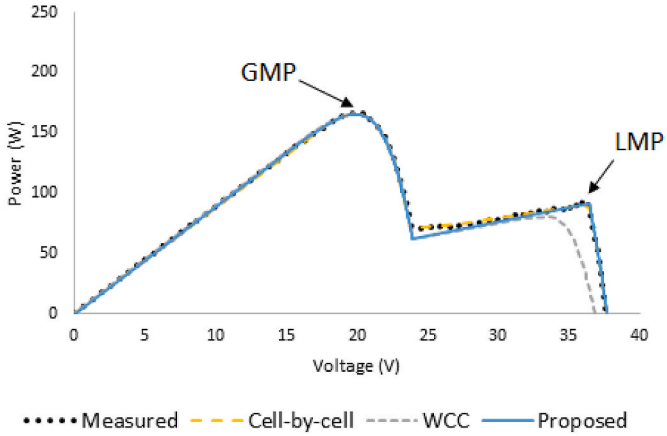

Fig. 15. Measured and modeled P–V curves of Module A with a cell 75% shaded (NS1 = 1; FS1 = 75%).

$$Difference = \frac{P_{modeled} - P_{measured}}{P_{measured}} \; x\; 100\% \tag{15}$$

When all cells in a submodule were uniformly shaded, the three methods had very similar and accurate results compared to the measurements. Differences between the methods appeared in situations where not all cells in the submodule were shaded. In these cases, the

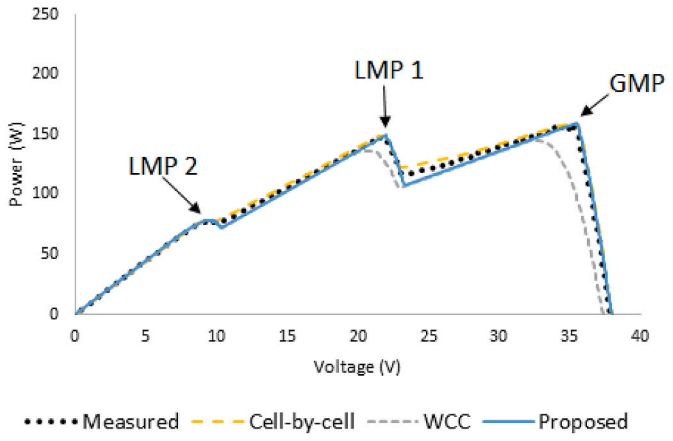

Fig. 16. Measured and modeled P–V curves of Module A with one cell 25% shaded of submodule 1 and a cell 50% shaded of submodule 2 (NS1 = 1 NS2 = 1; FS1 = 25% FS2 = 50%).

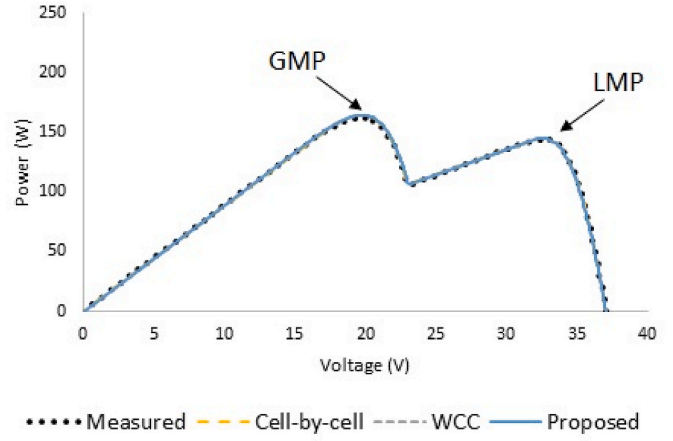

Fig. 17. Measured and modeled P–V curves of Module A with all cells of submodule 1 50% shaded (NS1 = 20; FS1 = 50%).

WCC method led to significant differences in the modeled I–V and P–V curves and presented a higher MAPE in GMP and LMP than the other methods. In contrast, the cell-by-cell method showed the most accurate curves but has disadvantages such as the number of I–V curves required and more simulation steps. The proposed method has adaptations that simplify the modeling and result in an accuracy of the I–V and P–V curves that is very similar to the cell-by-cell method and has the same MAPE.

4.2. Simplified calculation of generated electrical energy

The PV system was analyzed using an hourly and a monthly database for the measurement period. The simplified methods are abbreviated as SM, and the method proposed by Martínez-Moreno et al. [15] is referred as "Reference". The five methods used were described in Section 3.2.

4.2.1. Hourly database

For the analysis of the PV system, the power was first estimated for each hour of the measurement period. Fig. 18 shows, as an example of numerous situations observed over time, the measured PV power, modeled PV power, and solar irradiation on the PV module per hour on October 16, 2020. When the PV system is unshaded, the proposed method has results that coincide with the measured values. When the PV system is under PSC, SM 2 is the less accurate method. All other methods underestimate the shading losses, but the proposed method shows results closer to the measured values. Fig. 19 shows the measured energy and the energy calculated by summing the hourly values of each month. Fig. 20 shows the absolute percentage difference between the calculated and measured energy and the MAPE for each month.

SM 2 and the proposed method had the monthly results closest to the measured values. The energy estimated using SM 2 was lower than the measured energy in the first two months and higher than the measured

Table 4
Difference in GMP and LMP between the modeled and measured P–V curve of Module B for one, two and three cells with 50% shaded area.

Number of shaded cells	Cell-by-cell		WCC		Proposed	
	GMP	LMP	GMP	LMP	GMP	LMP
1	−0.2%	−0.6%	0.0%	**−7.6%**	0.0%	−0.7%
2	−0.3%	−0.8%	−0.1%	**−7.3%**	−0.2%	−0.4%
3	−0.2%	−1.0%	0.0%	**−7.1%**	−0.2%	−0.2%

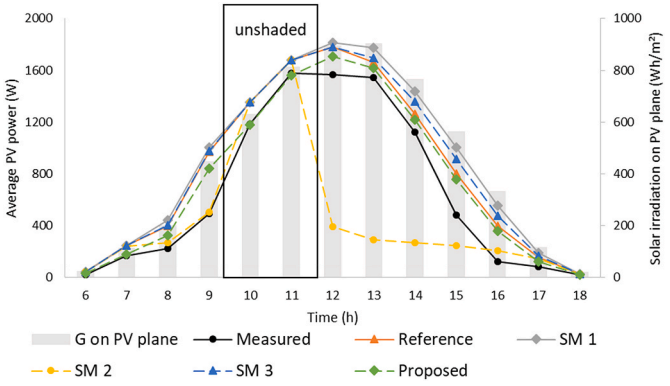

Fig. 18. Measured PV power, modeled PV power and measured solar irradiation on October 16, 2020. Time range without shading are highlighted.

Table 3
Difference in GMP and LMP between the modeled and measured P–V curve of Module A.

Condition	Cell-by-cell			WCC			Proposed		
	GMP	LMP 1	LMP 2	GMP	LMP 1	LMP 2	GMP	LMP 1	LMP 2
A cell with 25% shaded area (NS1 = 1; FS1 = 25%).	−0.3%	−0.4%	–	**−7.0%**	−0.3%	–	0.2%	−0.3%	–
A cell with 50% shaded area (NS1 = 1; FS1 = 50%).	−0.5%	−0.9%	–	−0.3%	**−8.9%**	–	−0.4%	−0.7%	–
A cell with 75% shaded area (NS1 = 1; FS1 = 75%).	−0.6%	−3.3%	–	−0.4%	**−13.2%**	–	−0.7%	−2.2%	–
A cell with 100% shaded area (NS1 = 1; FS1 = 100%).	−0.4%	**−17.9%**	–	−0.3%	**−26.7%**	–	−0.8%	**−19.1%**	–
A cell 25% shaded and another cell 50% shaded (NS1 = 1 NS2 = 1; FS1 = 25% FS2 = 50%).	0.1%	0.1%	−0.1%	**−9.4%**	**−8.2%**	0.7%	0.1%	0.4%	0.3%
A submodule evenly 50% shaded (NS1 = 20; FS1 = 50%).	0.6%	0.0%	–	0.8%	0.1%	–	0.8%	0.1%	–
Two submodules evenly shaded with fraction of 50% e 30% (NS1 = 20 NS2 = 20; FS1 = 30% FS2 = 50%).	−3.2%	1.4%	−1.1%	−3.2%	1.6%	−0.2%	−3.2%	1.6%	−0.2%

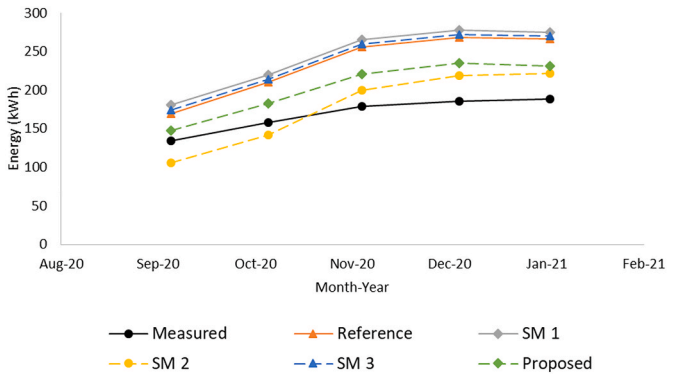

Fig. 19. Monthly measured and calculated electrical energy using hourly database.

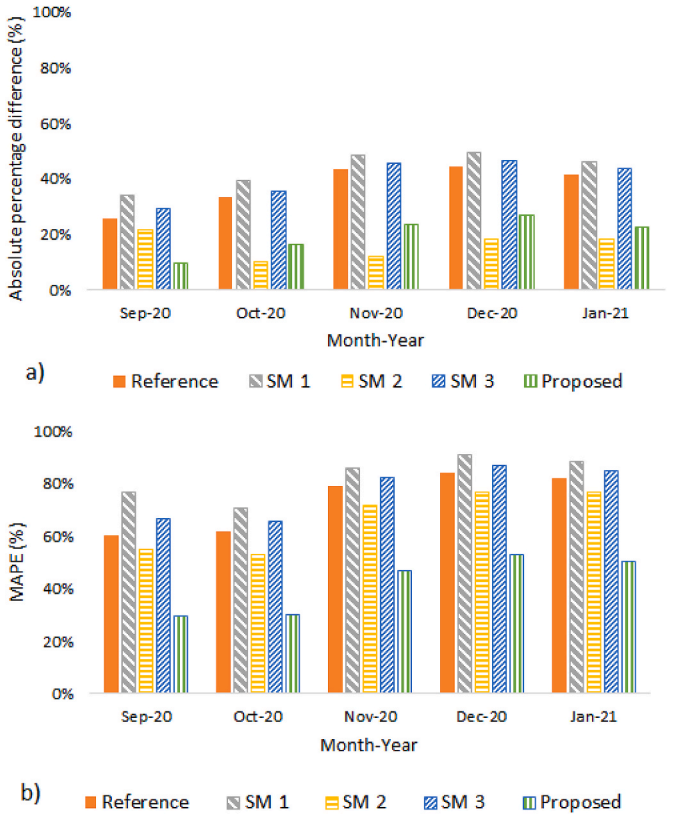

Fig. 20. (a) Difference between calculated and measured electrical energy and (b) MAPE per month for an hourly database.

energy in the last months. SM 2 assumes that any shadow in a submodule cancels the total beam radiation, i.e., the effective shading fraction is equal to 1; therefore, this simplified method leads to an overestimation of the losses in a few months. About MAPE, SM 2 showed higher values than the proposed improvement. SM 1 and SM 3 showed similar results to the reference calculation, underestimating the shading losses. The increase in accuracy due to the use a diffuse shading factor becomes clear when comparing the results of the reference and proposed calculations.

4.2.2. *Monthly database*

For the analysis with the monthly database, monthly average values for the shading factor and number of shaded submodules were used. The beam and diffuse fractions (BDF) of solar radiation were obtained in two ways: the average of the fractions for each month (monthly average hourly fraction) and the total monthly fraction. Fig. 21 shows the results of both BDF calculations, and Fig. 22 shows the absolute percentage differences. The proposed improvement with a fraction of diffuse shading resulted in differences of up to about 10% for both options for calculating the BDF.

Table 5 shows the absolute differences in the total electrical energy of the measurement period considering the different databases. The differences between the measured and calculated values with a monthly database were smaller than those with an hourly database, except for the results of SM 2. For both monthly database options, the proposed method showed a difference of less than 5%.

Considering only the shading fraction (SM 1) or only the number of shaded submodules (SM 3) for the calculation of the effective shading fraction were approximations that resulted in optimistic losses and significant differences compared to the measured values. The simplified calculations and the reference calculation do not consider diffuse radiation losses due to surrounding elements, so these methods tend to underestimate shading losses in PV systems with many surrounding elements, as in the case studied. Using the proposed diffuse shading factor led to results that were closer to the measured values in all the analyzes performed. SM 2 is more pessimistic in terms of radiation losses, so the differences were smaller compared to the other methods at times. All methods, except SM 2, showed more accurate results when a monthly rather than an hourly database was used. The monthly database also has the advantage of being smaller and requiring fewer calculation steps.

All of these simplified methods assume that the PV system is always operating at maximum power. Chepp et al. [18] found that the GMP of the PV system is outside the operating voltage range of the inverter at certain times of the day; therefore, the PV system is biased away from the GMP at these times. This type of loss cannot be accounted if the I–V curve is not calculated. Nevertheless, these methods are more suitable for analyzing the performance of PV systems and show low differences

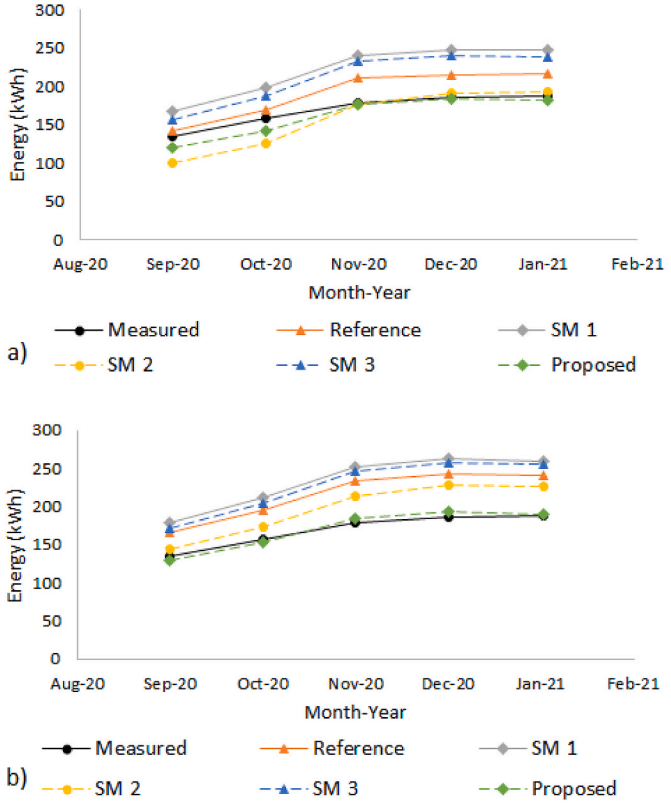

Fig. 21. Monthly output measured and calculated considering: (a) BDF of monthly solar radiation and (b) monthly average hourly BDF.

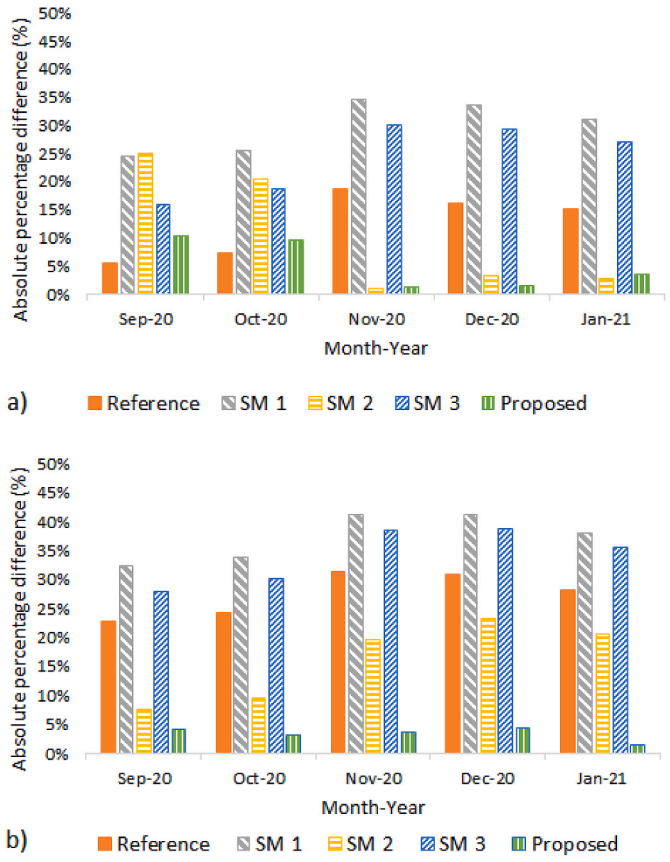

Fig. 22. Absolute percentage difference between the measured and calculated energy considering: (a) BDF of monthly solar radiation and (b) monthly average hourly BDF.

Table 5
Absolute difference between the measured total energy and the total energy calculated by the five methods using different databases.

Database	Reference	SM 1	SM 2	SM 3	Proposed
Hourly	38.5%	44.2%	5.2%	40.9%	20.5%
Monthly – BDF of total solar radiation	13.1%	30.3%	6.7%	24.8%	4.7%
Monthly – average hourly BDF	27.9%	37.8%	16.8%	34.7%	0.8%

compared to the measured values when a diffuse shading factor is applied.

5. Limitations of the proposed methods

The proposed method for modeling the I–V curve for PSC proved to be significantly accurate and simpler compared to the other methods studied. However, both the proposed and the cell-by-cell methods require data of avalanche breakdown of PV cells, which are not provided by PV module manufacturers. Therefore, these data may be a limitation in the application of the proposed method.

A diffuse shading factor was proposed for simplified calculations of the electrical energy generated by PV systems under PSC. This simple improvement in the calculation resulted in much more accurate energy values. However, the difficulty of calculating the diffuse shading factor as well as the shaded area of the PV modules depends on the characteristics and complexity of the PV system.

6. Conclusions

The aim of this article can be divided into two parts: (1) to propose an accurate method for determining I–V curves and (2) to propose an improvement to the simplified methods for estimating the energy generated by PV systems under PSC. Measured I–V curves of two PV modules and measured data from a PV system were compared with results modeled using different methods from the literature and the proposed methods in this article.

When comparing the measured and modeled I–V and P–V curves, the three analyzed methods showed similar and accurate results for the situation where all cells of a submodule are uniformly shaded. For situations where some cells of the submodule are shaded, the modeled curves showed differences. The proposed method provided accurate results, is simple and requires only a few simulation steps.

The results of the comparison between the simplified methods for calculating the electrical generation of a shaded PV system, which do not require estimation of the I–V curve, confirm that the use of the proposed diffuse shading factor provides more accurate results. The proposed improvement using a diffuse shading factor produced results that were closer to the measured values. Using the monthly database increased the accuracy of the results compared to using the hourly database.

The method proposed in this article for modeling I–V curves proved to be simple and accurate. When applied to the PV system, the addition of only a diffuse shading factor proposed in this article contributed to significantly more accurate results. Therefore, both proposed methods had significant advantages in terms of simplification of the simulation and accuracy of the results.

Future analyzes of the methods for modeling I–V curves using outdoor experimental data and the simplified methods for calculating the generated energy using a database of different PV systems will be important to broaden and deepen the comparisons between the studied methods.

CRediT authorship contribution statement

Ellen David Chepp: Investigation, Formal analysis, Methodology, Software, Writing – original draft. **Fabiano Perin Gasparin:** Conceptualization, Writing – review & editing, Resources, Supervision. **Arno Krenzinger:** Writing – review & editing, Supervision.

Declaration of competing interest

The authors declare that they have no known competing financial interests or personal relationships that could have appeared to influence the work reported in this paper.

Acknowledgments

This study was financed in part by Coordenação de Aperfeiçoamento de Pessoal de Nível Superior – Brazil (CAPES) – Finance Code 001 and by Conselho Nacional de Desenvolvimento Científico e Tecnológico – Brazil.

References

[1] T. Güney, Solar energy, governance and CO2 emissions, Renew. Energy 184 (2022) 791–798, https://doi.org/10.1016/j.renene.2021.11.124.
[2] IRENA - International Renewable Energy Agency, Renewable Energy Statistics (2021) 2021.
[3] L.S. Chan, Neighbouring shading effect on photovoltaic panel system: its implication to green building certification scheme, Renew. Energy 188 (2022) 476–490, https://doi.org/10.1016/j.renene.2022.02.058.
[4] N.M. Loulas, M.M. Karteris, P.A. Pilavachi, A.M. Papadopoulos, Photovoltaics in urban environment: a case study for typical apartment buildings in Greece, Renew. Energy 48 (2012) 453–463, https://doi.org/10.1016/j.renene.2012.06.009.
[5] M.K. Al-Smadi, Y. Mahmoud, Analysis of photovoltaic systems power losses in partial shading conditions, Proc. IECON 2018 - 44th Annu. Conf. IEEE Ind. Electron. Soc. (2018) 1699–1704, https://doi.org/10.1109/IECON.2018.8591806.

[6] A. Dolara, G.C. Lazaroiu, S. Leva, G. Manzolini, Experimental investigation of partial shading scenarios on PV (photovoltaic) modules, Energy 55 (2013) 466–475, https://doi.org/10.1016/j.energy.2013.04.009.
[7] H. Mohammed, M. Kumar, R. Gupta, Bypass diode effect on temperature distribution in crystalline silicon photovoltaic module under partial shading, Sol. Energy 208 (2020) 182–194, https://doi.org/10.1016/j.solener.2020.07.087.
[8] I.M. Mehedi, Z. Salam, M.Z. Ramli, V.J. Chin, H. Bassi, M.J.H. Rawa, M. P. Abdullah, Critical evaluation and review of partial shading mitigation methods for grid-connected PV system using hardware solutions: the module-level and array-level approaches, Renew. Sustain. Energy Rev. 146 (2021), 111138, https://doi.org/10.1016/j.rser.2021.111138.
[9] G. Sai Krishna, T. Moger, Reconfiguration strategies for reducing partial shading effects in photovoltaic arrays: state of the art, Sol. Energy 182 (2019) 429–452, https://doi.org/10.1016/j.solener.2019.02.057.
[10] M.C. Di Vincenzo, D. Infield, Detailed PV array model for non-uniform irradiance and its validation against experimental data, Sol. Energy 97 (2013) 314–331, https://doi.org/10.1016/j.solener.2013.08.030.
[11] S. Gallardo-Saavedra, B. Karlsson, Simulation, validation and analysis of shading effects on a PV system, Sol. Energy 170 (2018) 828–839, https://doi.org/10.1016/j.solener.2018.06.035.
[12] V.M.R. Tatabhatla, A. Agarwal, T. Kanumuri, Improved power generation by dispersing the uniform and non-uniform partial shades in solar photovoltaic array, Energy Convers. Manag. 197 (2019), 111825, https://doi.org/10.1016/j.enconman.2019.111825.
[13] H. Hanifi, M. Pander, B. Jaeckel, J. Schneider, A. Bakhtiari, W. Maier, A novel electrical approach to protect PV modules under various partial shading situations, Sol. Energy 193 (2019) 814–819, https://doi.org/10.1016/j.solener.2019.10.035.
[14] C. Saiprakash, A. Mohapatra, B. Nayak, S.R. Ghatak, Analysis of partial shading effect on energy output of different solar PV array configurations, Mater. Today Proc. (2020), https://doi.org/10.1016/j.matpr.2020.08.307.
[15] F. Martínez-Moreno, J. Muñoz, E. Lorenzo, Experimental model to estimate shading losses on PV arrays, Sol. Energy Mater. Sol. Cells 94 (2010) 2298–2303, https://doi.org/10.1016/j.solmat.2010.07.029.
[16] P. Rodrigo, E.F. Fernández, F. Almonacid, P.J. Pérez-Higueras, A simple accurate model for the calculation of shading power losses in photovoltaic generators, Sol. Energy 93 (2013) 322–333, https://doi.org/10.1016/j.solener.2013.04.009.
[17] M.A. Mikofski, M. Lynn, J. Byrne, M. Hamer, A. Neubert, J. Newmiller, Accurate Performance Predictions of Large PV Systems with Shading Using Submodule Mismatch Calculation, 2018 IEEE 7th World Conf. Photovolt. Energy Conversion, WCPEC 2018 - A Jt, Conf. 45th IEEE PVSC, 28th PVSEC 34th EU PVSEC, 2018, pp. 3635–3639, https://doi.org/10.1109/PVSC.2018.8547323.
[18] E.D. Chepp, F.P. Gasparin, A. Krenzinger, Accuracy investigation in the modeling of partially shaded photovoltaic systems, Sol. Energy 223 (2021) 182–192, https://doi.org/10.1016/j.solener.2021.05.061.
[19] D. Jena, V.V. Ramana, Modeling of photovoltaic system for uniform and non-uniform irradiance: a critical review, Renew. Sustain. Energy Rev. 52 (2015) 400–417, https://doi.org/10.1016/j.rser.2015.07.079.
[20] H.S. Moreira, J. Lucas de Souza Silva, M.V. Gomes dos Reis, D. de Bastos Mesquita, B.H. Kikumoto de Paula, M.G. Villalva, Experimental comparative study of photovoltaic models for uniform and partially shading conditions, Renew. Energy 164 (2021) 58–73, https://doi.org/10.1016/j.renene.2020.08.086.
[21] C. Deline, A. Dobos, S. Janzou, J. Meydbray, M. Donovan, A simplified model of uniform shading in large photovoltaic arrays, Sol. Energy 96 (2013) 274–282, https://doi.org/10.1016/j.solener.2013.07.008.
[22] N. Thakkar, D. Cormode, V.P.A. Lonij, S. Pulver, A.D. Cronin, A simple non-linear model for the effect of partial shade on PV systems, Conf. Rec. IEEE Photovolt. Spec. Conf. 1 (2010) 2321–2326, https://doi.org/10.1109/PVSC.2010.5614450.
[23] X. Qing, H. Sun, X. Feng, C.Y. Chung, Submodule-based modeling and simulation of a series-parallel photovoltaic array under mismatch conditions, IEEE J. Photovoltaics 7 (2017) 1731–1739, https://doi.org/10.1109/JPHOTOV.2017.2746265.
[24] S. MacAlpine, M. Brandemuehl, R. Erickson, Beyond the module model and into the array: mismatch in series strings, Conf. Rec. IEEE Photovolt. Spec. Conf. (2012) 3392–3396, https://doi.org/10.1109/PVSC.2012.6318298.
[25] R. Ayop, C.W. Tan, M.S.A. Mahmud, S.N. Syed Nasir, T. Al-Hadhrami, A.L. Bukar, A simplified and fast computing photovoltaic model for string simulation under partial shading condition, Sustain. Energy Technol. Assessments 42 (2020), 100812, https://doi.org/10.1016/j.seta.2020.100812.
[26] M. Kermadi, V. Jack, S. Mekhilef, Z. Salam, A fast and accurate generalized analytical approach for PV arrays modeling under partial shading conditions, Sol. Energy 208 (2020) 753–765, https://doi.org/10.1016/j.solener.2020.07.077.
[27] Y. Zhang, J. Su, C. Zhang, Z. Lang, M. Yang, T. Gu, Performance estimation of photovoltaic module under partial shading based on explicit analytical model, Sol. Energy 224 (2021) 327–340, https://doi.org/10.1016/j.solener.2021.06.019.
[28] E.D. Chepp, A. Krenzinger, A methodology for prediction and assessment of shading on PV systems, Sol. Energy 216 (2021) 537–550, https://doi.org/10.1016/j.solener.2021.01.002.
[29] O. Bingöl, B. Özkaya, Analysis and comparison of different PV array configurations under partial shading conditions, Sol. Energy 160 (2018) 336–343, https://doi.org/10.1016/j.solener.2017.12.004.
[30] H. Zheng, S. Li, R. Challoo, J. Proano, Shading and bypass diode impacts to energy extraction of PV arrays under different converter configurations, Renew. Energy 68 (2014) 58–66, https://doi.org/10.1016/j.renene.2014.01.025.
[31] K. Lappalainen, S. Valkealahti, Number of maximum power points in photovoltaic arrays during partial shading events by clouds, Renew. Energy 152 (2020) 812–822, https://doi.org/10.1016/j.renene.2020.01.119.
[32] C. Zomer, R. Rüther, Simplified method for shading-loss analysis in BIPV systems – part 1: theoretical study, Energy Build. 141 (2017) 69–82, https://doi.org/10.1016/j.enbuild.2017.02.042.
[33] S. Macalpine, C. Deline, Simplified method for modeling the impact of arbitrary partial shading conditions on PV array performance, 2015, IEEE 42nd Photovolt. Spec. Conf. PVSC 2015 (2015), https://doi.org/10.1109/PVSC.2015.7355938.
[34] G. Trzmiel, D. Głuchy, D. Kurz, The impact of shading on the exploitation of photovoltaic installations, Renew. Energy 153 (2020) 480–498, https://doi.org/10.1016/j.renene.2020.02.010.
[35] J.W. Bishop, Computer simulation of the effects of electrical mismatches in photovoltaic cell interconnection circuits, Sol. Cell. 25 (1988) 73–89, https://doi.org/10.1016/0379-6787(88)90059-2.
[36] M.G. Villalva, J.R. Gazoli, E. Ruppert Filho, Modeling and circuit-based simulation of photovoltaic arrays, 2009 Brazilian Power Electron, Conf. COBEP2009 (2009) 1244–1254, https://doi.org/10.1109/COBEP.2009.5347680.
[37] W. De Soto, S.A. Klein, W.A. Beckman, Improvement and validation of a model for photovoltaic array performance, Sol. Energy 80 (2006) 78–88, https://doi.org/10.1016/j.solener.2005.06.010.
[38] C.S. Ruschel, F.P. Gasparin, A. Krenzinger, Experimental analysis of the single diode model parameters dependence on irradiance and temperature, Sol. Energy 217 (2021) 134–144, https://doi.org/10.1016/j.solener.2021.01.067.
[39] J. Peroza, A. Krenzinger, D. Aguiar, RUPTURA por avalanche em células FOTOVOLTAICAS E suas implicações em análises de associações no software CREARRAY, in: VII Congr. Bras. Energ. Sol., 2018.

3 INTEGRAÇÃO DOS ARTIGOS

Durante o período de mestrado, a autora realizou uma pesquisa com a finalidade de propor uma metodologia intuitiva para a análise de sistemas FV parcialmente sombreados (CHEPP, 2018). Essa pesquisa foi continuada no doutorado, sendo realizada uma extensa revisão da literatura da área, descrição da metodologia de forma mais detalhada e melhoria nos resultados, o que culminou na elaboração e publicação do artigo científico. A metodologia proposta foi demonstrada por meio de um estudo do efeito de diferentes padrões de sombreamento de um módulo FV e a influência da sua orientação retrato ou paisagem. Também foram analisadas as perdas por sombreamento em uma usina FV localizada em Porto Alegre. As análises utilizaram ferramentas computacionais disponíveis a todos, que são os programas SketchUp, EnergyPlus, RadiaSol 2 e Crearray (os dois últimos foram desenvolvidos pelo LABSOL).

Existem programas computacionais comerciais para projeto FV que são analisados em diversos trabalhos da literatura a fim de verificar a exatidão dos resultados em condições de radiação solar uniforme. Esses programas comumente apresentam opções para cálculo do sombreamento de forma simples ao usuário. Entretanto, não é amplamente conhecida a exatidão dos resultados simulados para um sistema FV em condições de sombreamento parcial. Complementando o estudo realizado no primeiro artigo, o segundo artigo teve o objetivo de comparar os resultados obtidos por programas computacionais de energia solar, os programas PVsyst e SAM, com dados experimentais de um sistema FV instalado no LABSOL, em Porto Alegre. Para uma definição precisa dos parâmetros de entrada dos programas estudados, foram medidas curvas I-V do sistema FV. Foram simuladas curvas I-V para as mesmas condições a fim de ajustar os parâmetros de entrada, albedo do entorno e a perda por poeira nos módulos FV, de modo que as curvas simuladas coincidissem com as medidas. A metodologia proposta no primeiro artigo foi necessária para a obtenção dessas curvas I-V, permitindo uma análise detalhada do sistema FV em condição de sombreamento parcial e um melhor ajuste dos parâmetros de entrada. Esse segundo trabalho apresentou uma análise detalhada das diferenças entre os valores medidos e simulados pelos programas PVsyst e SAM, mostrando as diferenças nos resultados obtidos utilizando as diferentes opções de cálculo de sombreamento disponíveis em cada programa.

A medição ou modelagem das curvas I-V e P-V de um sistema FV é importante para análises detalhadas do comportamento do sistema. Nos casos de sombreamento parcial, as curvas apresentam descontinuidades (“degraus”) que são uma característica dessa condição. Dada a complexidade na modelagem de curvas I-V e P-V nessas condições de sombreamento parcial, considerações para facilitar os cálculos são feitas muitas vezes. No primeiro artigo, assim como em outros trabalhos da literatura, foi considerado que todo o submódulo estava nas mesmas condições da sua célula mais sombreada. Porém, essa consideração pode levar a diferenças principalmente na região de circuito aberto das curvas. Nesse contexto, o terceiro artigo teve o objetivo de propor uma metodologia simples para modelagem precisa de curvas I-V e P-V. Curvas I-V de módulos em diferentes condições de sombreamento parcial foram medidas em um simulador solar. Essas curvas medidas foram comparadas às curvas modeladas utilizando o novo método proposto e dois métodos da literatura. Além da análise das curvas, existem métodos simplificados de estimativa de energia elétrica produzida por sistemas FV que não necessitam do cálculo da curva I-V. Esse terceiro artigo também propôs uma melhoria a um método simplificado encontrado na literatura. Para isso, quatro métodos de cálculo simplificado de energia produzida em situações de sombreamento parcial foram aplicados ao sistema FV instalado no LABSOL, e foi proposta uma melhoria através do uso de um fator de sombreamento difuso. Portanto, esse terceiro artigo teve o foco de melhorar os métodos encontrados na literatura para modelagem de curvas I-V e de cálculo simplificado de energia produzida por sistemas FV parcialmente sombreados.

4 CONCLUSÕES

Esta tese teve o objetivo de aprimorar a modelagem da operação de sistemas FV parcialmente sombreados. Os objetivos específicos foram desenvolvidos nos três artigos publicados.

O primeiro artigo publicado teve o objetivo de desenvolver uma metodologia intuitiva para analisar sistemas FV sombreados. A metodologia permitiu a análise das perdas em diferentes padrões de sombreamento e análise das perdas por sombreamento em uma usina FV. Foi verificado que a posição retrato ou paisagem dos módulos FV em um sistema FV e o padrão de sombreamento podem influenciar significativamente as perdas. A metodologia se mostrou aplicável para sistemas FV de microgeração distribuída (potência instalada de até 75 kW), havendo possíveis limitações para sistemas FV de maior potência, devido ao nível de detalhamento das análises.

No segundo artigo, foi analisada a exatidão dos cálculos de sombreamento realizados por programas computacionais da área de energia solar. O programa PVsyst possui três opções de cálculo de sombreamento, enquanto o programa SAM possui duas opções. Quanto mais detalhado o cálculo de sombreamento, mais os resultados simulados se aproximaram dos medidos. A diferença entre a energia medida e a simulada pelo PVsyst utilizando o modelo detalhado chegou a 9% e o modelo mais simples (linear) chegou a 24% para todo período analisado. Portanto, o modelo linear apresentou uma diferença em comparação às medições 15% maior que o modelo detalhado. Em relação ao SAM, ambos os modelos de cálculo de sombreamento resultaram em diferenças em torno de 20%. Também foi verificado que quanto mais detalhado for o modelo geométrico do entorno, maior a precisão dos resultados. A opção de cálculo de sombreamento escolhida e o nível de detalhamento da representação 3D realizada influenciaram significativamente a precisão dos resultados obtidos nas simulações.

O terceiro artigo propôs uma metodologia simples e precisa para modelar curvas I-V de módulos FV parcialmente sombreados e uma melhoria a um método simplificado de cálculo da energia produzida por sistemas FV parcialmente sombreados. Em relação à modelagem de curvas I-V, o método proposto e os demais analisados para comparação foram precisos quando todas as células de um submódulo são sombreadas uniformemente. Entretanto, a metodologia proposta

possui vantagens quando o submódulo não é uniformemente sombreado, apresentando curvas I-V precisas de uma maneira simplificada. Um método simplificado para análise da eletricidade produzida por sistemas FV sombreados (sem modelagem da curva I-V) foi melhorado com o uso de um fator de sombreamento difuso, e os resultados foram comparados com os obtidos utilizando outros métodos da literatura. A realização dos cálculos simplificados com dados mensais aumentou a precisão dos resultados em comparação aos cálculos horários, com exceção do método 2 analisado. Usando uma base de dados mensal, a diferença entre a energia elétrica produzida medida e a energia estimada do sistema FV instalado no LABSOL, considerando o fator de sombreamento difuso, foi menor que 5%. Portanto, as duas metodologias propostas nesse artigo se mostraram simples e precisas.

Sistemas FV parcialmente sombreados podem ser analisados por meio de diferentes métodos com diferentes níveis de complexidade e exatidão dos resultados. Nesta tese foram abordados esses diferentes métodos e propostas melhorias. Portanto, esta tese contribuiu com a melhoria da modelagem de sistemas FV parcialmente sombreados, analisando tanto a modelagem de curvas I-V como modelos simplificados de estimativa de energia produzida. A partir dos resultados, pode-se concluir que as previsões de energia elétrica produzida por sistemas FV parcialmente sombreados devem ser realizadas com cautela, uma vez que o método de cálculo escolhido pode influenciar significativamente a exatidão dos resultados e que métodos mais simplificados tendem a ser menos precisos.

Nesta tese, não foram analisados os módulos FV de meia célula com sombreamento parcial. Como continuidade do trabalho, sugere-se a realização de estudos com módulos FV de meia célula sobre os efeitos do sombreamento parcial e a modelagem de curvas I-V nessa condição. Também são sugeridos estudos mais detalhados para validação experimental da metodologia proposta no artigo 1.

REFERÊNCIAS

ANEEL, Agência Nacional de Energia Elétrica. **Geração Distribuída**. Disponível em: <https://app.powerbi.com/view?r=eyJrIjoiY2VmMmUwN2QtYWFiOS00ZDE3LWI3NDMtZDk0NGI4MGU2NTkxIiwidCI6IjQwZDZmOWI4LWVjYTctNDZhMi05MmQ0LWVhNGU5YzAxNzBlMSIsImMiOjR9>. Acesso em: 25 set. 2023a.

ANEEL, Agência Nacional de Energia Elétrica. **Sistema de Informações de Geração da ANEEL**. Disponível em: <https://app.powerbi.com/view?r=eyJrIjoiNjc4OGYyYjQtYWM2ZC00YjllLWJlYmEtYzdkNTQ1MTc1NjM2IiwidCI6IjQwZDZmOWI4LWVjYTctNDZhMi05MmQ0LWVhNGU5YzAxNzBlMSIsImMiOjR9>. Acesso em: 25 set. 2023b.

AYOP, R. et al. A simplified and fast computing photovoltaic model for string simulation under partial shading condition. **Sustainable Energy Technologies and Assessments**, v. 42, n. September, p. 100812, 2020.

CHEPP, E. D. **Metodologia para análise de perdas por sombreamento em instalações fotovoltaicas**. [s.l.] Universidade Federal do Rio Grande do Sul, 2018.

CHEPP, E. D.; GASPARIN, F. P.; KRENZINGER, A. Accuracy investigation in the modeling of partially shaded photovoltaic systems. **Solar Energy**, v. 223, n. May, p. 182–192, 2021.

CHEPP, E. D.; GASPARIN, F. P.; KRENZINGER, A. Improvements in methods for analysis of partially shaded PV modules. **Renewable Energy**, v. 200, n. September, p. 900–910, 2022.

CHEPP, E. D.; KRENZINGER, A. A methodology for prediction and assessment of shading on PV systems. **Solar Energy**, v. 216, n. January, p. 537–550, 2021.

DOLARA, A. et al. Experimental investigation of partial shading scenarios on PV (photovoltaic) modules. **Energy**, 2013.

HANIFI, H. et al. A novel electrical approach to protect PV modules under various partial shading situations. **Solar Energy**, v. 193, n. July, p. 814–819, 2019.

IRENA, INTERNATIONAL RENEWABLE ENERGY AGENCY. **Renewable Capacity Statistics 2023**. [s.l: s.n.].

MACALPINE, S.; DELINE, C. Simplified method for modeling the impact of arbitrary partial shading conditions on PV array performance. **2015 IEEE 42nd Photovoltaic Specialist Conference, PVSC 2015**, p. 1–6, 2015.

MARTÍNEZ-MORENO, F.; MUÑOZ, J.; LORENZO, E. Experimental model to estimate shading losses on PV arrays. **Solar Energy Materials and Solar Cells**, v. 94, n. 12, p. 2298–2303, 2010.

MERMOUD, A.; LEJEUNE, T. Partial shadings on PV arrays: By-pass diode benefits analysis. **European Photovoltaic Solar Energy Conference**, p. 6–10, 2010.

RIGO, P. D. et al. Competitive business model of photovoltaic solar energy installers in Brazil. **Renewable Energy**, v. 181, n. August 2021, p. 39–50, 2022.

TRZMIEL, G.; GŁUCHY, D.; KURZ, D. The impact of shading on the exploitation of photovoltaic installations. **Renewable Energy**, v. 153, p. 480–498, 2020.

WIJERATNE, W. M. P. U. et al. Design and development of distributed solar PV systems: Do the current tools work? **Sustainable Cities and Society**, v. 45, n. November 2018, p. 553–578, 2019.